C.P. No. 344
(18,186)
A.R.C. Technical Report

C.P. No. 344
(18,186)
A.R.C. Technical Report

MINISTRY OF SUPPLY

AERONAUTICAL RESEARCH COUNCIL

CURRENT PAPERS

LIBRARY
ROYAL AIRCRAFT ESTABLISHMENT
BEDFORD.

An Experimental Introduction to the Jet Flap

By

N. A. Dimmock

LONDON . HER MAJESTY'S STATIONERY OFFICE

1957

TEN SHILLINGS NET

ADDENDUM

For Reference 2, reference may be made to:

(a) B. S. Stratford — Early thoughts on the jet flap. The Aeronautical Quarterly, Vol. VII. February, 1956.

(b) I. M. Davidson — The Jet Flap. The Journal of the R. Ae. Soc. January, 1956.

See also:

B. S. Stratford — Mixing and the jet flap. The Aeronautical Quarterly, Vol. VII. May, 1956.

B. S. Stratford — A further discussion on mixing and the jet flap. The Aeronautical Quarterly, Vol. VII. August, 1956.

DB 62269/1/BS.200098 301 7/57 R

U.D.C. No.533.691.152:533.691.13

C.P. No. 344
NGTE R 175

NATIONAL GAS TURBINE ESTABLISHMENT

An experimental introduction to the jet flap

- by -

N. A. Dimmock

SUMMARY

This paper records the experimental results obtained with two two-dimensional aerofoils, each having a 12.5 per cent thick elliptical cross section with a narrow full span jet slot at the trailing edge, the jet deflections being respectively 90° and 31.4°. It is shown that the values of the force and moment coefficients and derivatives obtained experimentally agree satisfactorily with those suggested by the theory of Reference 2. Support is given to the thrust hypothesis in that the measured thrust was greater, under appropriate conditions, than the reaction component from the deflected jet. The losses in the system have been considered and some of them investigated, those due to Reynolds number and jet entrainment effects being included. Also, the influence of ground proximity on the lift and centre of lift of the 31.4° model was measured at zero incidence and found not to be prohibitive. A tentative empirical expression is suggested for the pitching moment coefficient.

TABLES

APPENDIX

ILLUSTRATIONS

ILLUSTRATIONS (cont'd.)

ILLUSTRATIONS (cont'd.)

1.0 Introduction

It has been known for some time that if a moving aerofoil is provided with a high velocity jet sheet in its trailing edge region, having a momentum more than sufficient for boundary layer control, its lift will be greater than could be predicted using only classical theory[1]. Late in 1952 it was suggested at the N.G.T.E. that a worthwhile increase in lift might result if, instead of an auxiliary jet, most or all of the propulsive jet of an aircraft were discharged downwards through a narrow full span nozzle forming the trailing edge of the wing. After some purely qualitative, unreported, preliminary experiments, work was begun on a theoretical and an experimental investigation of a system comprising an uncambered aerofoil of fixed geometry with a full span "propulsive" jet issuing from its trailing edge - see Figure 2.

The aims of the experimental work were the provision of such basic information as would assist in an understanding of the jet flap mechanism, and of a check on the theory which was being developed in parallel with the experiments - see Reference 2. Thus a comparison with that theory is made wherever appropriate.

2.0 The equipment

2.1 The model

For practical reasons and since any theoretical work involving transformations would thus be simplified, an uncambered aerofoil of elliptical section was chosen for the experiments, it being thought, moreover, that an orthodox aerofoil section might be no more suitable for use in conjunction with the jet flap than would the ellipse. For ease of manufacture the model was made in brass and as large as the wind tunnel facilities would permit, but even so the size was insufficient for the avoidance of considerable Reynolds number effects. The basic model comprised an aerofoil body with an accurately machined register to which could be attached alternative trailing edge assemblies.

The structural and geometric details are broadly illustrated by Figures 1 and 2, two trailing edge units being used, each conforming to the elliptical section and having a full span jet slot of which the centre line passed through the centre of the trailing edge radius. The jet efflux angles were 90.0° and 31.4° (nominally 90° and 30°) and the average slot widths were both 0.018 in., the variation being less than ± 0.001 in., for the 90° model and as illustrated in Figure 5 for the 30° model. Care was taken to ensure a uniform spanwise jet total pressure distribution (see Figure 1(b)) and to rid the model of leaks which might well upset its boundary layers. The jet total pressure was measured within the body of the aerofoil where the flow area was more than forty times that of the jet slot, whilst the external static pressure holes (1 - 26 in Figure 2), which of necessity were staggered near the leading and trailing edges, were all within $\frac{1}{8}$ in. of the mid-span station.

2.2 The wind tunnel etc.

In view of the large vertical displacement to be expected of the mainstream, the tunnel working section was made 12 in. wide by $56\frac{1}{2}$ in. deep and 6 ft long, and it was connected by a two dimensional contraction to the $56\frac{1}{2}$ in. square settling chamber of an existing low speed cascade tunnel as shown in Figure 3. The sides of the working section could be adjusted by screw jacks to clamp the model when pressure plotting and to provide a small clearance, about 0.05 in. on each side, to permit the thrust balance to be used. Air speeds up to 115 ft/s could be attained in the working section where the velocity profile was fair, although the boundary layer was about 0.75 in. thick on the side walls in the region of the aerofoil leading edge due to a bulge near the exit of the contraction.

The maximum jet flow was about 0.17 lb/s of air and this was provided by a mobile compressor feeding the model via the normal laboratory ring main and reservoir, a stop valve, a high efficiency filter, two reducing valves in series, a centrifugal water separator and a throttling valve. With this arrangement the long period fluctuations of the jet total pressure, due to the compressor governing mechanism, were reduced to about 0.02 in. mercury within the normal working range of the regulator valves. With large airflows, however, variation could be considerably larger and, when necessary, the manual control of a blow-off valve ensured that the percentage fluctuation of the jet total pressure was reduced to a negligible value at all times. It was found essential to remove the condensed water from the air since if any passed through the jet slot it gave rise to a large, erratic reduction in thrust and could even affect the static pressure distribution. All drain valves were, therefore, left "cracked" during test runs to give a continuous blow down of condensate and oil which on occasions amounted to more than two gallons per hour.

The vertical lengths of rubber tubing connecting the model inlets to the supply points (see Figure 4) were kept straight and taut, whatever the attitude of the aerofoil, to avoid any Bourdon tube effect when under pressure during the thrust measurements.

The thrust balance consisted of a parallelogram linkage on either side of the working section, the lower links being clamped to the air supply tube so as to prevent rotation of the model (see Figure 4). The two forward arms were fixed to a torsion tube which carried the balance arms centrally, while the rear pair were freely pivotted. The need for haste in the construction of the balance led to the use of ball races for the pivots and these, when lubricated with light machine oil after being thoroughly washed in a grease solvent, proved remarkably reliable in spite of the very small angular movements made. The use of a sensitive pneumatic relay valve and pressure gauge as a null point indicator made it possible to measure thrust and drag forces reliably to 0.002 lb, while 0.0005 lb could be detected. A full scale deflection of the pressure gauge (0 - 20 p.s.i.) corresponded to an angular movement of the balance arms of about 1.5 minutes of arc when the coupling link was positioned to give the maximum practicable sensitivity. Thus, with a heavy model and suspension system and large inverted lift forces, the pendulum effect was negligible providing that the initial precaution was taken of setting the balance point to correspond with a vertical alignment of the four parallel arms.

Zero geometric incidence was obtained by setting the chord line scribed on the model parallel to the wind tunnel centre line marked on one of the transparent walls. A pointer clamped to the air supply tube was then zeroed on a protractor fixed to one of the side links (see Figure 4) and a preliminary test without "blow" confirmed that no lift force resulted when the model was set at zero incidence in this way.

3.0 The jet calibration

3.1 Efflux angle

The measurement of the jet angle for the 90° model - the first to be tested - proved fairly simple, for the parallel portion of the slot was twice its width and accurate machining had left the external corners sharp. Long fine strands of wool attached to the trailing edge close to and on either side of the slot indicated a mean jet direction perpendicular to the chord when sighted against a reference line scribed on the tunnel wall. Also, with the model set at zero incidence, the balance registered zero thrust until the strength of the jet was sufficient to produce unstable secondary effects. These were caused by the jet impinging on the top tunnel wall and turning towards either the inlet or the outlet of the working section, the choice apparently being determined by draughts in the building since an initiation or a reversal of the effect could be obtained by blocking the tunnel exit. The ejector action of the jet stream induced a flow of air through the wind tunnel which gave rise to an apparent drag or thrust on the aerofoil. However, the direct measurement of angle using wool tufts, supported by the null point thrust measurement with small jet flows, was considered sufficiently conclusive for the jet deflection angle to be taken as 90.0°.

With the 30° model a different technique was attempted in order to obtain the high degree of accuracy necessary. After a preliminary trial with wool tufts had indicated that the jet deflection was nearly 31°, the model was set at -31.0° so that the jet issued very nearly horizontally. A thrust calibration was then performed, as described in Section 3.2, a small error in jet angle making little difference to the results. The aerofoil was then turned to +59.0° incidence, to give a nearly vertical jet, and the thrust balance plus pressure plotting used to determine the small thrust or drag which would permit a correction to be made to the nominal jet angle. However, because of the large area of the model - at 59° incidence - presented to the induced tunnel flow, the effects described above relating to the 90° model were pronounced even at the low values of jet total pressure and the method had to be abandoned. As for the 90° model, direct observation of the angle was then resorted to, but this time three pairs of very fine cotton threads were speced along the span, the tests covering a range of tuft lengths and jet total pressures. The jet angle was determined as 31.4° and a number of discreet measurements using the same method gave this value consistently over several days. As an additional check the model was set to zero incidence and the thrust measured for a number of jet total pressure settings. To this thrust was added the pressure force acting parallel to the chord line and, when the total was divided by the cosine of the estimated angle of 31.4°, the quotient agreed well with the measured values of corrected thrust as shown on the curve in Figure 7.

3.2 The thrust

With the 90° model set at -90° incidence, the thrust was measured over the complete range of jet total pressure that could safely be used. The balance was not fully operative until after the tests on this model, but the thrust was "weighed" using the completed suspension arms and links together with cord, pulleys, a yoke and a scale pan. The manometer connected to the static holes in the model showed that a considerable pressure force was "induced" by the jet stream and it amounted to a "drag" of about nine per cent of the measured thrust. With this correction added the total thrust, J, was found to agree reasonably with the estimated value. Figure 6 illustrates the result with the direct measurement, the induced effect and the corrected curve shown separately.

The same procedure was adopted for the 30° model, the incidence for calibration being -31.4° and the pressure forces both normal and parallel to the chordline being resolved parallel to the thrust line and added. Figure 7 shows the result.

4.0 Behaviour at zero incidence

4.1 The jet shape

As an aid to an understanding of the jet flap mechanism and to test the validity of some of the assumptions[2] concerning the jet sheet, experiments were made using the 30° and 0° models (see Section 5.2 for 0° model) to discover the path of the jet, the extent of its penetration into the mainstream and its rate of diffusion. Two pitot combs were used to measure the distribution of total pressure in the vicinity of the jet stream, one consisting of 31 tubes each 1 mm. outside diameter and evenly spaced in 2.90 inches for use at stations B and C (see Figure 8) and the other having 20 tubes of 0.5 mm. diameter pitched closely together for use at station A where the "wake" was narrow and the gradients of total pressure were steep. At these stations the pitot combs, which projected through the tunnel wall, were fixed in such a manner that the peak of each "wake" was recorded for all values of the jet coefficient, C_J, between 0 and 1.0 (see Section 4.2 for the definition of C_J) the centre line of the wake for $C_J = 0$ providing a datum from which the jet penetration could be measured. At station A the narrow comb was aligned approximately with the jet centre line but it was not wide enough to record the peak of the "no blow" wake. At station D, the remotest plane possible within the limit of the transparent panels, the width of the larger pitot comb also was insufficient to include the centres of both the jet stream and the wake with $C_J = 0$. Thus, since there was no means of moving the instrument stem a measured vertical distance, a simple total head tube 1.5 mm. outside diameter was traversed manually to obtain the necessary information, the entry being positioned visually between scales marked on both transparent side walls of the working section. Examples of the "wake" shapes at $C_J = 0.30$ are shown for the four stations in Figure 8, together with the jet path derived from these explorations, whilst the penetration of the jet into the mainstream at stations B, C and D is shown in Figure 9.

For the purpose of plotting the jet path, the measurement of the penetration at only three planes proved inadequate, and obstructions prevented the mounting of the pitot combs in intermediate positions. The simple pitot tube was, therefore, used to explore and find the position of maximum total pressure in any one plane and a distant, carefully aligned, spotlight then indicated the position of the pitot entry on tracing paper affixed to the tunnel wall. Figure 10 is a fair copy of the result with the check points obtained from pitot comb measurements added as corroborative evidence.

These brief, somewhat unrefined experiments formed the background for a part of the argument for the validity of the theoretical jet flap model in Reference 2.

4.2 Lift

The integrated pressure force in the y direction, (see Figure 46) which is the pressure lift, L_p, since $\alpha = 0$, was added to the vertical component of the jet thrust to give the total lift L_o. Or, in coefficient form,

$$C_{L_o} = C_{L_p} + C_J \sin\theta \quad \ldots \ldots \ldots \ldots \ldots \ldots \quad (1)$$

where C_J, the jet coefficient, is given by

$$C_J = \frac{\text{Gross thrust per unit span (J)}}{\frac{1}{2}\rho U_o^2 c} \quad \ldots \ldots \ldots \quad (2)$$

(For nomenclature see Appendix I and Figure 46).

Figures 11 and 12 show both the total and the pressure lift coefficients, C_{L_o} and C_{L_p}, plotted against the jet coefficient, C_J, for the 90° and 30° models.

In Reference 2 it is shown that:-

$$C_{L_o} = 2k \sin\theta \sqrt{2\pi}\, C_J^{\frac{1}{2}} \left[1 + \frac{\pi}{48} \cdot \frac{C_J}{k^2} + O(C_J^2)\right] \qquad (3)$$

and the magnification factor - a useful practical concept - by:-

$$\mathcal{M}_o = \frac{\text{Total lift}}{\text{Jet lift}} \equiv \frac{L_o}{J \sin\theta}$$

$$= 2k \left(\frac{2\pi}{C_J}\right)^{\frac{1}{2}} \left[1 + \frac{\pi}{48} \cdot \frac{C_J}{k^2} + O(C_J^2)\right] \quad \ldots \quad (4)$$

The experimental values of $\mathcal{M}_o$ are plotted against C_J in Figures 13 and 14.

The above equations for C_{L_o} and $\mathcal{M}_o$ are derived from the parametric relationships:-

$$\left.\begin{aligned} \mathcal{M}_o &= \frac{\pi}{\psi}\left(1 + \frac{\sin\psi}{\psi}\right) \\ \text{and} \qquad C_J &= \frac{2\psi^2}{\pi} \cdot k^2 \cdot \frac{2}{1 + \cos\psi} \end{aligned}\right\} \quad \ldots \ldots \ldots \ldots \quad (5)$$

where ψ defines the size of the simple analogous flap.

The factor k, for the purposes of this Report, may be considered as a practical jet shape factor that is given by

$$k^2 = \frac{\eta}{\sin\theta},$$

where η is the angle of deflection of an analogous hinged flap on the equivalent thin aerofoil. With a thin aerofoil the value of k would be such as to account for the difference between the pressure distribution on the curved jet flap surface and that on the simple straight flap with the same total lift. In practice, however, it is affected also by the shape of the aerofoil section in the trailing edge region, by the Reynolds number, and by the jet coefficient and efflux angle. So far no theoretical value has been suggested for k although it is expected to be in the region of 1.0, i.e. for small jet angles $\eta \mp \theta$.

The experimental values of k obtained through equations (5) include all the effects of boundary layer separation from the model. Curves of k plotted against C_J are shown in Figures 15 and 16.

A comprehensive selection of pressure distribution curves is given for general information in Figures 17 to 20 for the 90° model, and in Figures 23 to 26 for the 30° model, whilst in Section 4.3 the evidence provided by a number of these distributions is used to interpret certain of the observed phenomena.

4.3 Some Reynolds number effects

For all the tests on both models with a jet coefficient of 0.5 or less the chordal Reynolds number was 4.25×10^5 (mainstream speed = 100 ft/s) but, with the pressure inside the model aerofoil limited to about 15 p.s.i. gauge, values of C_J above 0.5 - 30° model only - could only be obtained by reducing the air speed in the tunnel with a consequent reduction in Reynolds number. The value of $\frac{U_0 c}{\nu}$ has been included in the relevant illustrations.

The following points were noted from the results of the 90° model tests:-

(i) A discontinuity in the C_{L_0} - C_J curve at a value of $C_J = 0.04$ (Figure 11). This is more obvious in the $\mathcal{M}_0$ - C_J curve (Figure 13) and still more so in the k - C_J curve (Figure 15).

(ii) The lack of a suction peak near the trailing edge until a C_J of 0.039 is reached (pressure distribution curves (a), (b) and (c) in Figure 17).

(iii) The sudden reduction of pressure after a partial recovery on the upper surface at the trailing edge at all values of C_J (pressure distribution curves (a) to (k) in Figures 17 to 20).

These observations prompted some experiments with transition wires fitted to the aerofoil which, by then, had been rebuilt with its 30° trailing edge. Figures 21 and 22 show C_{L_0} and $\mathcal{M}_0$, respectively, plotted against C_J for the aerofoil with and without trip wires, the results for various arrangements of the wires being added from a separate test, whilst the pressure distributions obtained from that test are shown in curves (a) to (e) of Figure 23 in order of increasing lift. It should be noted that the remainder of the testing on the 30° model was done with both transition wires in the position shown at (e) in Figure 23.

A study of the pressure distributions, reinforced by the evidence from lift measurements and by explorations with wool tufts and a smoke probe, suggests the following interpretation.

In general the momentum deficiency in the boundary layer at the trailing edge of the aerofoil, which would be shed as a wake in the absence of a jet, causes a diminution in the effective jet strength issuing from the slot. Reference 3 considers how this interaction affects thrust and drag, but since it is a net loss to the jet system the lift also can be modified, and the rapid increase of k - the flap shape factor and the most sensitive indicator to the functioning of the jet flap system - with C_J at small values of the latter is to be expected as the ratio of the aerofoil drag coefficient to the jet coefficient becomes small. (See Figures 15 and 16 and Section 5.1).

Consider the conditions where the peak leading edge static pressure coefficient, C_p, is less than about -1.2, the value corresponding to a C_J of 0.039 for the 90° model - Figure 17 (d) - and between 0.15 and 0.20 for the 30° model - Figure 23 (g) and (h) - and where discontinuities in the curves of C_{L_o}, $\mathcal{M}_o$, and k occur - Figures 11 to 16. An arbitrary but relevant local Reynolds number is $\frac{U_{max}\, s}{\nu}$, where U_{max} is the local peak velocity and s the surface distance from the front stagnation point to the point of inflection of the pressure curve, which was considerably less than that at which laminar separation or transition occurred in classical work on flows around circular cylinders - as for example in References 4 and 5 - and so it appeared that the laminar boundary layer must have persisted to near the trailing edge when no trip wires were fitted. (Note here observations (ii) and (iii) above concerning the 90° model, also the shape of the pressure distribution for the 30° model without a trip wire on the upper surface, Figure 23 (a) and (b)). This laminar separation near the trailing edge might be expected to cause a greater loss to the jet lifting system than would the delayed separation of a turbulent boundary layer.

It follows that the increase in lift at low values of C_J, found when trip wires were placed aft on the 30° model, were due probably to the benefits bestowed by a laminar boundary layer over the majority of the aerofoil surface and a delayed, or even non-existent, separation at the trailing edge brought about by transition to turbulent flow at the wires. (Note also the lower measured drag on the model with trip wires added - Section 5.1).

Above the critical value of C_J required to give a C_p of about -1.2 the suction peak and adverse pressure gradient near the leading edge were sufficiently large, apparently, to cause transition there, possibly following a small bubble of laminar separation although this could not be detected. For the 90° model this transition might have delayed the separation at the trailing edge to some extent, but the resulting thick boundary layer offset this and thus accounted for the abrupt check in the rate of increase of k with C_J (Figure 15). Separation at the trailing edge of the 90° model was present at all times during the tests in spite of several attempts to improve the flow in that region by the addition of "plasticine" fairings and, behind the model above the jet sheet, reversed flow with considerable turbulence was observed using wool tufts.

The convergence, at the critical value of $0.15 < C_J < 0.20$, of the curves of C_{L_0}, $\mathcal{M}_0$ and k for the 30° model with and without trip wires (Figures 21, 22 and 15 and 16) supports the above interpretation since it shows that, above this value of C_J, the trip wires had no further effect. In both instances the onset of transition near the leading edge must have resulted in a thicker boundary layer which would diminish the strength of the jet and so explain the reduced increase of C_{L_0} and k with C_J (Figures 12 and 16).

Additional evidence from the pressure distributions is the noticeable kink in some of the curves where the pressure rises after the forward suction peak and this normally indicates a transition from laminar to turbulent flow in the boundary layer[4]. The lack of sufficiently closely spaced static holes in the region, however, prevents the consistency needed for a definite conclusion. It is significant also that the shape of the curve of k plotted against C_J (Figure 16), with k calculated from pressure measurements, is similar to the curve of $\frac{C_{T_0}}{C_J}$ against C_J (Figure 30) although C_{T_0} was obtained from balance measurements in a separate test. Other points of discontinuity in both curves of k and $\frac{C_{T_0}}{C_J}$ occur at a C_J of about 0.5, 0.75 and 1.0 and no explanation of these is offered, but it should be remembered that the Reynolds number does not remain constant above a value for C_J of 0.5 except for the three points: C_J = 1.0, 1.5 and 2.0.

Leading edge separation occurred with both models after a pressure coefficient of about -6.7 had been reached, this value corresponding to $C_J = 0.38$ for the 90° model and $C_J = 1.50$ for the 30° model - Figures 18 (h) and 25 (m). The pressure distributions after the onset of leading edge separation are shown in Figures 19 and 20 for the 90° model and in Figures 25 (n) and 26 for the 30° model, and it will be seen from Figures 11 to 16 that the lift continues to increase smoothly in spite of this separation, as does the suction peak near the trailing edge of the 30° model where, it was thought, no separation occurred.

4.4 The centre of lift

The first moment of area of the pressure distribution curves about the mid-chord point was obtained by graphical integration, and the addition of the moment due to the jet reaction gave the total pitching moment on the aerofoil and hence the position of the centre of lift. With the 90° model the moment due to pressures acting parallel to the chordline was included, although amounting only to about two per cent of the other induced moment and less than one per cent of that due to the jet reaction. Therefore, when computing the results for the 30° model only a few sample pressure distributions were plotted against y and, when found to contribute less than 0.5 per cent to the total pitching moment, this correction was ignored to save time.

The position of the centre of lift is shown plotted against C_J in Figures 27 and 28, together with the theoretical curve given by[2]

$$\frac{d_o}{c} = \frac{\pi}{48} \cdot \frac{C_J}{k^2} \left[1 - \frac{1}{\sqrt{2\pi}} \cdot \frac{C_J^{\frac{1}{2}}}{k} - \frac{\pi}{120} \cdot \frac{C_J}{k^2} ---\right] \qquad (6)$$

where d_o is measured aft the mid-chord point of the aerofoil at zero incidence. The value taken for k was that obtained experimentally as described in Section 4.2.

5.0 Evidence on the thrust hypothesis

5.1 Experiments using the 30° and 90° models

The "thrust" hypothesis states[2] that "in an idealized jet flap system, the gross thrust experienced by the structure will equal the total jet reaction whatever the angle of deflection of the jet" since, with potential flow in the mainstream, a thin non-mixing jet sheet must experience a pressure drag force of $J(1 - \cos\theta)$ as well as the lifting force of $J \sin\theta$ in order that the pressure difference across it becomes zero at infinity. Thus, with no net drag exerted on the combined system of the aerofoil plus its jet, the aerofoil must receive a thrust equal to $J(1 - \cos\theta)$ in addition to the direct component of the jet reaction, $J \cos\theta$. In practice the amount by which the horizontal force acting on the aerofoil exceeds $J \cos\theta$, and which is termed the pressure thrust, may be more or less than $J(1 - \cos\theta)$. The 'augmented' induced thrust is considered in Reference 3, as is the first of the two main factors tending to reduce the pressure thrust, namely, the process of mixing between the jet and the mainstream air. The second factor is the onset of a separation bubble at the leading edge.

It was with these problems in mind that the first build of the model aerofoil was fitted with a trailing edge having its jet slot at 90° to the chordline so that, with the aerofoil at zero incidence, any thrust measured could only be pressure thrust and its determination would not depend upon the accuracy of measurement of the difference of two large forces. With the thrust balance not completed, the forces of thrust and drag were initially computed from the pressure distribution. Later the temporary balance described in Section 3.2 was used as a check and the results obtained from both methods are plotted in Figure 29 in the form $\frac{C_{T_o}}{C_J}$ against C_J (where $C_{T_o} = \frac{\text{measured thrust}}{\frac{1}{2}\rho U_o^2 c}$) where it will be seen that the pressure thrust reached a maximum of only 37 per cent of the jet reaction. An exploration of the airflow with wool tufts and a smoke probe revealed that the mainstream air below the aerofoil was entering the jet stream perpendicularly over a distance of the order of an inch from the slot and, close to the jet exit, was even being turned to meet the jet before entrainment. If, for example, a proportion of the ultimate loss to the system is assumed to bear some relationship to the momentum flux of the entrained air, which enters the jet at right angles, then, taking a local velocity of 84 ft/s and a flow area 1 in. x 12 in., this quantity is of the order of 1.4 lb or nearly half the loss actually experienced. In addition there was a large region above the jet sheet where reversed flow and considerable turbulence were present and this might have been an even greater source of loss than the rapid entrainment of mainstream air. The exact mechanism of the thrust loss is not yet resolved but the qualitative assessment of the large volume of 'spoilt' flow indicates that, with the model used, the measurement of any pressure thrust is encouraging. As expected, the onset of leading edge separation at $C_J \doteqdot 0.4$ caused a sudden reduction in measured thrust.

At this point in the programme a simple model with an undeflected jet was made and used to investigate the effect termed "jet drag", but for convenience the results are collected together in Section 5.2, q.v.

The thrust balance was completed in time for the 30° model tests so that only a few sample pressure distributions were plotted against y, these being necessary mainly to check that their contribution to the pitching moment was, as assumed, insignificant (see Section 4.4). The thrust, measured by both methods, is plotted as $\frac{C_{T_0}}{C_J}$ against C_J in Figure 30, where it will be seen that only a small proportion (a maximum of about 15 per cent) of the possible pressure thrust was realised. However the measured thrust included all the drag on the model which was composed of the following items:-

(1) Pressure or form drag (other than jet drag) - coefficient C_{D_p} - included in both methods of thrust measurement.

(2) Skin friction - coefficient C_{D_f} - included only in the balance measurements.

(3) Induced drag (three-dimensional drag) due to the thick boundary layer on the side walls of the working section - included to some extent in pressure distribution and

(4) greater three-dimensional drag when there was clearance between the aerofoil and the tunnel walls - thrust balance only.

(5) Jet drag - affects pressure distribution and therefore included in both methods of measurement.

The following table summarises the result of some measurements and estimates concerning items (1) and (2) with "no-blow" conditions.

Table of measured and estimated drag coefficients for $C_J = 0$

C_{D_p} from pressure distribution	C_{D_f} Estimated	$C_{D_p} + C_{D_f}$	C_{D_o} from measured values $= C_{D_p} + C_{D_f} + ?$	Details of model
0.0103	0.0039 (a) 0.011 (b)	0.0140 0.0211	0.0236 (? = separation near T.E. + tip clearance effect)	90° model - no trip wires
not measured	-	-	0.0214 (? = separation rear T.F. + tip clearance effect)	30° model - no trip wires
0.0081	0.0049 (c)	0.013	0.0173 (? = tip clearance effect only)	30° model with trip wires

(a) Assuming laminar boundary layer to T.E.

(b) Assuming fully turbulent boundary layer from L.E.

(c) Assuming transition at the wires.

No measurement of the three-dimensional drag - items (3) and (4) above - could be made, but it was established that, by increasing the gap between the aerofoils and the tunnel walls with the thrust balance in use, the measured thrust decreased and, with "no blow", the drag increased. The "jet" drag, again, could not be measured for a model with a deflected jet but, for an aerofoil with a more orthodox trailing edge and an undeflected jet of cold air, it is shown in Section 5.2, that this amounts to some six per cent of the jet reaction at small values of C_J. It is to be expected that, for an elliptical section trailing edge, the jet drag would be increased[3].

For the 30° model there appeared to be an increase in the thrust measured by balance and a slight decrease in that computed from the pressure distributions when leading edge separation occurred, but since only the pressure thrust could be affected to a first order, and little of this was present, no noticeable loss could be expected and the apparent increase in thrust by balance may have been in reality a decrease in the relevant drag items - see (2) and (4) above - due to the reduced suction peak.

5.2 Jet drag experiments with an undeflected jet

The observation of the very large entrainment angle of the mainstream entering the jet sheet from below the 90° model, which suggested a "loss" in the mixing process, prompted the construction of a simple aerofoil having an undeflected jet slot situated in a comparatively thin trailing edge; the section is shown in Figure 31. At first, with only the temporary balance available, no "jet drag" could be detected but, with the sensitivity of the completed balance, a reduction in the measured thrust, greater than the "no blow" drag on the aerofoil, was found. With the simply constructed model the trailing edge was not absolutely rigid and, as the relationship between thrust and jet total pressure was not constant from day to day, each test was preceded by a thrust calibration, there being a continuous trend of decreasing thrust for a given jet total pressure amounting to just less than five per cent of the initial jet reaction from start to finish of the tests in spite of frequent, careful cleaning of the jet slot. No drag correction was made to the thrust calibration since it was thought that, with the model at zero incidence to the small flow of air induced through the wind tunnel by the jet (see Section 3.1), it would be negligible. Later, when the same model was required for some further tests, the trailing edge was modified to prevent the variation of the thrust calibration and the 'induced' drag correction was computed and found to be about 0.6 per cent of the measured thrust. The result of these tests and another made after the modification to the trailing edge is presented in the same form as that for the 90° and 30° models so that an overall comparison may be made (Figure 31) while in Figure 32 the effective drag coefficient, given by $C_J - C_{T_0}$, is plotted against the jet coefficient for values of the latter up to 0.10, over which range the increase in $C_{D_{eff}}$ with C_J is linear. When C_{D_0} was artificially increased by adding a strip of metal to the leading edge there was no significant difference in the rate of increase of $C_{D_{eff}}$ with C_J, and the same result was found when C_{D_0} was decreased by adding a "plasticine" fairing to improve the leading edge profile; both these effects are shown in Figure 32. The final reduction of all this data to a common basis for comparison was made by subtracting the "no blow" drag coefficient, C_{D_0}, from the effective drag coefficient, $C_{D_{eff}}$, to get the jet drag coefficient, C_{D_J}, and this is shown, plotted against C_J, in Figure 33. The average value of C_{D_J} appears to be about $0.06\ C_J$ until $C_J \doteqdot 0.10$ and thereafter it increases at the reduced rate of 0.017 per unit increment of C_J. When the model, fitted with nose fairing, was tested at 50 f.p.s. tunnel speed $\left(\frac{U_0 c}{\nu} = 2.13 \times 10^5\right)$ the higher rate of increase of C_{D_J} was maintained to a value of C_J of about 0.25 and then dropped so that $\frac{\partial C_{D_J}}{\partial C_J} = 0.0104$.

It should be noted that the jet drag measured in these experiments is for a cold air jet with a density roughly equal to that of the mainstream. In practice, the propulsive jet will be hot and it is to be expected theoretically, that in cruising flight, when $\frac{\rho U}{\rho_J U_J} \doteqdot 1.0$, there will be little or no jet drag[3]. (ρ and ρ_J are the densities of the undisturbed mainstream air and the jet fluid respectively; U_J = the jet velocity at mainstream pressure before mixing). This conclusion is supported by the results of some tests on the same model with hydrogen as the jet fluid - see Reference 3.

6.0 The lift at incidence

The total lift coefficient for the aerofoil at incidence was computed from the integration of the pressure distributions parallel and normal to the chordline and from a knowledge of the jet reaction and its line of action. For the 30° model the pressure forces acting parallel to the chordline were neglected apart from sample checks which showed that the error produced by this approximation was less than 0.40 per cent.

The experimental values of the total lift coefficient, C_L, are plotted against incidence in Figures 34 and 35, the broken lines being given by

$$C_L = C_{L_0} + \alpha \left[\frac{\partial C_L}{\partial \alpha}\right]_{\alpha=0} \quad .. \quad .. \quad .. \quad .. \quad .. \quad .. \quad (7)$$

where[2]

$$\left[\frac{\partial C_L}{\partial \alpha}\right]_{\alpha=0} = 2\pi \left\{ 1 + \frac{k}{\sqrt{2\pi}} \cdot C_J^{\frac{1}{2}} + \frac{\pi}{24} \cdot \frac{C_J}{k^2} + \frac{1}{24\pi k} \left(\frac{\pi C_J}{2}\right)^{\frac{3}{2}} ---- \right\} \quad (8)$$

and k is given the value found experimentally from the tests at zero incidence. It can be seen that the stalling point $\left(\frac{\partial C_L}{\partial \alpha} = 0\right)$ occurs at an incidence which decreases with increasing C_J, but that the decrease itself diminishes at the higher values of C_J and, for the 30° model, this stalling incidence tends to a limiting value of about +5° (Figure 35). As the 90° model was not tested at a jet coefficient higher than 0.50, at which value the stall occurred at +2° incidence, it is difficult to estimate the limiting value, but the trend indicates that this aerofoil might stall at small negative angles of incidence with large jet coefficients. The theoretical curves and experimental points for

$$\left[\frac{\partial C_L}{\partial \alpha}\right]_{\alpha=0}$$

are plotted in Figures 36 and 37, where it can be seen that there is good agreement.

7.0 Longitudinal stability

The pitching moment on the aerofoil at incidence was found by the method described in Section 4.4, again neglecting the pressure distribution plotted against thickness for the 30° model except for sample checks which, in general, showed the resultant error to be less than 0.40 per cent of the uncorrected moment. Where the latter itself was small and of the same order as the correction, the error in the value of d was only 0.12 per cent of the chord.

From a knowledge of the lift and pitching moment coefficients the distance of the aerodynamic centre aft the quarter-chord point was found and is plotted against C_J in Figures 27 and 28. Theoretical curves have been added, and are given by[2]

$$\frac{a}{c} = \frac{k}{4} \cdot \frac{C_J^{\frac{1}{2}}}{\sqrt{2\pi}}$$

again using values of k obtained experimentally in the tests at zero incidence.

Knowing the induced force normal to the chord line, as well as the direct thrust and its line of action, the centre of lift position was found and $^d/_c$ is plotted against α in Figures 38 and 39. From plots on a larger scale

$$\left[\frac{\partial\left(\frac{d}{c}\right)}{\partial\alpha}\right]_{\alpha=o} \quad \ldots \quad \ldots \quad \ldots \quad \ldots \quad (9)$$

was determined and the result is shown in Figures 40 and 41 together with the theoretical curves from Reference 2:-

$$\left[\frac{\partial\left(\frac{d}{c}\right)}{\partial\alpha}\right]_{\alpha=o} = -\frac{\sqrt{^\pi/_2}}{4k\sin\theta} \cdot \frac{1}{C_J^{\frac{1}{2}}} \left\{1 + 0.6\ C_J - 0.4\ C_J^{\frac{3}{2}} ----\right\} \qquad (10)$$

which is applicable only for small angles of incidence as various terms of the order $(\alpha/\theta)^2$ were omitted in the simplification of the expression.

Finally, Figures 42 and 43 show the variation of the pitching moment coefficient, C_m, with lift coefficient, it being noted that the straight lines drawn through the experimental points for both models at C_J values of 1.0 or less converged very near the point $C_L = -2\pi$, $C_m = -^\pi/2$, whilst even at the high values of $C_J = 3.0$ and 4.0 the tangent to the curve at $\alpha = 0°$ passed fairly close to the same point. These observations suggest the empirical relationship.

$$C_m = mC_L + 2\pi m - \frac{\pi}{2}$$

where m is the slope which by inspection appears to be

$$m = \frac{1}{4} - Z\ C_J^{\frac{1}{2}}$$

The value for Z seems to be reasonably constant, but different for the two model aerofoils, and it could be of the form,

$$Z = \frac{k\sin\theta}{\text{constant}}$$

The following table shows the experimental value of Z, and the numerical value of $\frac{k\sin\theta}{2\sqrt{2\pi}}$ is added for both models.

Comparison of experimental and empirical constants relating C_m to C_L

C_J	90° model		30° model	
	Z	$\frac{k\sin\theta}{2\sqrt{2\pi}}$	Z	$\frac{k\sin\theta}{2\sqrt{2\pi}}$
0.0095	0.129	0.0985		
0.024	0.142	0.138		
0.194	0.141	0.157		
0.20			0.0906	0.0902
0.466	0.142	0.154		
0.500			0.0948	0.0945
1.00			0.0963	0.0903

It seems very likely, from the experimental evidence, that for values of $C_J \leqslant 1.0$,

$$C_m = \frac{C_L}{4} - Z\, C_J^{\frac{1}{2}} \left[C_L + 2\pi\right] \quad \text{.. ..} \quad (11)$$

where Z is a constant for one aerofoil geometry and jet angle. It also seems probable that Z is proportional to $k\sin\theta$, and the two experiments so far completed suggest that,

$$Z = \frac{k\sin\theta}{2\sqrt{2\pi}} \quad \text{.. .. ..} \quad (12)$$

However, this last empiricism should be accepted only with considerable reserve.

8.0 Ground interference effects

The 30° model was used to investigate the effect of proximity to a "ground" made of 0.25 in. thick "Duralumin" plate stiffened at its edges with angle section members and extending the full length and breadth of the wind tunnel working section, its leading edge being two chords upstream from model leading edge. Care was taken in fitting the "ground" in any of its alternative positions to ensure that the surface was flat and parallel to the top and bottom walls of the tunnel, the undisturbed airflow through the working section being parallel to these in normal circumstances. Only tests at zero incidence were performed and no thrust balance measurements were made whilst, as before, the induced lift and pitching moment were obtained from the pressure forces normal to the chordline and the contribution of the thicknesswise distribution to the moment disregarded apart from the usual sample plots.

A range of C_J from 0.10 to 4.17 and of ground clearance from the chordline from 0.188c (1.5 in.) to 1.0c (8.0 in.) was covered by the tests, the results being illustrated in Figures 44 and 45, where C_{L_0} and $^{do}/_c$ respectively are plotted against ground clearance for the different values of C_J. It can be seen from these curves that, for values of C_J up to 2.0 and of ground clearance down to 0.30 x chord length, the effect is far from intolerable.

9.0 Conclusions

The experimental results from an elliptical aerofoil having a two dimensional jet deflected 90° from the chordline and from another with a jet deflection of 31.4° (nominally the 30° model) substantially support the theory proposed in Reference 2 for a simple jet flap aerofoil both with and without incidence. They also afford evidence which is favourable to the thrust hypothesis in that, in both instances, the measured thrusts were greater than the reaction component from the deflected jet (which, in the case of the 90° model, was zero). The losses in the system have been considered and, to some extent, investigated. For instance, the effect of Reynolds number was the subject of one experiment and transition wires added to the 30° model near the trailing edge were found to increase the lift at low values of the jet coefficient. Also measured was the "sink" (i.e. jet entrainment) drag acting on a model with an undeflected jet of cold air, although Reference 3 suggests that these results would be different for a practical jet flap scheme with a hot jet. A tentative, empirical relationship between pitching moment, lift and jet coefficients has been derived from the experimental results. Finally, the reduction of lift and the movement aft of the centre of lift position due to ground interference has been measured on the 30° model and found not to be prohibitive.

REFERENCES

No.	Author(s)	Title, etc.
1	Ph. Poisson-Quinton	Recherches theoretiques et experimentales sur le controle de la couche limite. Proc. Seventh Internat. Congress of Applied Mechanics. Vol. 2, Part II, 1948.
2*		
3	B. S. Stratford N. A. Dimmock	Mixing and the jet flap. N.G.T.E. Memorandum No. M.250, A.R.C. 18,422. October, 1955.
4	A. Fage	The airflow around a circular cylinder in the region where the boundary layer separates from the surface. R. & M. 1179. August, 1928.
5	A. Fage V. M. Falkner	Further experiments on the flow around a circular cylinder. R. & M. 1369. February, 1931.

*See addendum sheet

TABLE I

Test results for 90° model at zero incidence. (θ = 90.0°)

C_J	U_0 ft/s (corrected value)	$\frac{R_N}{10^5}$	C_{L_0}	$\frac{M}{M_0}$	C_{m_0}	d_0/c aft of mid-chord point %	C_{T_0} from pressure distn.	C_{T_0} from balance measurements
0.0095	100	4.25	0.241	25.37	-0.0082	3.40	-0.0066	
0.0143	100	4.25	0.348	24.03	-0.0035	2.44	-0.0069	
0.0190	100	4.25	0.451	23.75	-0.0061	1.35	-0.0059	
0.0239	101	4.29	0.532	22.27	-0.0087	1.63	-0.0029	
0.0286	101	4.29	0.629	22.07	-0.0036	0.57	-0.0037	
0.0387	101	4.29	0.808	20.87	-0.0112	1.39	+0.0060	
0.0484	101	4.29	0.891	18.45	-0.0160	1.80	0.0073	
0.0719	101	4.29	1.106	15.40	-0.0194	1.75	0.0154	
0.0955	102	4.34	1.257	13.23	-0.0344	2.74	0.0168	
0.1468	102	4.34	1.555	10.73	-0.0480	3.09	0.0404	
0.1946	103	4.37	1.751	9.02	-0.0644	3.68	0.0530	
0.266	105	4.46	2.126	7.46	-0.0953	4.48	0.0958	
0.378	106	4.50	2.456	6.52	-0.0988	4.02	0.1391	
0.431	107	4.55	2.610	6.10	-0.0987	3.77	0.0962	
0.451	107	4.55	2.691	5.98	-0.1079	4.01	0.0886	
0.0467	108	4.59	2.778	5.96	-0.1062	3.82	0.1007	
0							-0.0103	
0								-0.0236
0.008								-0.0177
0.0105								-0.0167
0.0150								-0.0147
0.0216								-0.0118
0.0334								-0.0039
0.0459								0
0.118								+0.0236
0.232								0.0568
0.337								0.0920
0.436								0.1157
0.521								0.1058

TABLE II

Test results for 90° model at incidence. (θ = 90.0°)

C_J	α degrees	C_L	C_m	d/c aft of mid-chord point %	C_J	α degrees	C_L	C_m	d/c aft of mid-chord point %
	-5.0	-0.182	-0.1288	-70.8		-5.0	0.063	-0.1287	206.5
	-2.5	+0.048	-0.0697	+147.5		-2.5	0.287	-0.0691	24.1
	-1.25	0.143	-0.0446	+31.2		-1.25	0.411	-0.0426	10.3
0.0095	0	0.241	-0.0082	+3.40	0.024	0	0.532	-0.0087	1.6
	+1.25	0.539	+0.0220	-4.09		+1.25	0.749	+0.0319	-4.3
	2.5	0.582	0.0547	-9.41		2.5	0.843	0.0570	-6.8
	5.0	0.797	0.1122	-14.15		5.0	1.094	0.1111	-10.2
	-10.0	0.572	-0.2765	48.1		+10.0	1.558	-0.3675	23.4
	-5.0	1.091	-0.1656	15.2		-5.0	2.190	-0.2588	11.7
	-2.5	1.522	-0.1224	8.0		-2.5	2.558	-0.2106	8.2
0.194	0	1.751	-0.0644	3.7	0.467	0	2.778	-0.1062	3.8
	+2.5	2.078	+0.0119	-0.6		+2.5	2.839	-0.0762	2.7
	5.0	2.148	+0.0803	-3.7		5.0	2.578	-0.1656	6.4
	10.0	1.756	-0.0786	+4.4		10.0	2.085	-0.2241	10.6
	15.0	1.613	-0.0852	+5.1		15.0	2.237	-0.2336	10.1

TABLE III

Test results for 30° model at zero incidence. $(\theta = 31.4^{\circ})$

C_J	U_0 ft/s	$\frac{R_N}{10^5}$	C_{L_0}	μ/μ_0	C_{m_0}	d_0/C aft of mid-chord point %	$C_{T_\bullet}$ from press. distn.	C_{T_0} from balance measurements	
0								-0.0214	These tests with no trip wires fitted.
0.02	100	4.25	0.080	7.73	-0.0014	1.74		-0.0082	
0.03	100	4.25	0.143	8.95	-0.0015	1.05		-0.0006	
0.04	100	4.25	0.189	9.07	-0.0036	1.90		+0.0088	
0.05	100	4.25	0.248	9.52	-0.0073	2.94		0.0138	
0.07	100	4.25	0.396	10.87	-0.0073	1.84		0.0365	
0.10	100	4.25	0.614	11.78	-0.0203	3.31		0.0616	
0.15	100	4.25	0.848	10.86	-0.0353	4.16		0.1032	
0								-0.0173	Trip wires fitted on both upper and lower surfaces 7/16 in. from T.E. Trip wire diameter = 0.0345 in.
0.02	100	4.25	0.196	18.77	-0.0025	1.27		-0.0013	
0.03	100	4.25	0.255	16.32	-0.0073	2.85		+0.0057	
0.04	100	4.25	0.349	15.73	-0.0055	1.58		0.0125	
0.05	100	4.25	0.398	15.28	-0.0114	2.86		0.0176	
0.07	100	4.25	0.528	14.48	-0.0125	2.37		0.0253	
0.10	100	4.25	0.662	12.70	-0.0220	3.32		0.0579	
0.15	100	4.25	0.838	10.72	-0.0306	3.66		0.0990	
0.20	100	4.25	1.029	9.83	-0.0401	3.90		0.1398	
0.30	100	4.25	1.256	8.04	-0.0648	5.16	0.2525	0.2210	
0.40	100	4.25	1.498	7.18	-0.0827	5.52		0.3082	
0.50	100	4.25	1.749	6.71	-0.1155	6.60	0.433	0.4015	
0.75	81.6	3.46	2.144	5.49	-0.1676	7.81	0.656	0.625	
1.00	50	2.12	2.441	4.69	-0.2256	9.23	0.871	0.807	
1.50	50	2.12	3.144	4.02	-0.3536	11.24		1.230	
2.00	50	2.12	3.747	3.59	-0.4172	11.14	1.720	1.689	
2.50	44.8	1.90	4.322	3.32	-0.510	11.79		2 120	
3.00	40.7	1.73	4.944	3.16	-0.646	13.08	2.581	2.580	
3.50	38.0	1.62	5.468	3.00	-0.728	15.29		2.970	
4.00	35.4	1.50	5.982	2.87	-0.867	14.51		3.416	
4.17	34.7	1.47	6.072	2.80	-0.965	15.90	3.596	3.50	

TABLE IV

Test results for 30° model at incidence. (θ = 31.4°)

C_J	U_0 ft/s	$\frac{R_N}{10^5}$	α degrees	C_L	C_m	d/c aft of mid-chord point %
			-10	-0.075	-0.2747	-602
			- 5	+0.428	-0.1590	+35.9
			- 2	0.803	-0.0898	11.10
0.20	100	4.25	0	1.029	-0.0401	3.90
			2	1.261	+0.0211	-1.68
			4	1.466	0.0652	-4.43
			6	1.634	0.6995	-6.12
			8	1.542	0.1410	-9.20
			10	1.498	0.1056	-7.08
			-10	0.335	-0.3575	86.0
			- 5	1.013	-0.2330	22.1
			- 2	1.417	-0.1567	10.9
0.50	100	4.25	0	1.750	-0.1155	6.60
			2	1.924	-0.0625	3.27
			4	2.159	-0.0045	0.21
			6	2.408	+0.0118	-0.50
			10	2.360	-0.0762	+3.28
			-10	0.842	-0.4805	47.90
			- 5	1.620	-0.3434	20.19
			- 2	2.126	-0.2714	12.60
1.00	50	2.12	0	2.441	-0.2256	9.23
			1	2.618	-0.1950	7.49
			2	2.652	-0.1342	5.12
			5	2.926	-0.0796	2.79
			-10	1.714	-0.7425	36.35
			- 5	2.735	-0.6126	21.18
			- 2	3.361	-0.5297	15.47
2.00	50	2.12	0	3.747	-0.4172	11.14
			2	4.078	-0.3487	8.68
			4	4.546	-0.3540	7.99
			8	4.379	-0.4817	11.53
			-10	2.565	-0.9856	32.30
			- 5	3.739	-0.8305	20.90
			- 2	4.391	-0.7080	15.80
3.00	40.7	1.73	0	4.944	-0.6460	13.08
			2	5.625	-0.5788	11.90
			4	6.317	-0.6264	10.18
			6	6.491	-0.7161	11.43
			8	5.727	-0.7570	13.96
			-10	3.262	-1.2676	32.36
			- 5	4.503	-1.1085	22.96
			- 2	5.402	-0.943	17.06
4.00	35.4	1.50	0	5.982	-0.867	14.51
			2	6.869	-0.850	12.57
			4	7.639	-0.897	12.06
			6	7.820	-0.967	12.89
			8	8.199	-1.008	12.92

APPENDIX I

Notation

Fluid properties

Symbol	Quantity	Where defined or first used
U	Local mainstream velocity relative to the aerofoil.	Section 5.2
U_o	Undisturbed mainstream velocity relative to the aerofoil.	Conventional
U_J	Jet fluid velocity relative to the aerofoil.	Section 5.2
ρ	Mainstream density (assuming incompressible flow)	Conventional
ρ_J	Jet fluid density.	Section 5.2
ν	Kinematic viscosity.	Conventional
p	Local static pressure.	Conventional and Figures 17-20 and 23 to 26
p_o	Static pressure of undisturbed mainstream	Conventional and Figures 17 to 20 and 23 to 26
p_t	Total head pressure.	Conventional and Figure 8

Geometrical

Symbol	Quantity	Where defined or first used
α	Angle of incidence.	Conventional and Figure 46
η	Analogous flap angle.	Section 4.2
θ	Jet deflection angle	Section 4.2 and Figure 46
ψ	An analogous flap size parameter.	Section 4.2
a	Distance of aerodynamic centre aft the quarter chord point.	Section 7.0
c	Aerofoil chord.	Conventional
d	Distance of centre of total lift aft the mid-chord point.	Section 7.0 and Figure 46
d_o	As for "d", but with the aerofoil at zero incidence	Section 4.4
x and y	Co-ordinates along and perpendicular to the aerofoil chord-line.	Figure 46.

Forces and moments

Symbol	Quantity	Where defined or first used
J	Total jet reaction or momentum flux at the nozzle.	Section 3.2 and Figure 46
L	Total lift.	Conventional and Figure 46.
L_o	Total lift at zero incidence.	Section 4.2 and Figure 46
L_p	Pressure lift.	Section 4.2 and Figure 46
M	Total pitching moment.	Figure 46 (only used in coefficient form - Section 7.0)
T_o	Measured thrust at zero incidence.	Figure 46 (only used in coefficient form - Section 5.1)

Force and moment coefficients

Symbol	Quantity	Where defined or first used
C_{D_o}	"No blow" drag coefficient i.e. when $C_J = 0$.	Section 5.1
C_{D_f}	Skin friction drag coefficient.	Conventional and Section 5.1
C_{D_p}	Pressure drag coefficient.	Section 5.1
$C_{D_{eff}}$	Effective drag coefficient = $C_J - C_{T_o}$.	Section 5.2 and Figure 32
C_{D_J}	Jet drag coefficient.	Section 5.2
C_J	Jet coefficient.	Section 4.2
C_L	Total lift coefficient.	Section 6.0
C_{L_o}	Total lift coefficient, aerofoil at zero incidence.	Section 4.2
C_{L_p}	Pressure lift coefficient.	Section 4.2
C_p	Pressure coefficient.	Section 4.3 and Figure 8 and Figures 17 to 20 and 23 to 26
C_m	Pitching moment coefficient.	Section 7.0
C_{T_o}	Thrust coefficient, aerofoil at zero incidence.	Section 5.1

Miscellaneous

Symbol	Quantity	Where defined or first used
k	The practical jet shape factor.	Section 4.2
$\mathcal{M}_o$	Magnification factor, aerofoil at zero incidence.	Section 4.2
m	Slope of C_m versus C_L curve.	Section 7.0
Z	An empirical constant.	Section 7.0
π	3.14159---	Conventional

FIG. 1

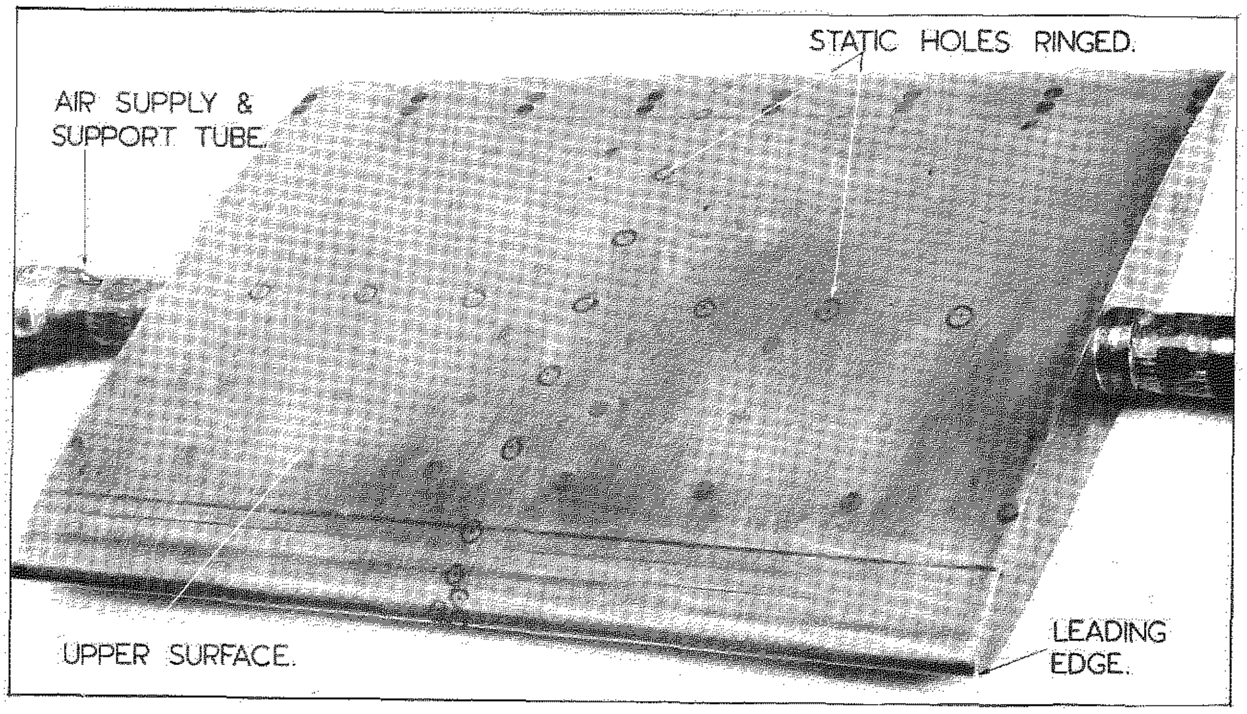

(a) THE MODEL-EXTERNAL.

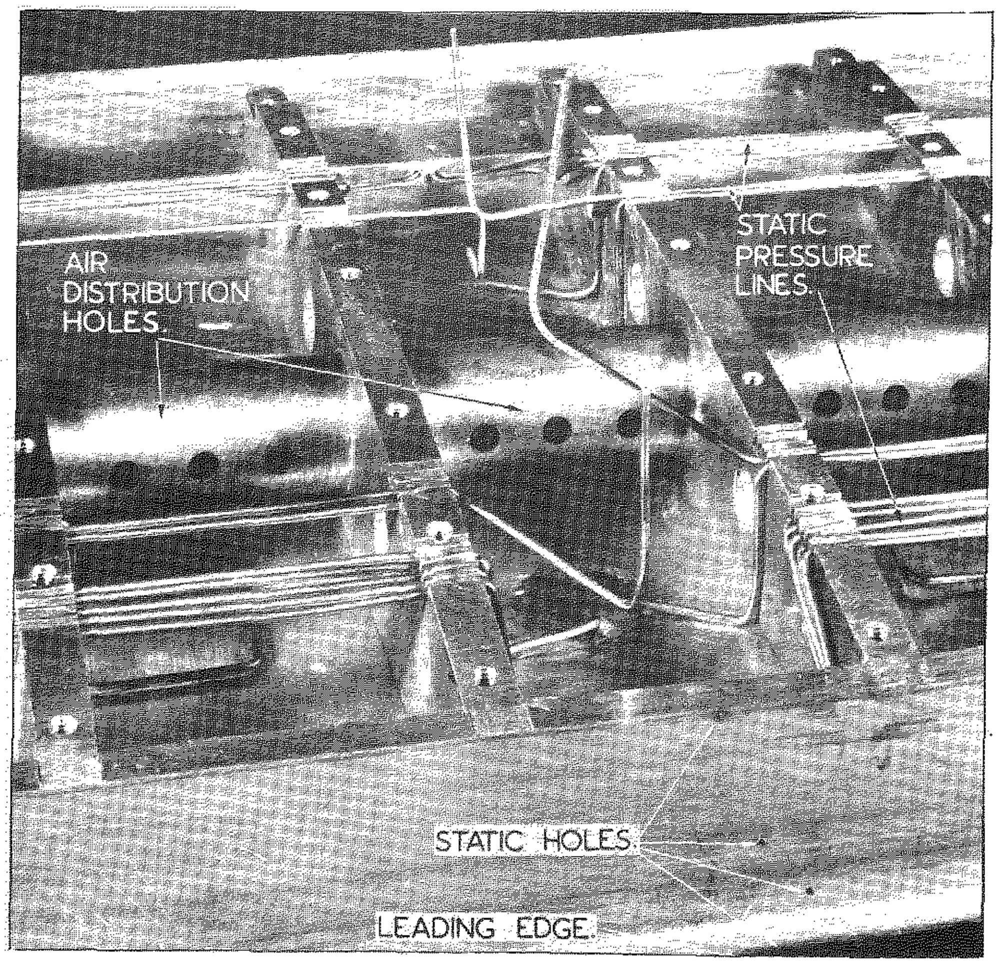

(b) VIEW SHOWING THE CONSTRUCTION OF THE MODEL.

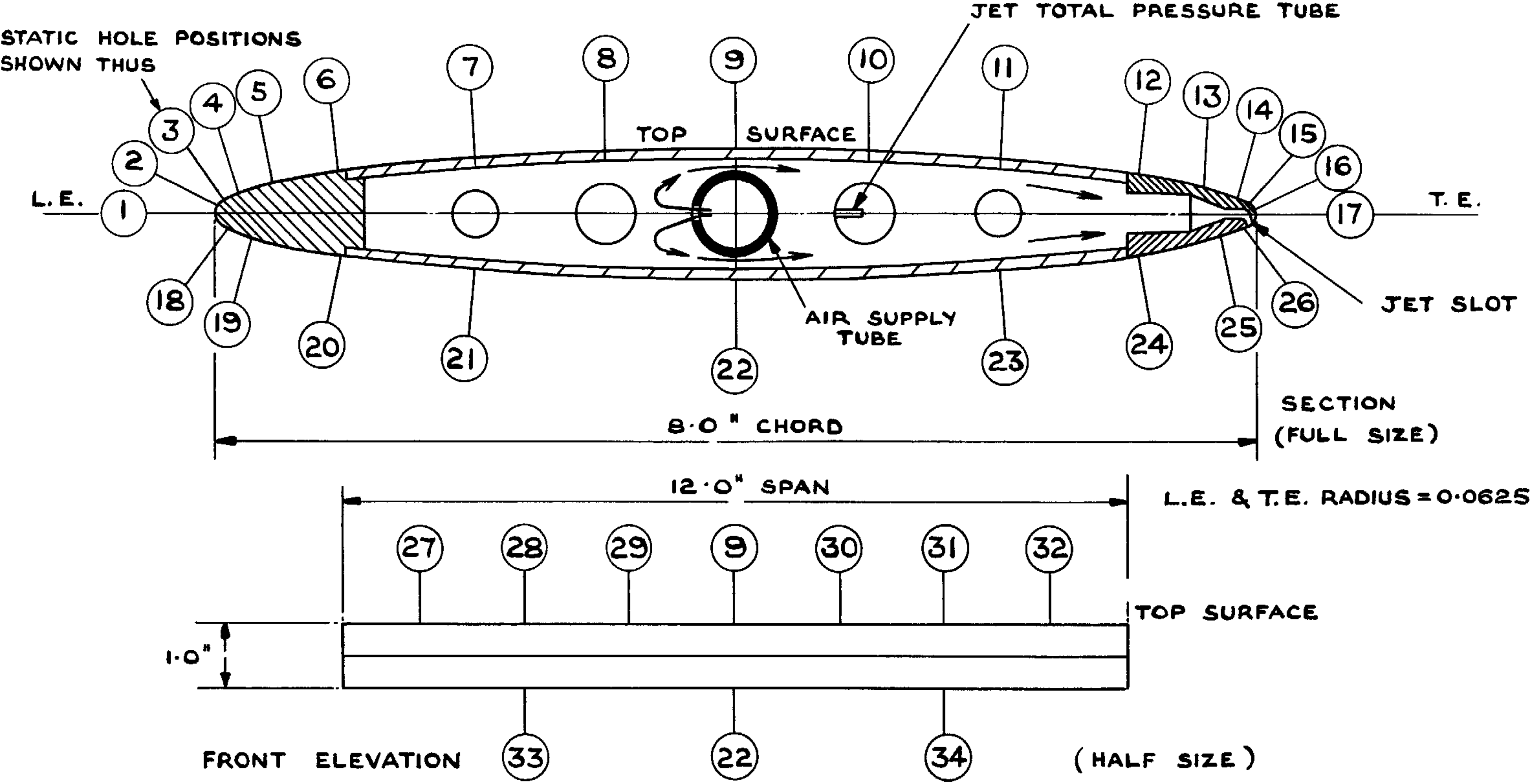

SECTION OF MODEL—12·5% THICK ELLIPSE.

FIG. 2

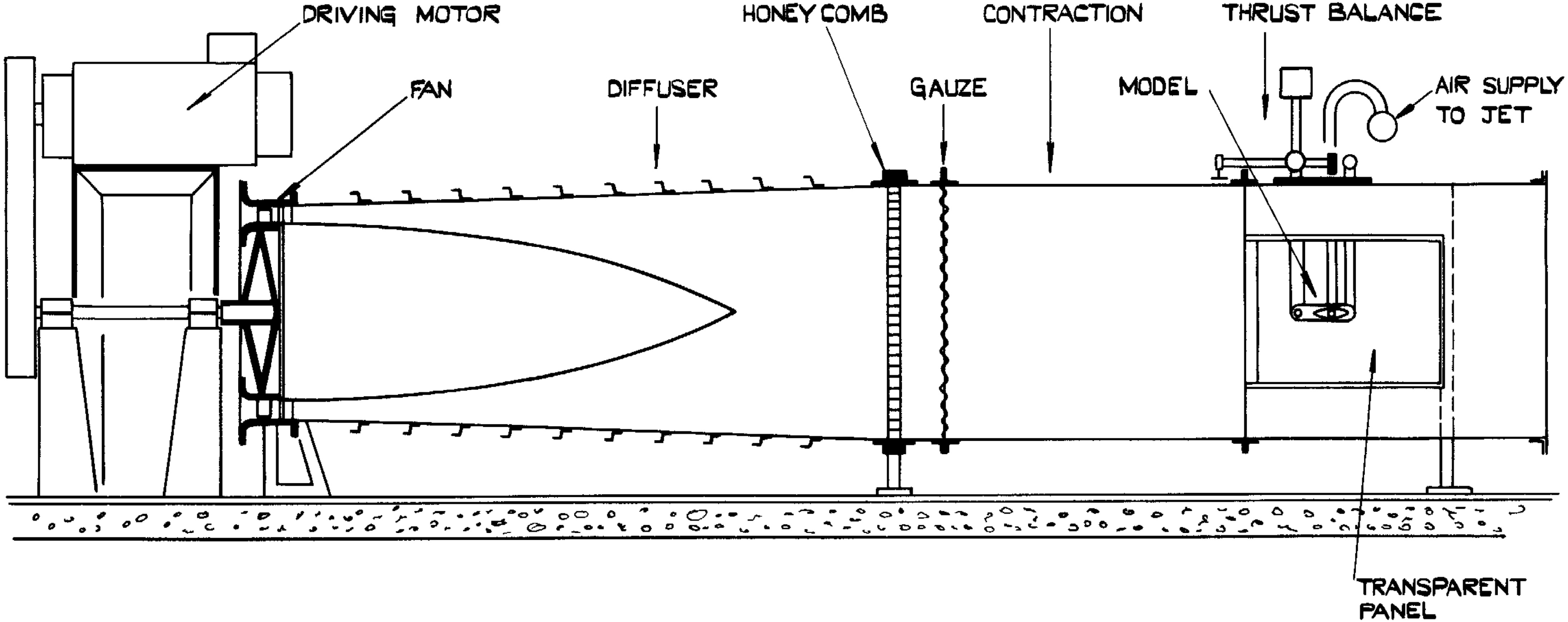

ARRANGEMENT OF WIND-TUNNEL.

FIG. 3

FIG. 4

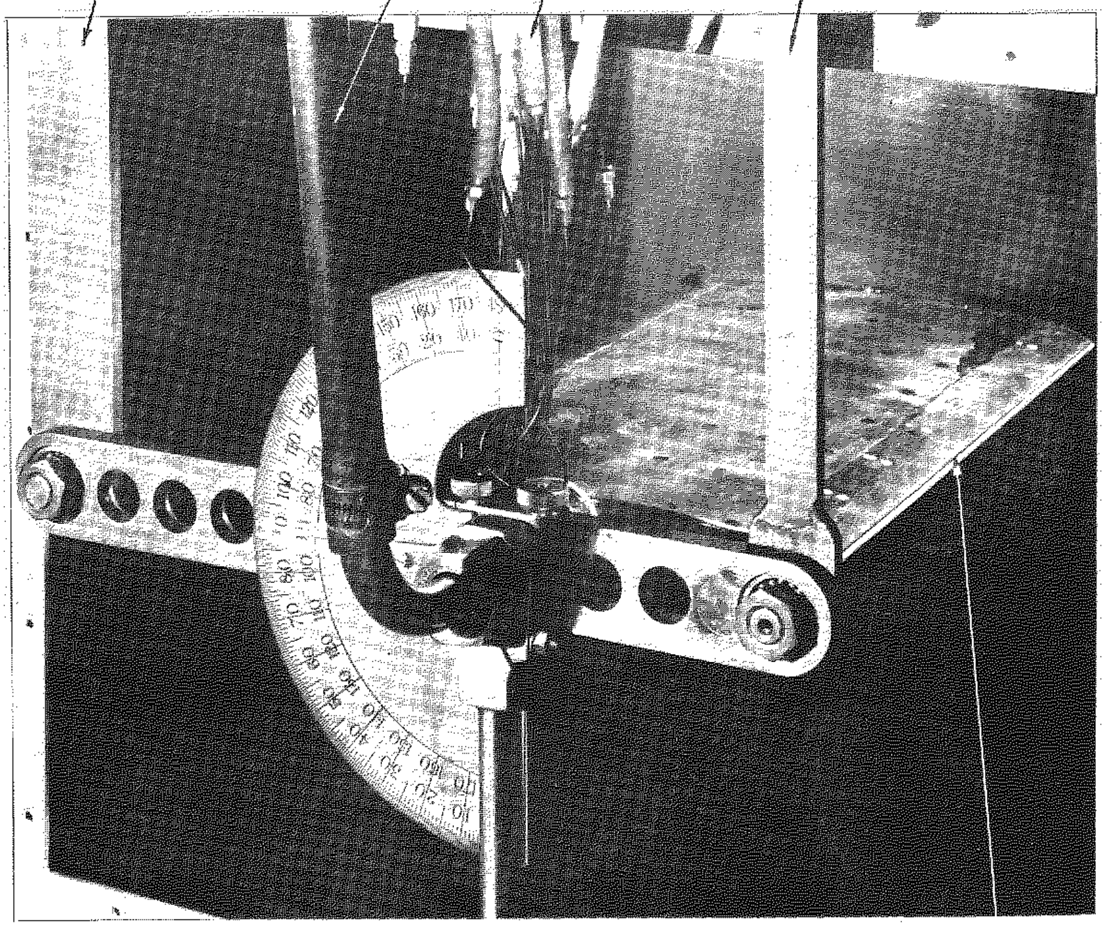

WORKING SECTION WITH MODEL.

FIG. 5

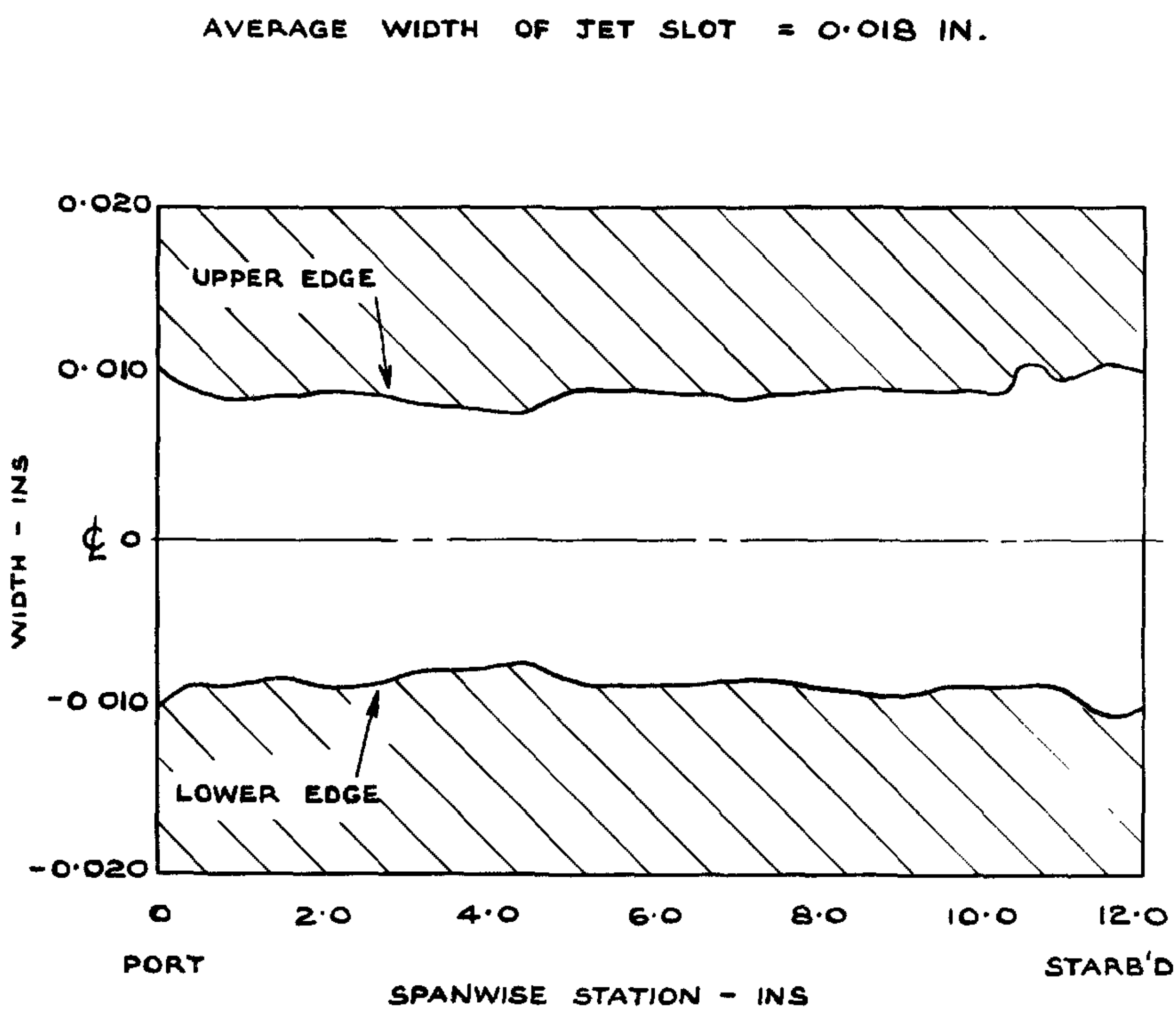

VARIATION OF JET SLOT — 30° MODEL.

FIG. 6

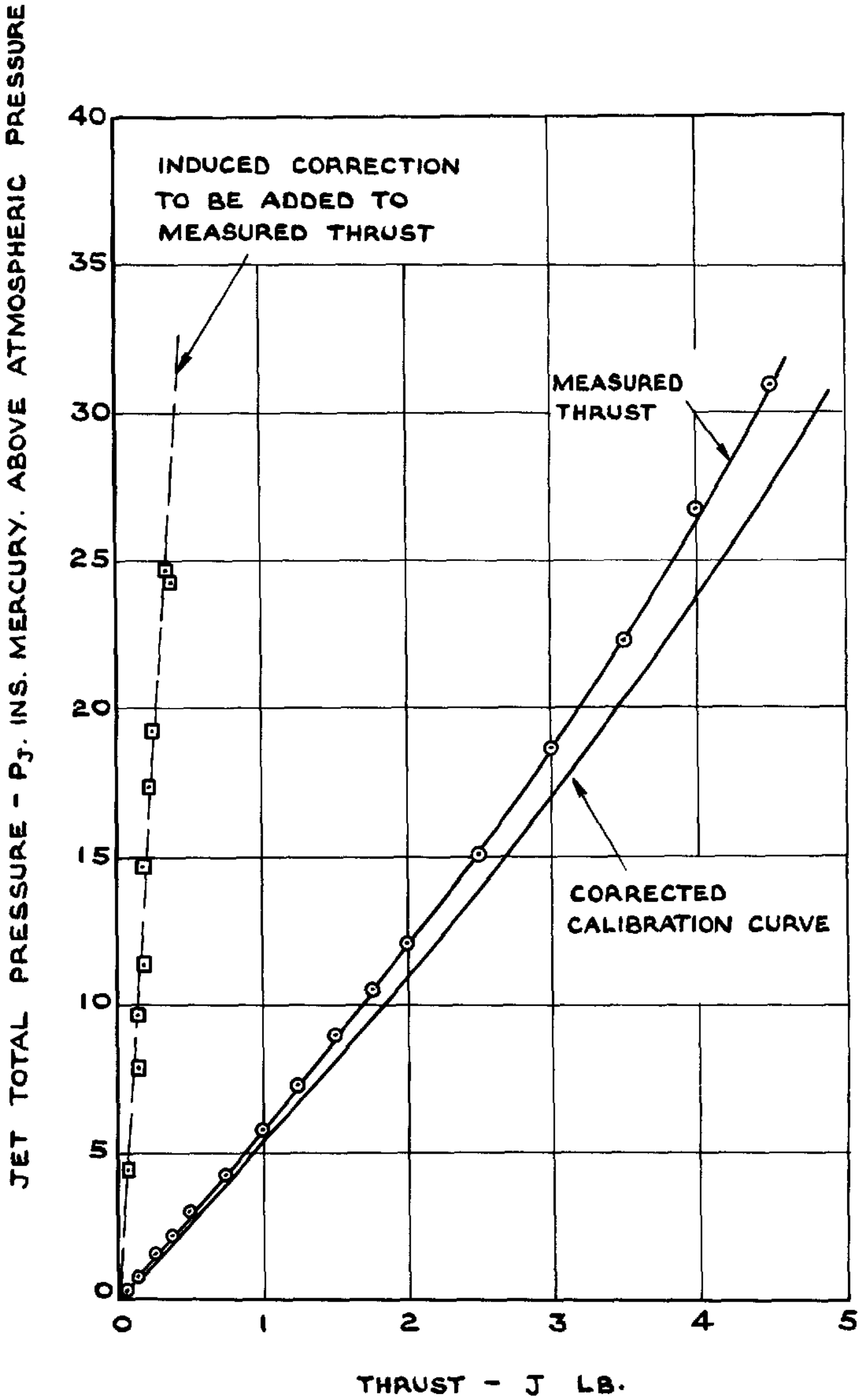

THRUST CALIBRATION CURVES - 90° MODEL.

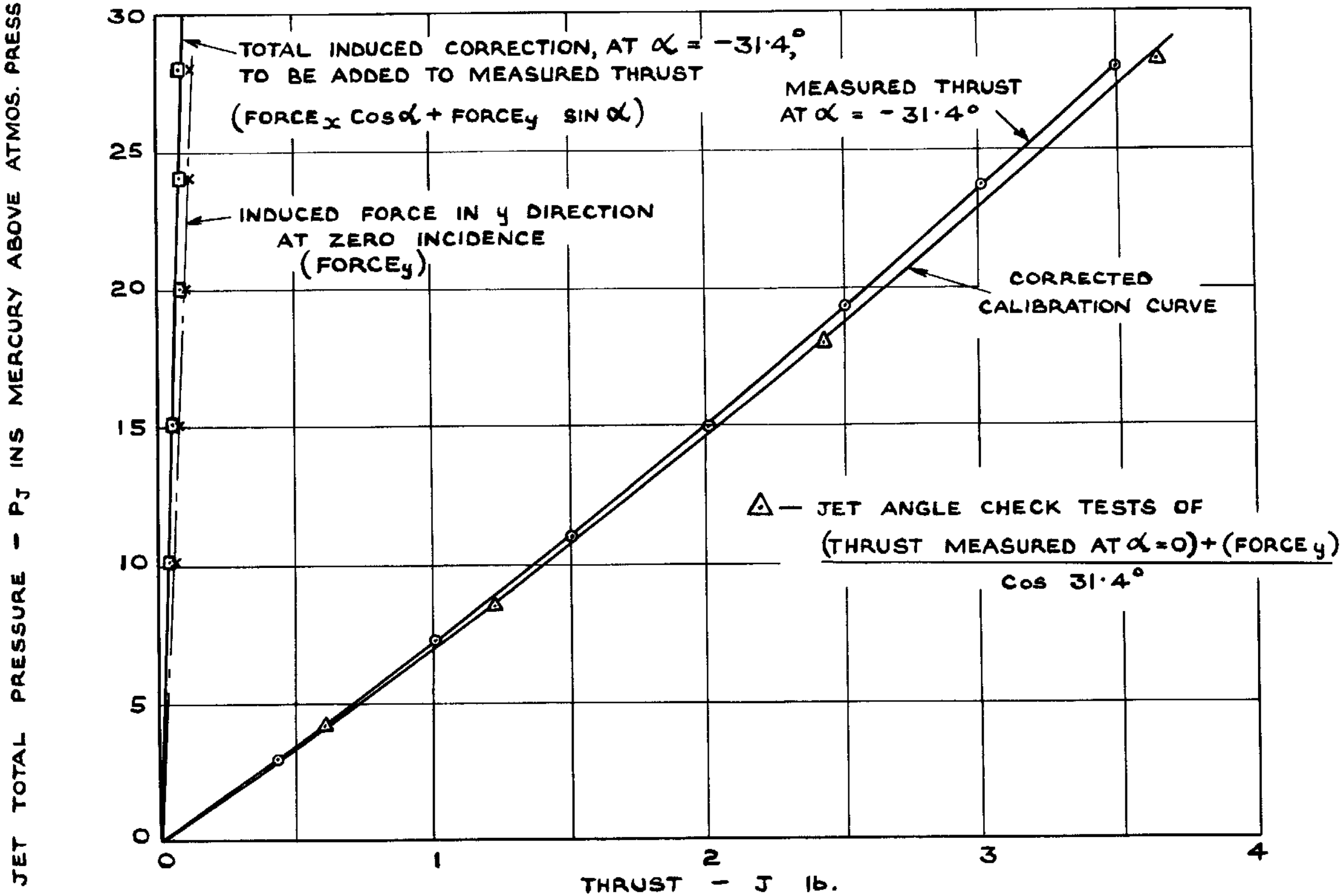

FIG. 7

THRUST CALIBRATION CURVES FOR MODEL WITH JET DEFLECTED 31·4°

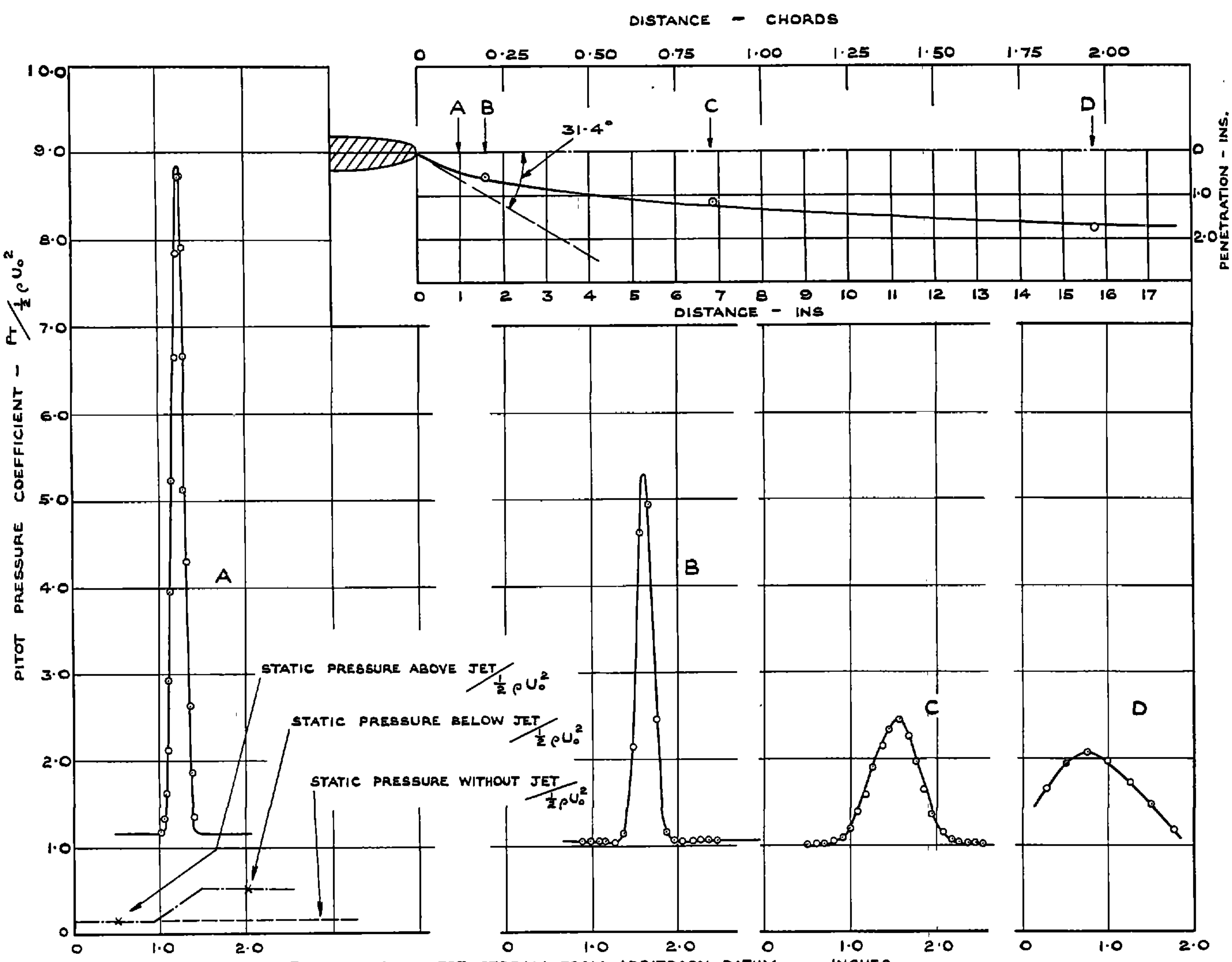

JET PATH & PROFILE AT C_J=0·30–30° MODEL.

FIG. 9

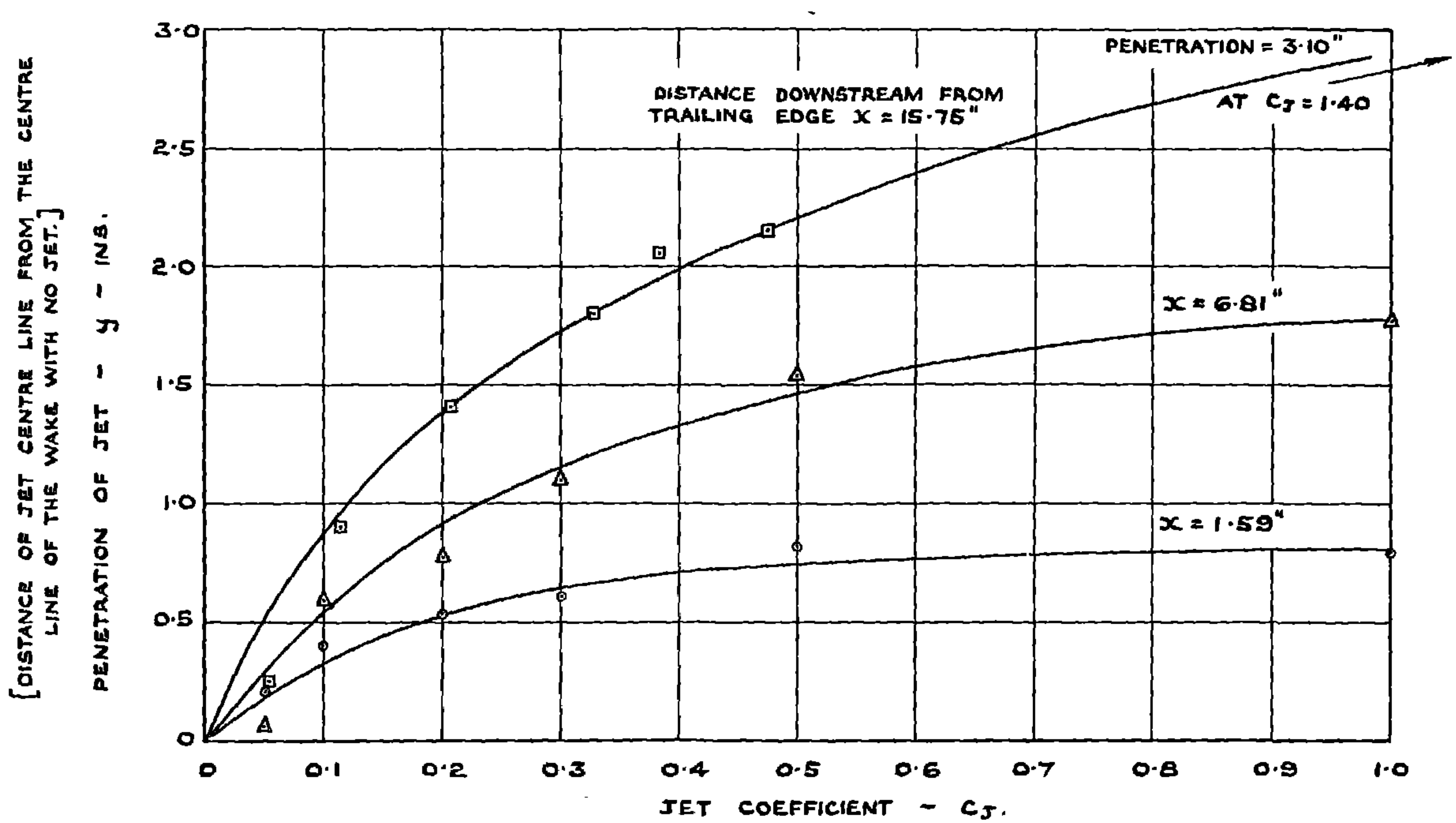

THE PENETRATION OF THE JET STREAM INTO THE MAINSTREAM. — 30° MODEL.

FIG. 10

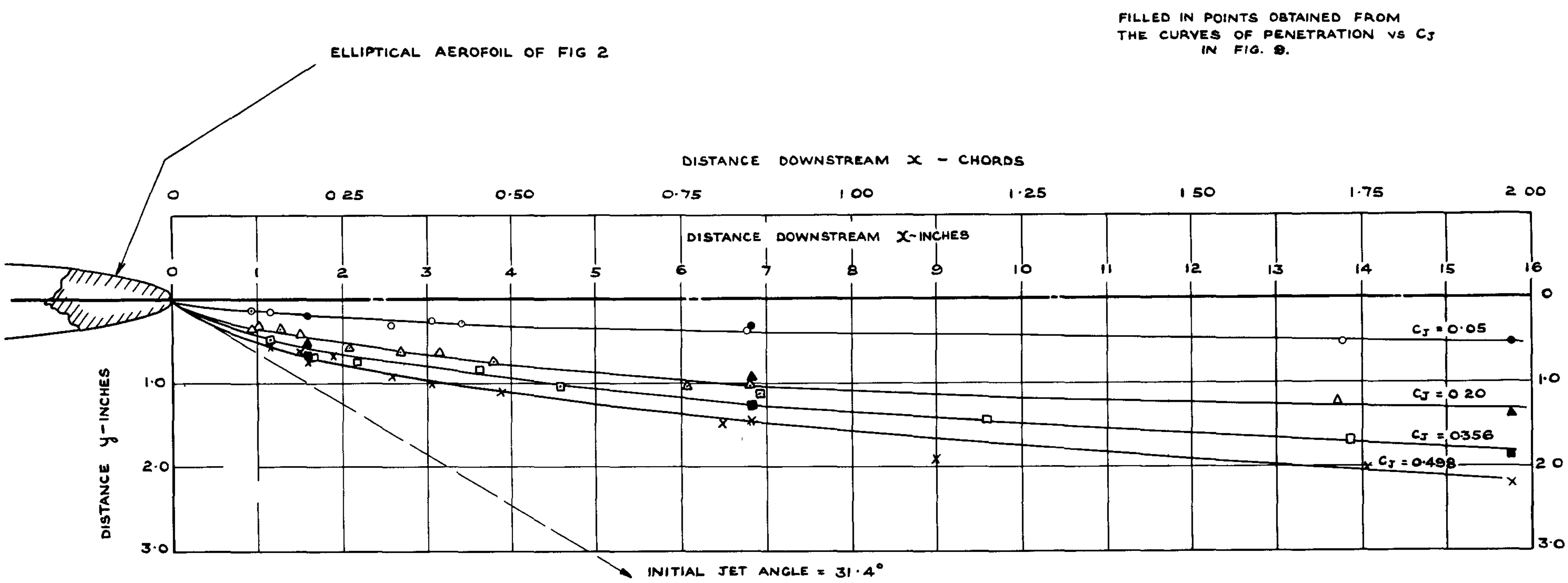

THE JET PATH — 30° MODEL.

FIG. 11

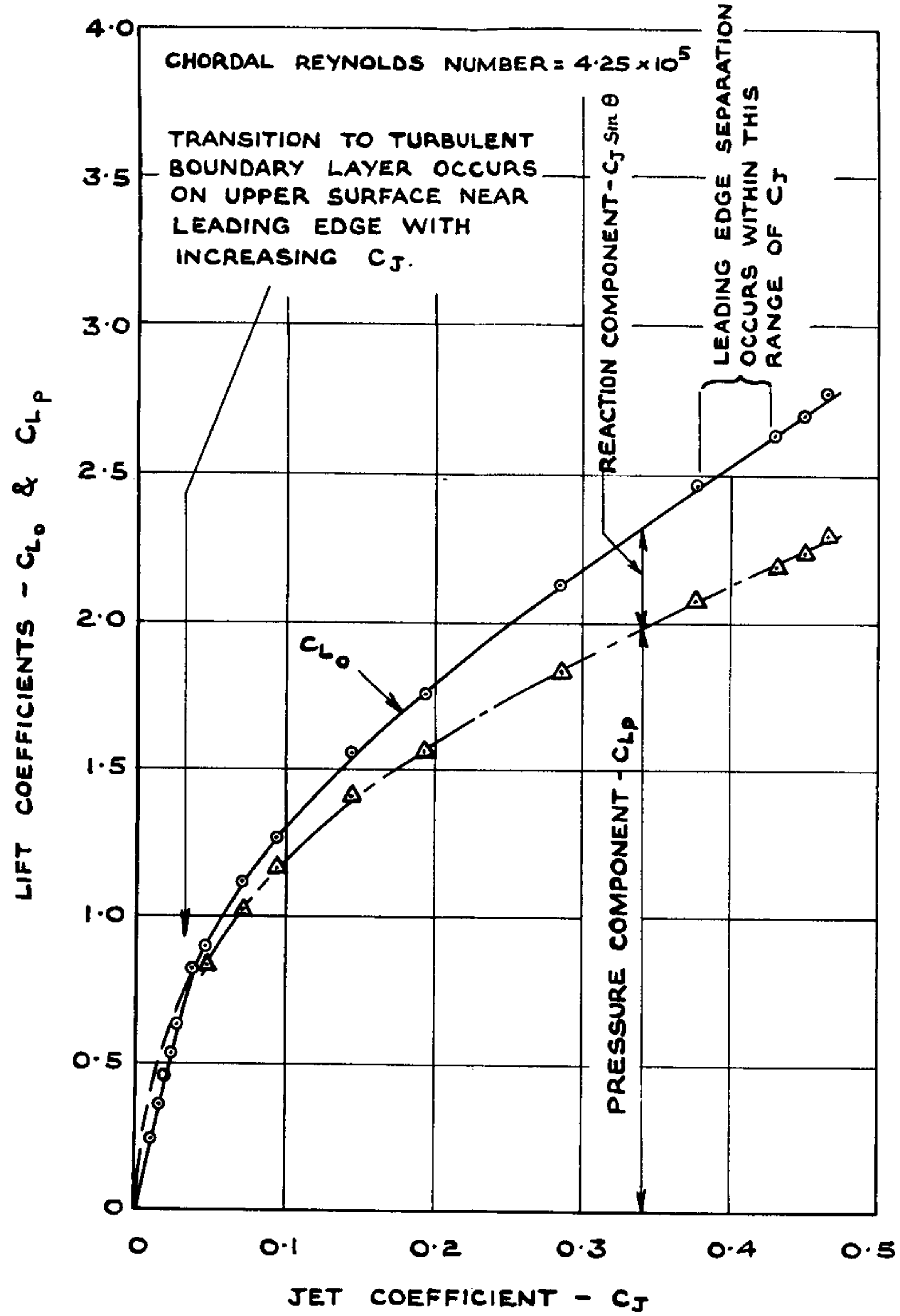

LIFT AT ZERO INCIDENCE - 90° MODEL.

FIG. 12

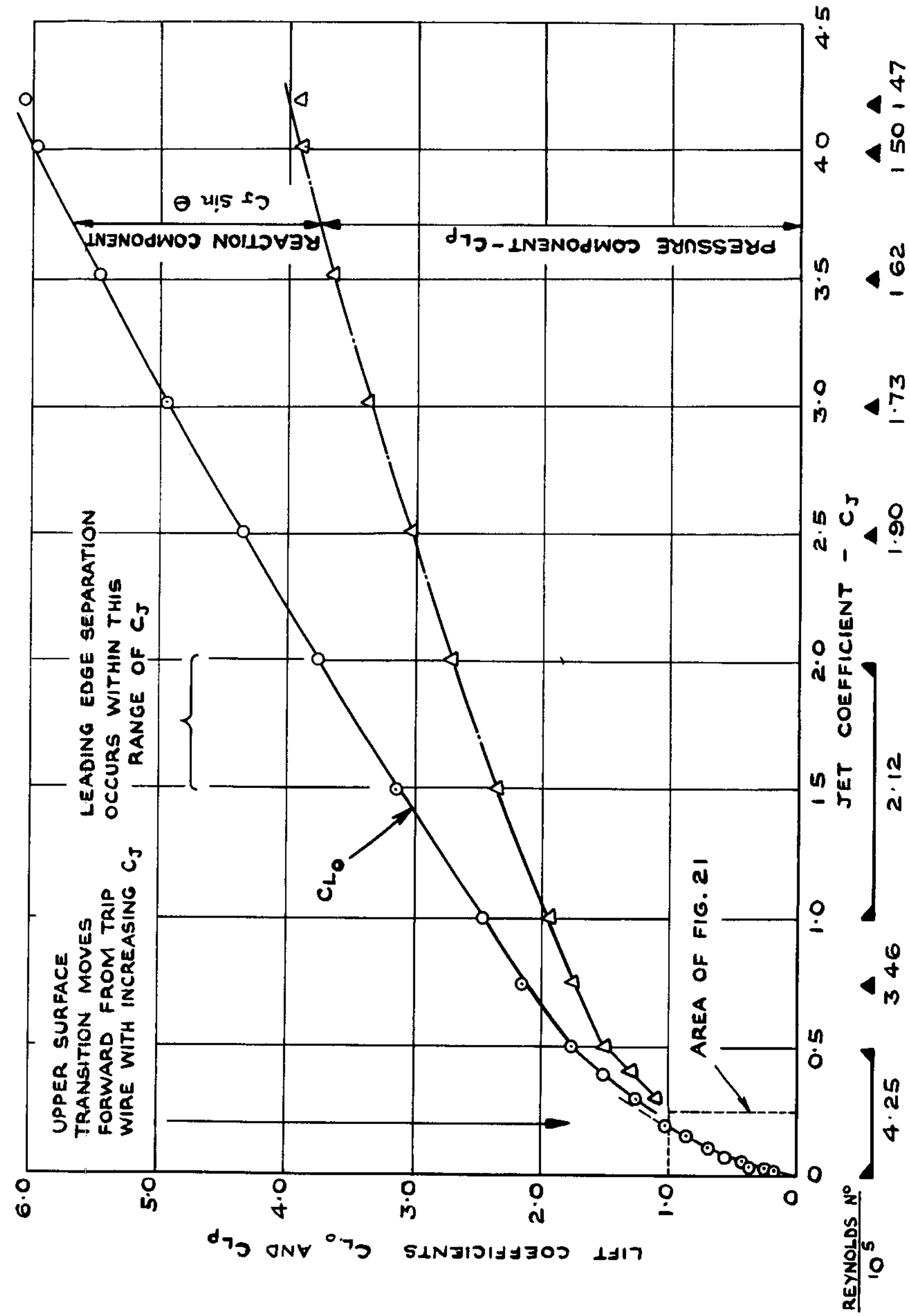

LIFT AT ZERO INCIDENCE-30° MODEL.

FIG. 13

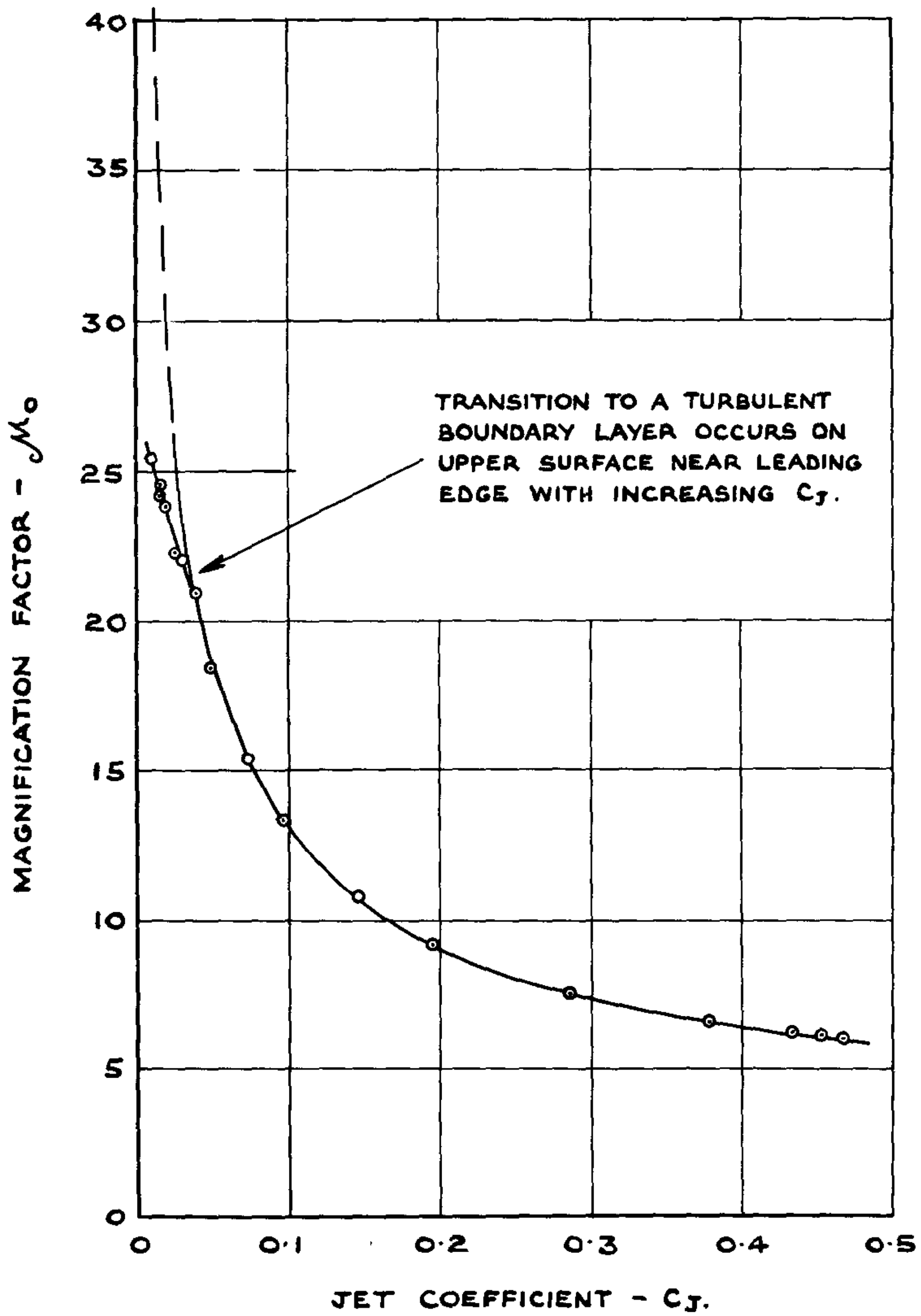

VARIATION OF $\mathcal{M}_0$ WITH C_J - 90° MODEL.

FIG. 14

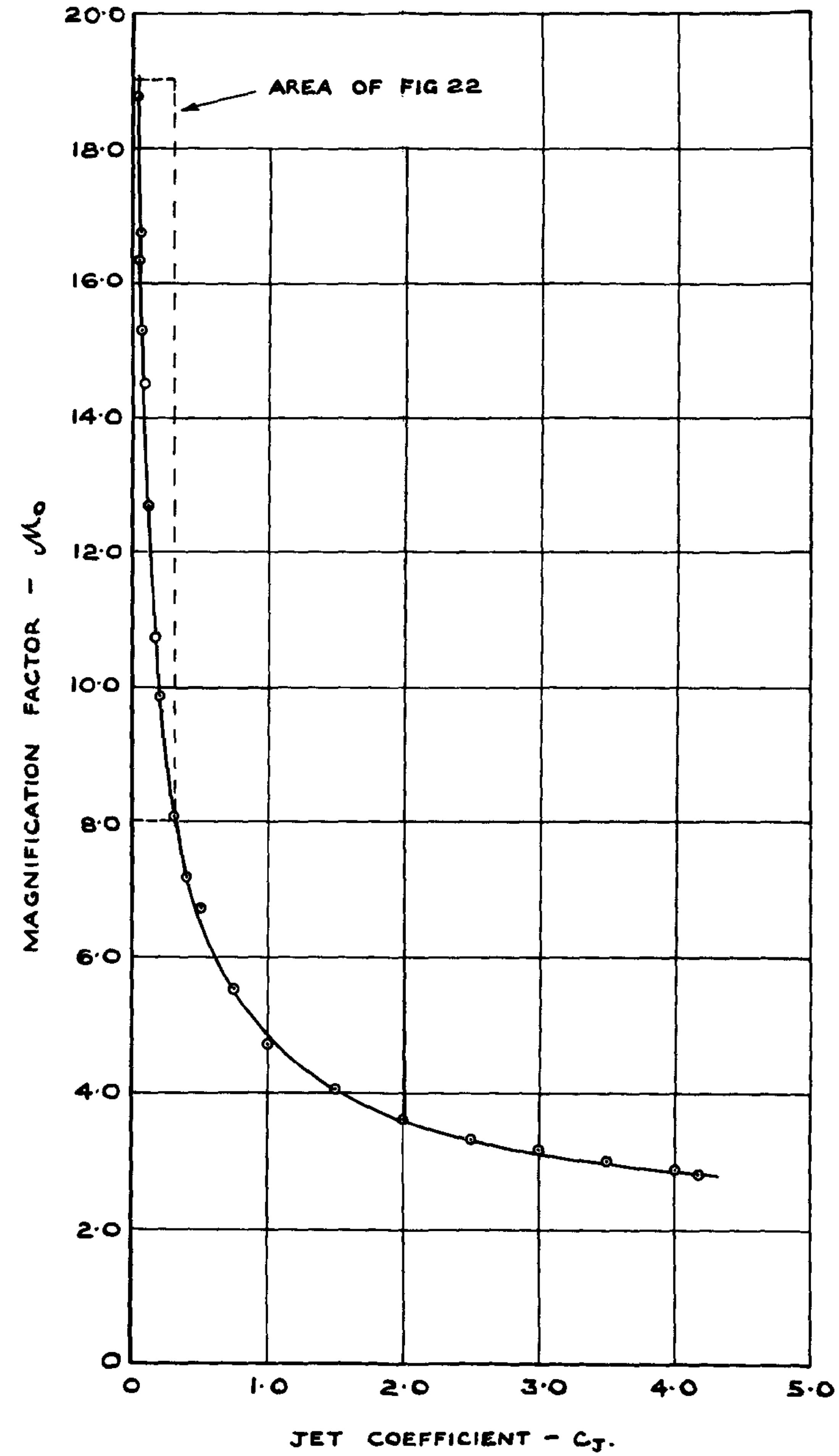

VARIATION OF $\mathcal{M}_0$ WITH C_J - 30° MODEL.

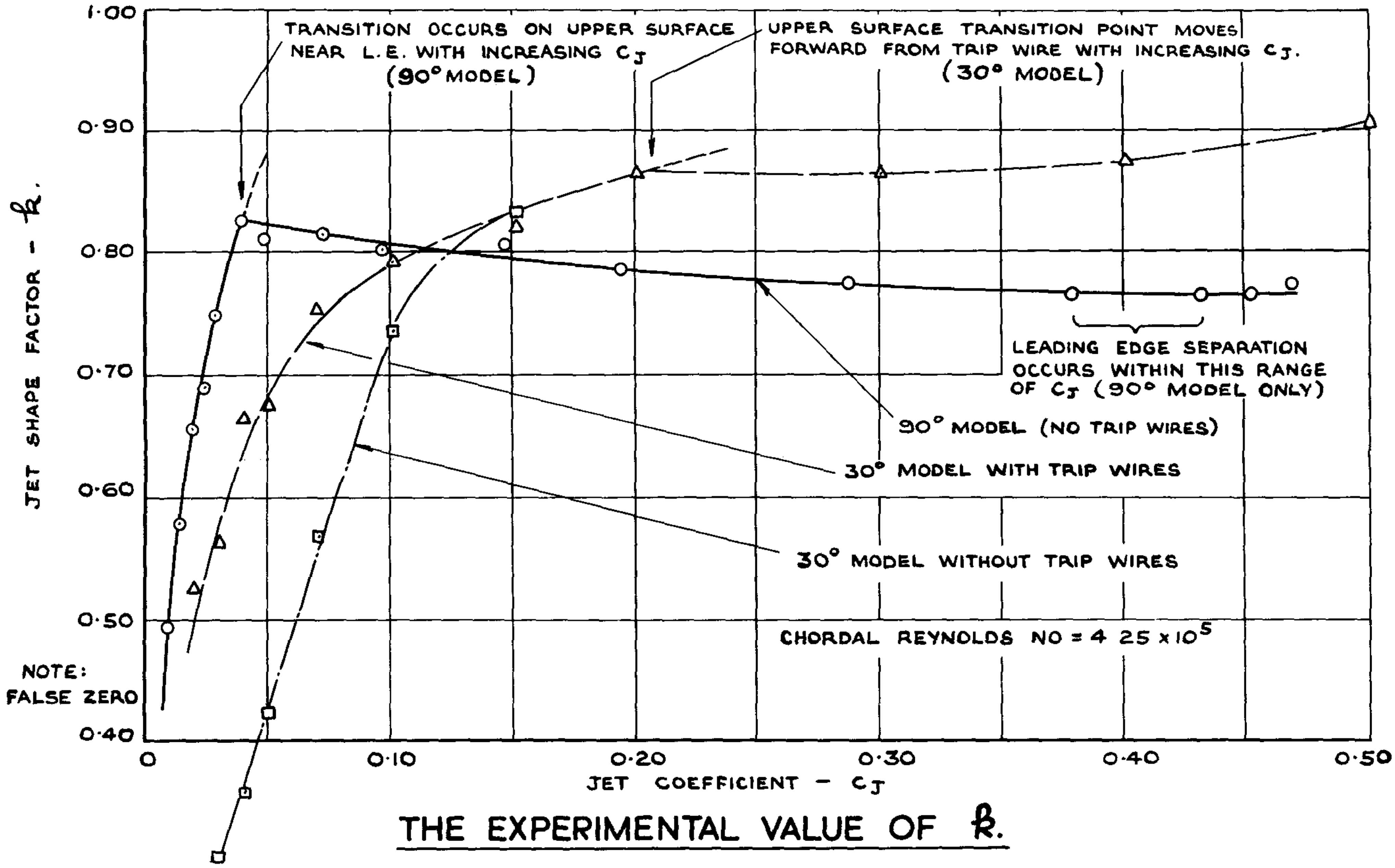

THE EXPERIMENTAL VALUE OF k.

FIG. 15

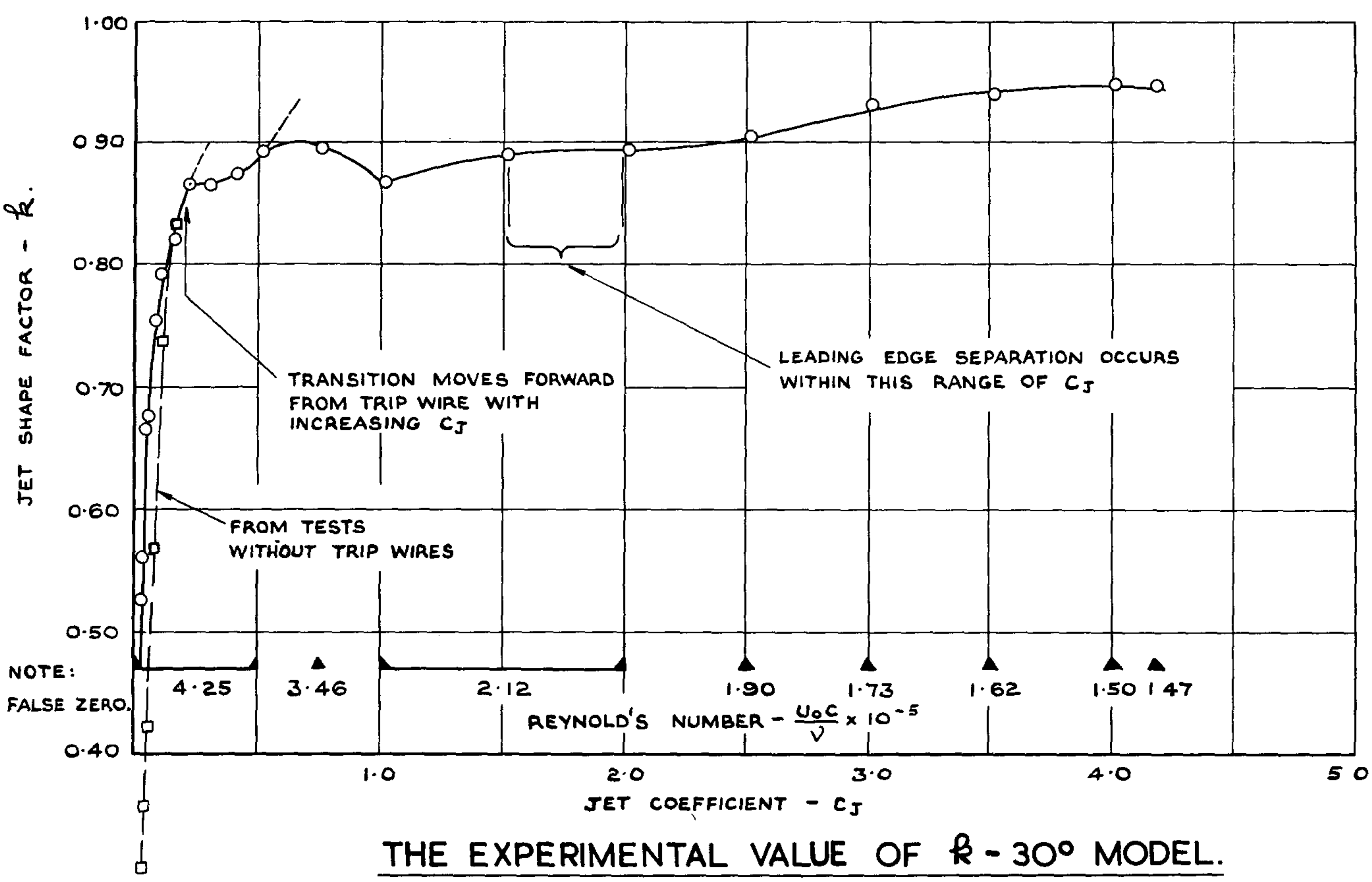

THE EXPERIMENTAL VALUE OF k - 30° MODEL.

FIG. 16

FIG. 17

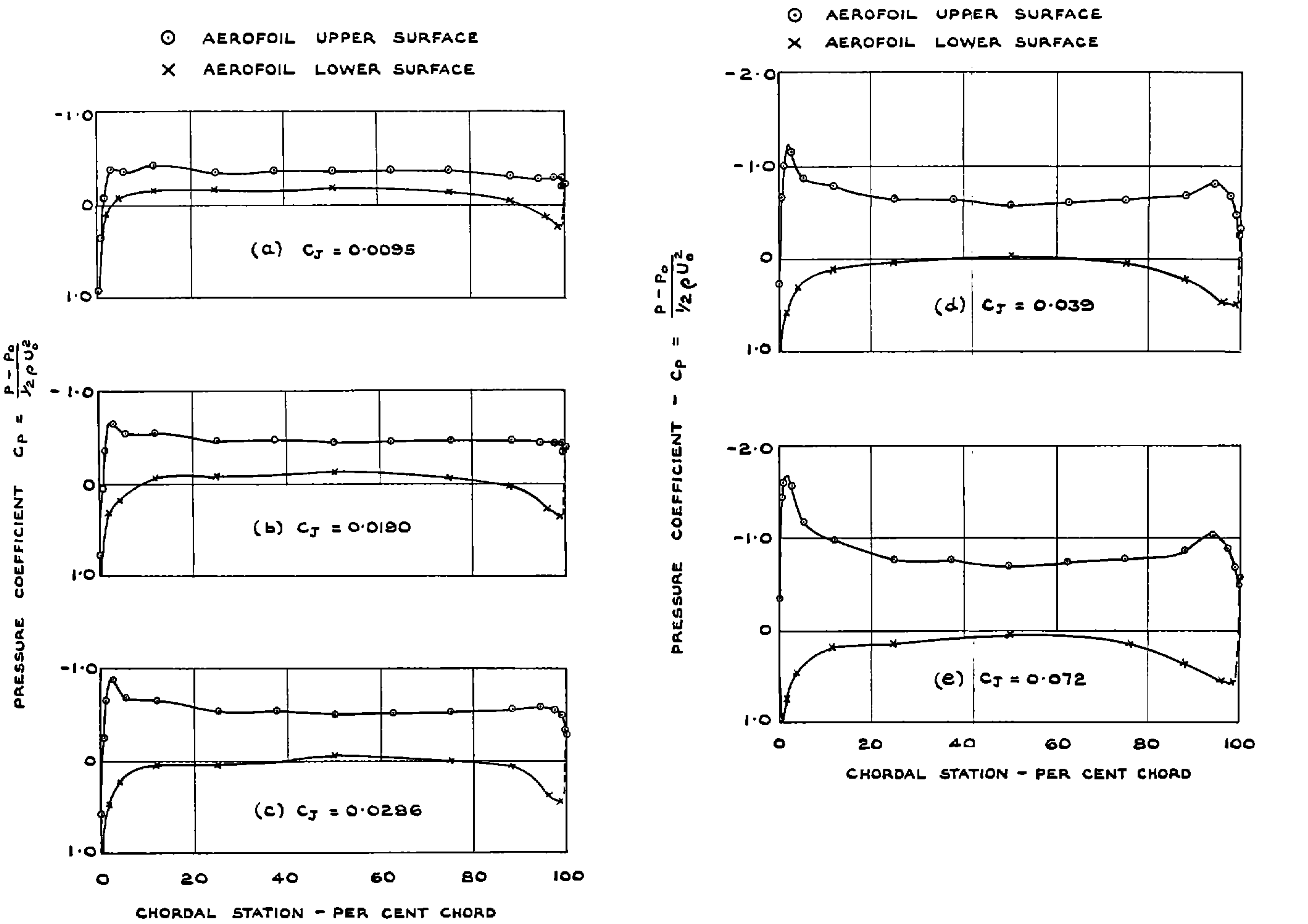

PRESSURE DISTRIBUTION AT ZERO INCIDENCE — 90° MODEL.

FIG. 18

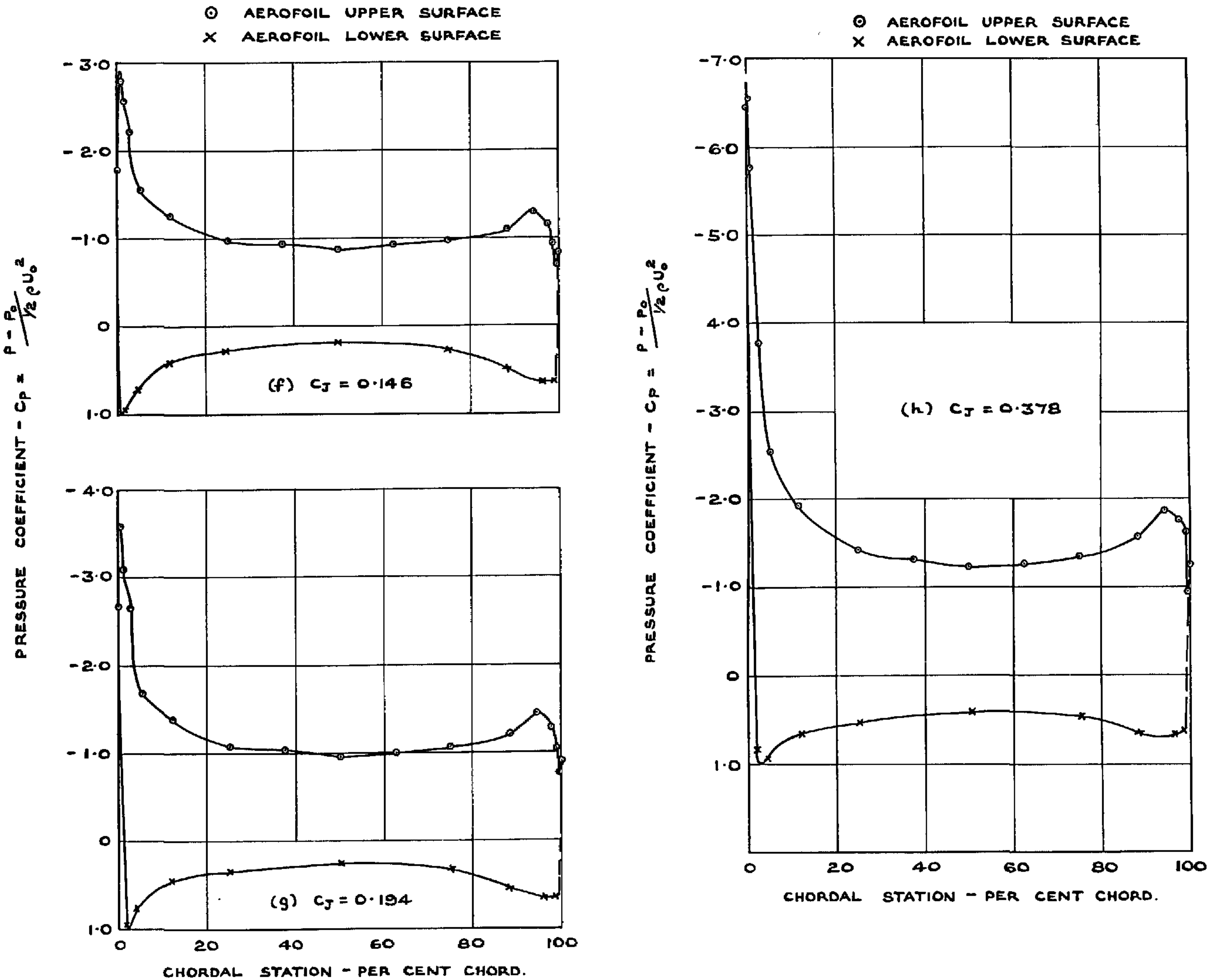

PRESSURE DISTRIBUTION AT ZERO INCIDENCE - 90° MODEL.

FIG. 19

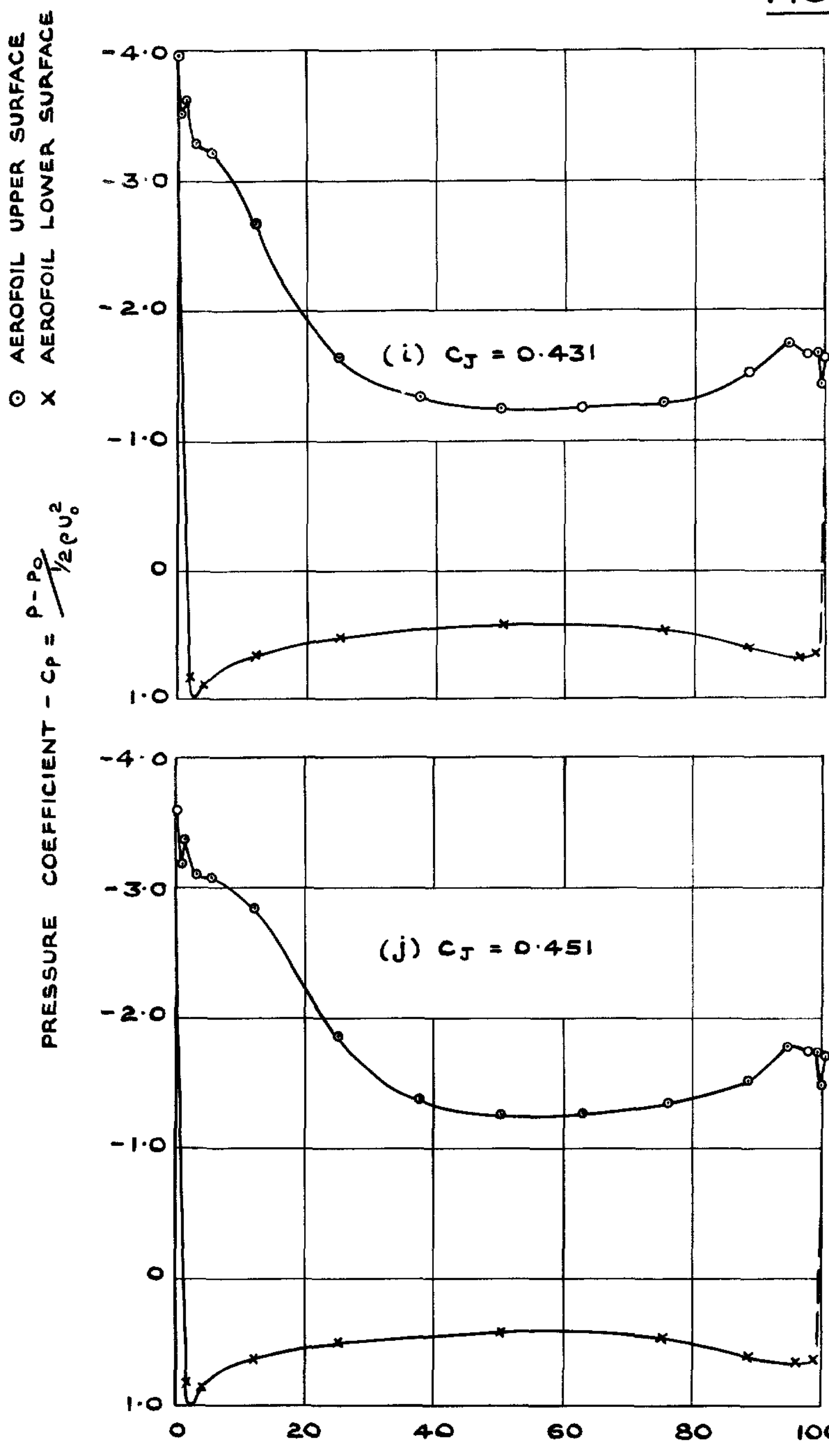

PRESSURE DISTRIBUTION AT ZERO INCIDENCE
90° MODEL.

FIG. 20

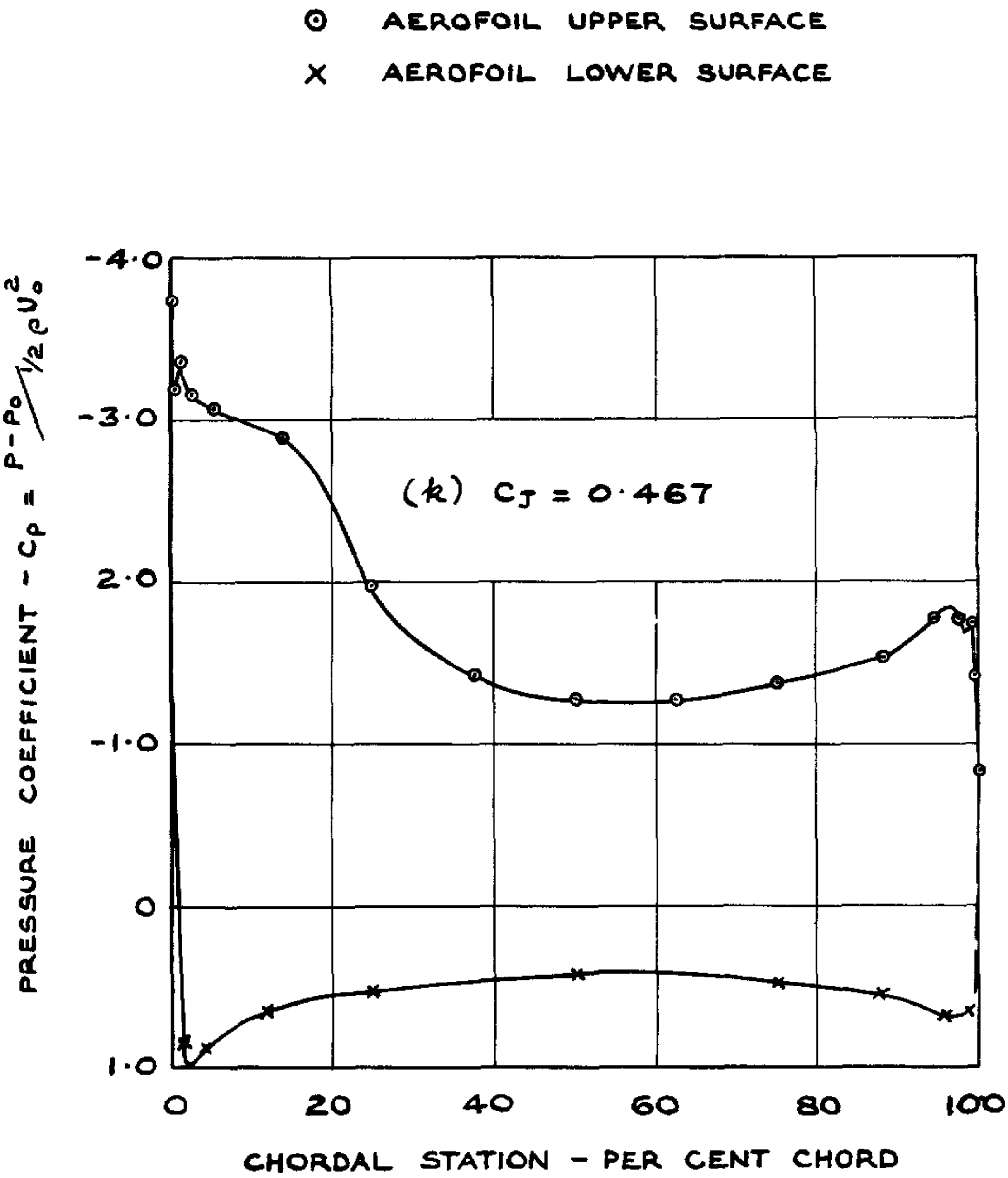

PRESSURE DISTRIBUTION AT ZERO INCIDENCE
90° MODEL.

FIG. 21

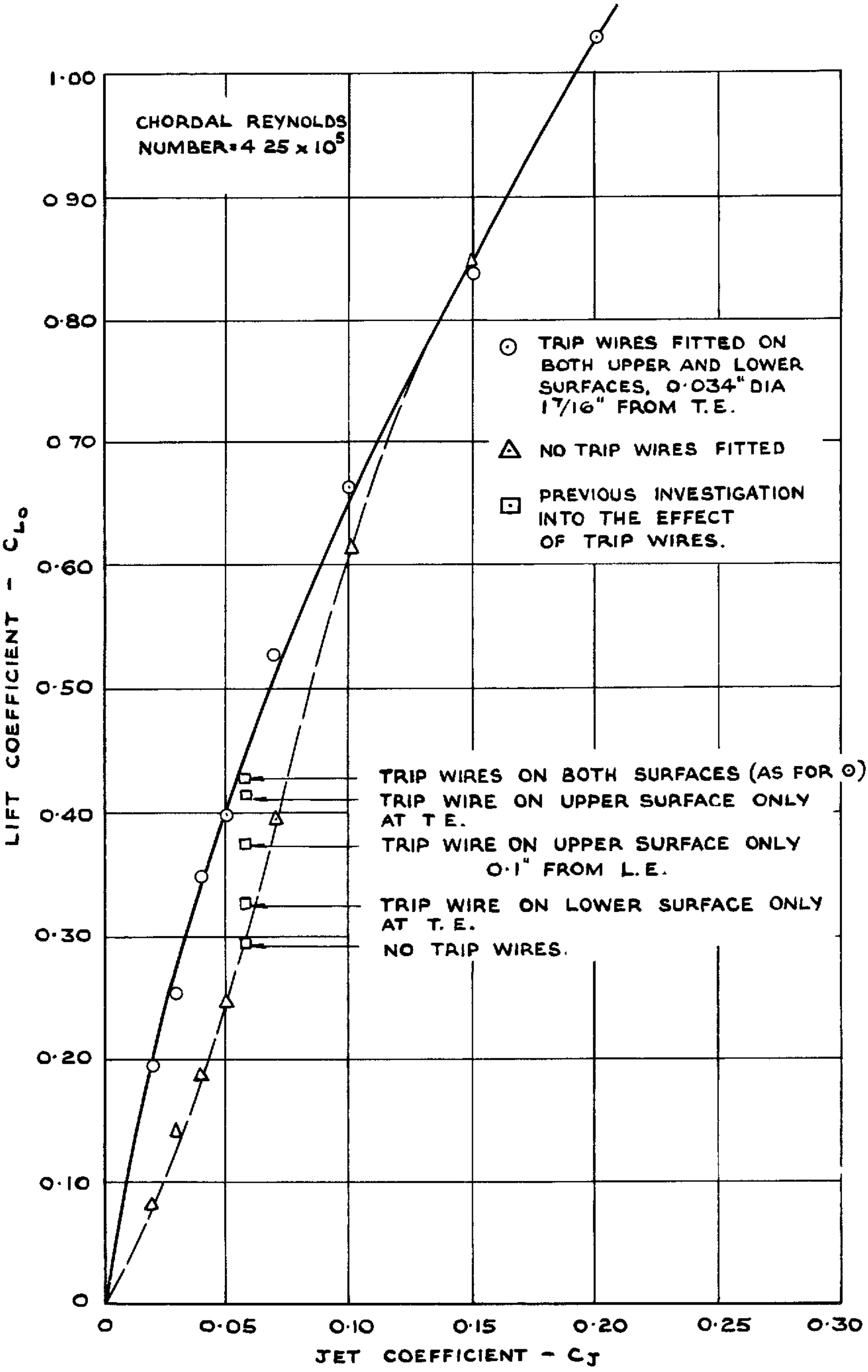

PRIMARY REYNOLDS NUMBER EFFECTS—30° MODEL.

FIG. 22.

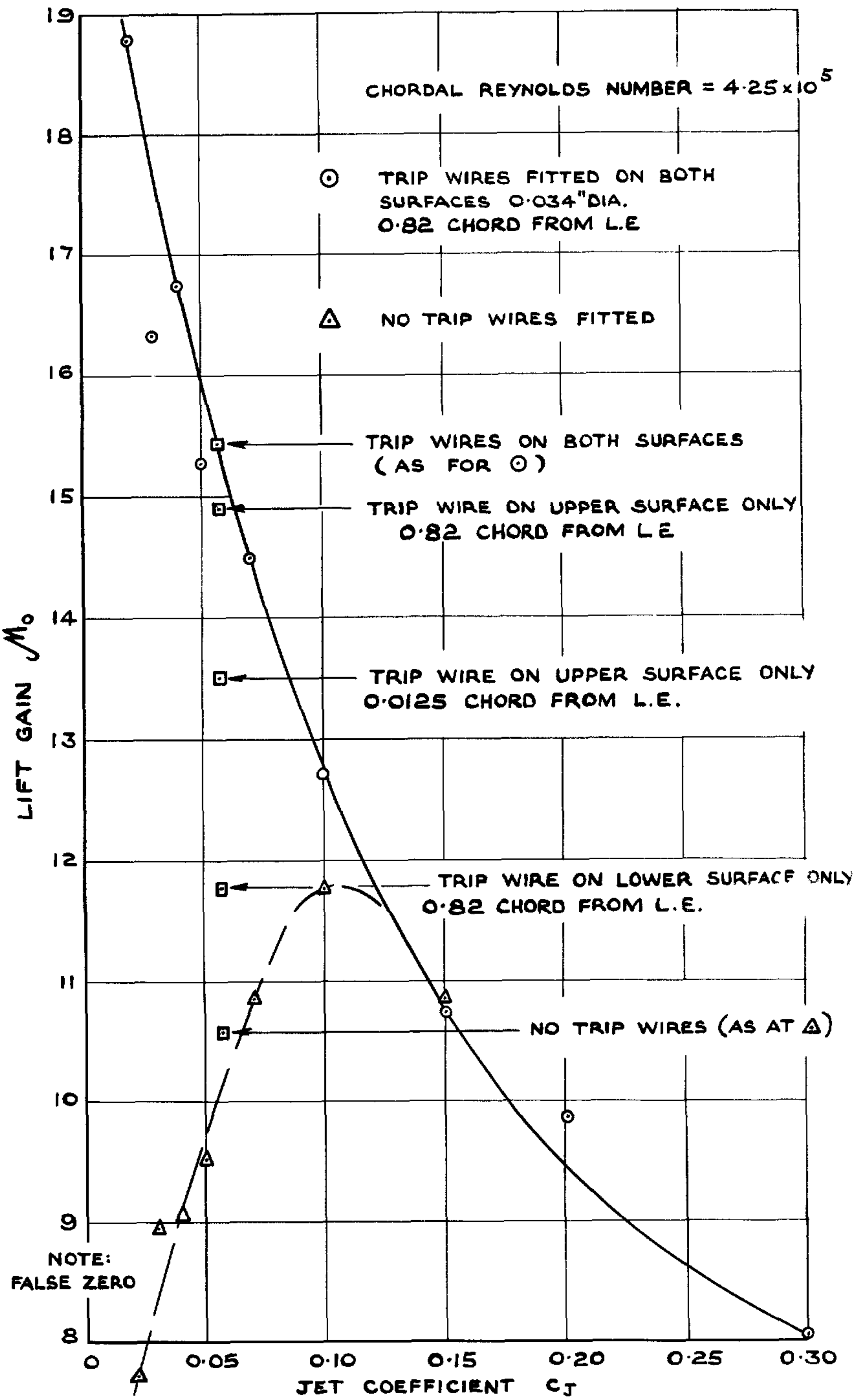

EFFECT OF TRANSITION WIRES ON $\mathcal{M}_0$ – 30° MODEL.

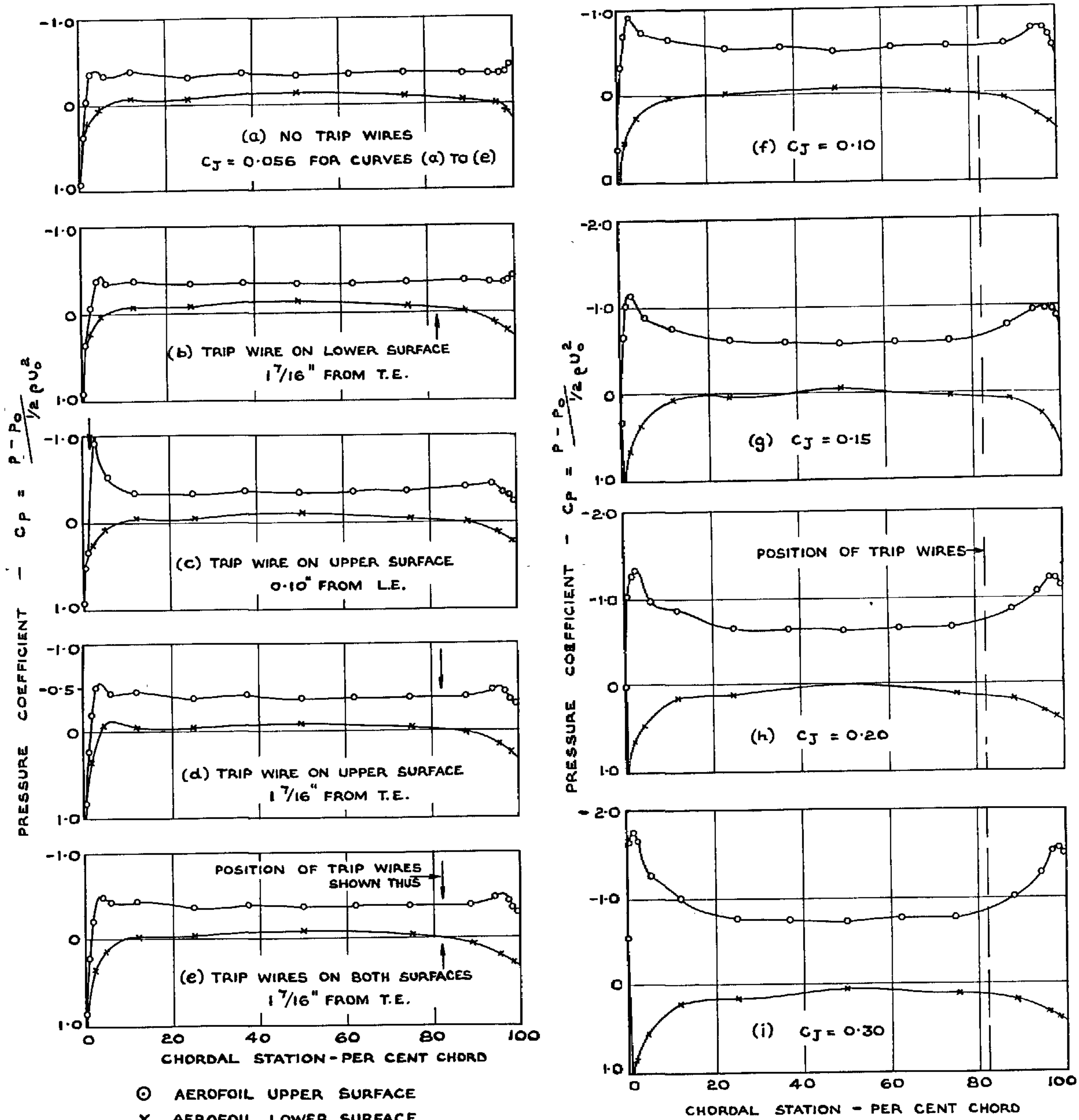

PRESSURE DISTRIBUTIONS AT ZERO INCIDENCE — 30° MODEL.

FIG. 23

FIG. 24

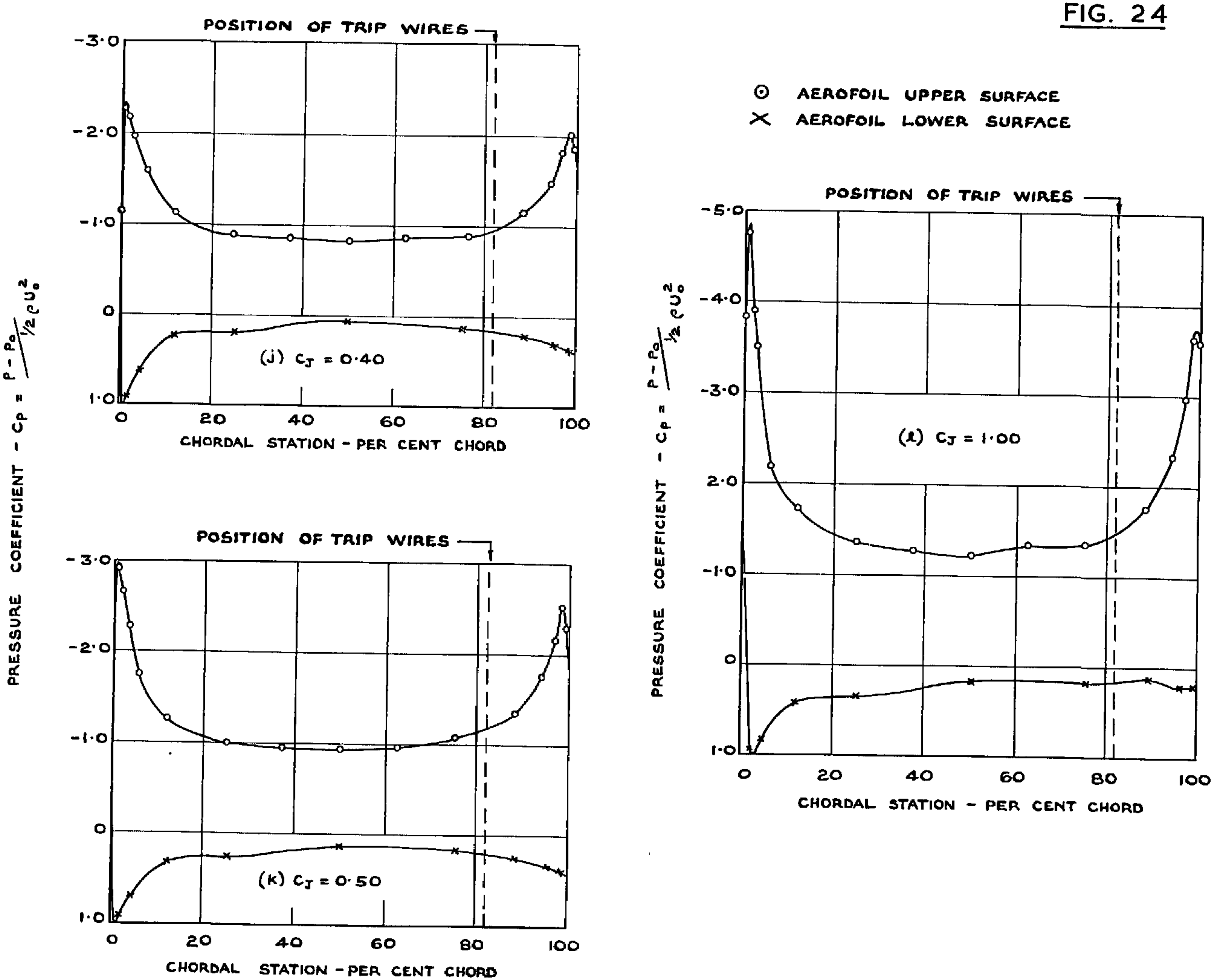

PRESSURE DISTRIBUTION AT ZERO INCIDENCE — 30° MODEL.

FIG. 25

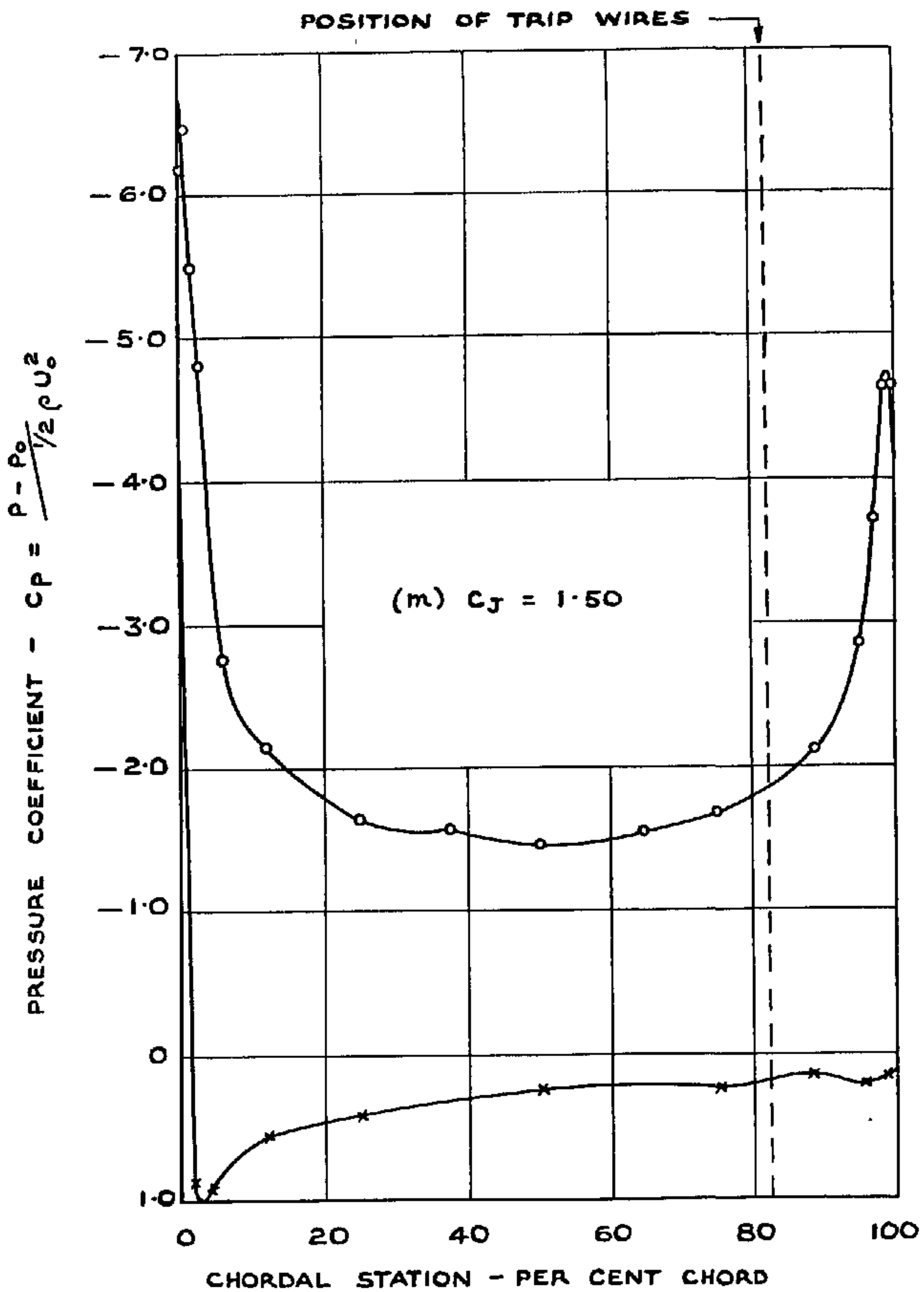

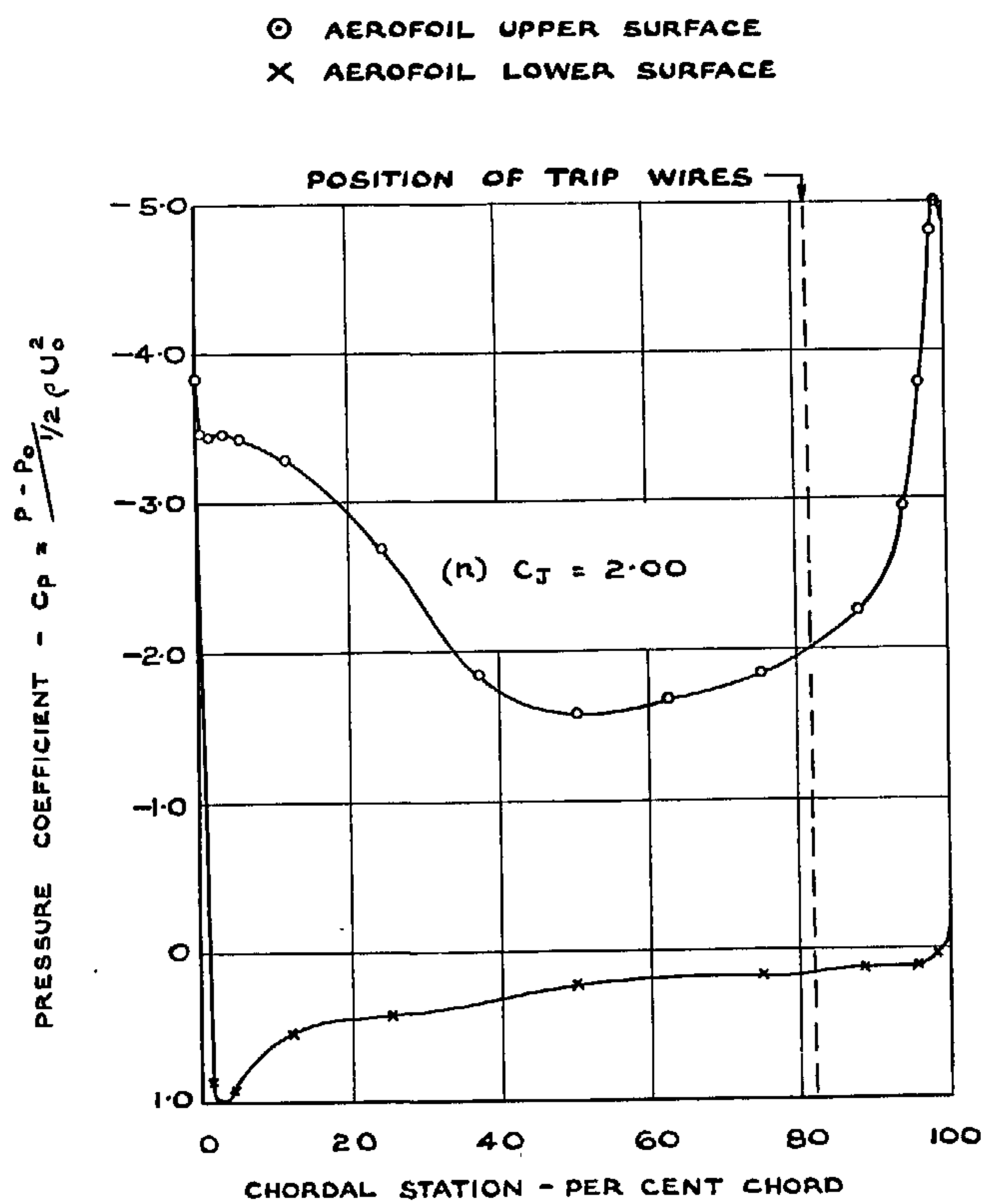

PRESSURE DISTRIBUTION AT ZERO INCIDENCE.— 30° MODEL.

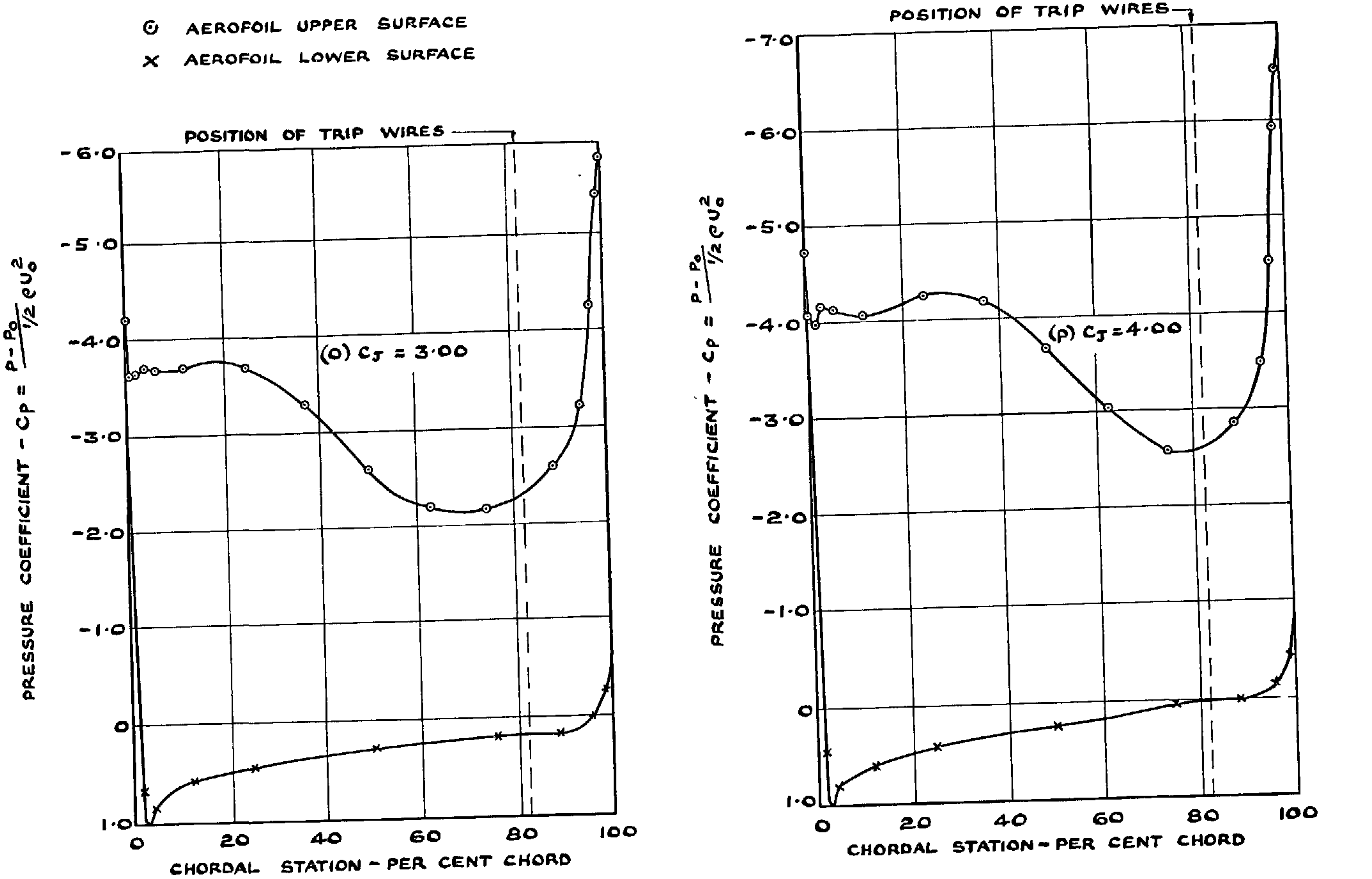

PRESSURE DISTRIBUTION AT ZERO INCIDENCE - 30° MODEL.

FIG. 27

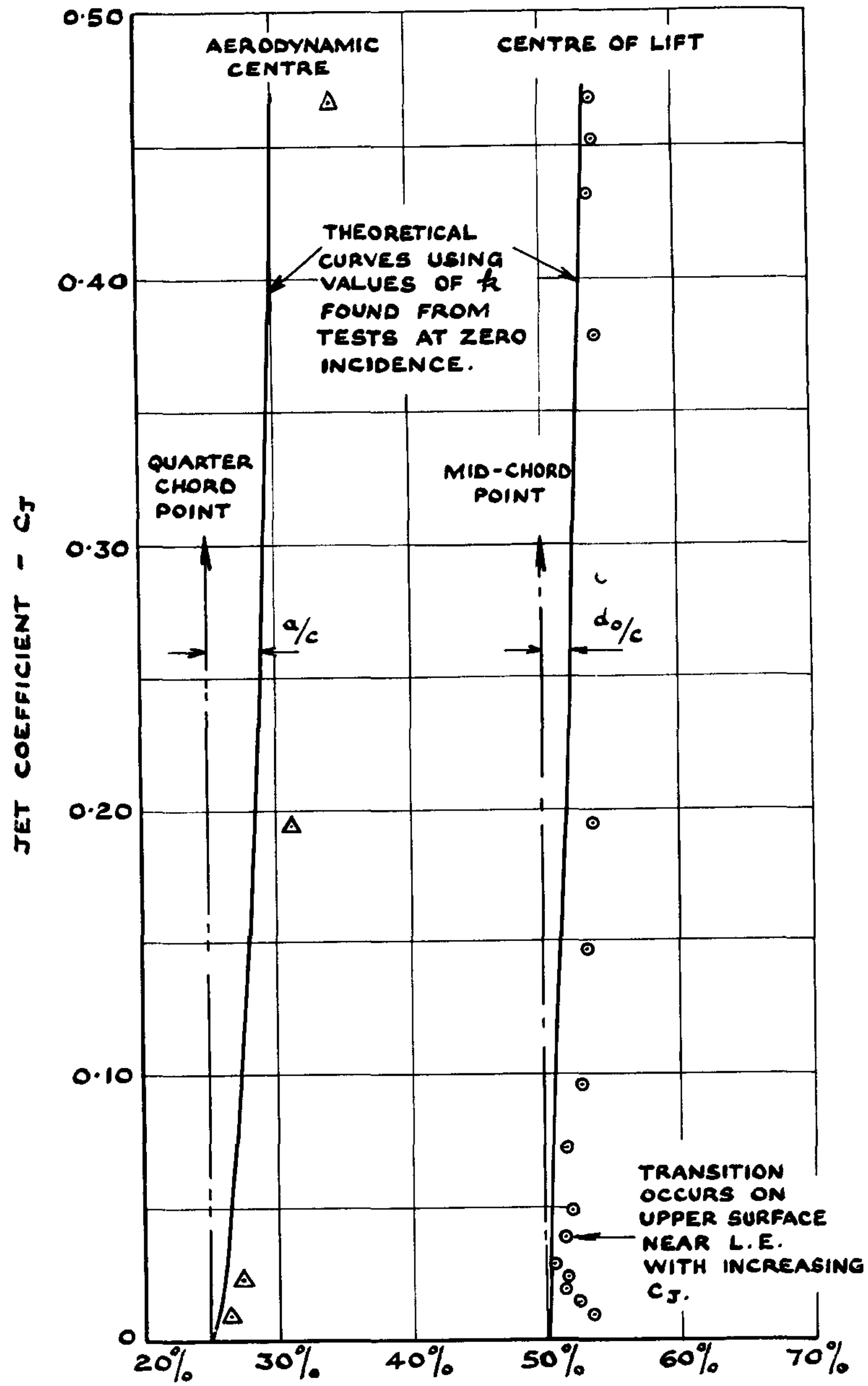

NOTE: FALSE ORIGIN.

AERODYNAMIC CENTRE & CENTRE OF LIFT 90° MODEL.

FIG. 28

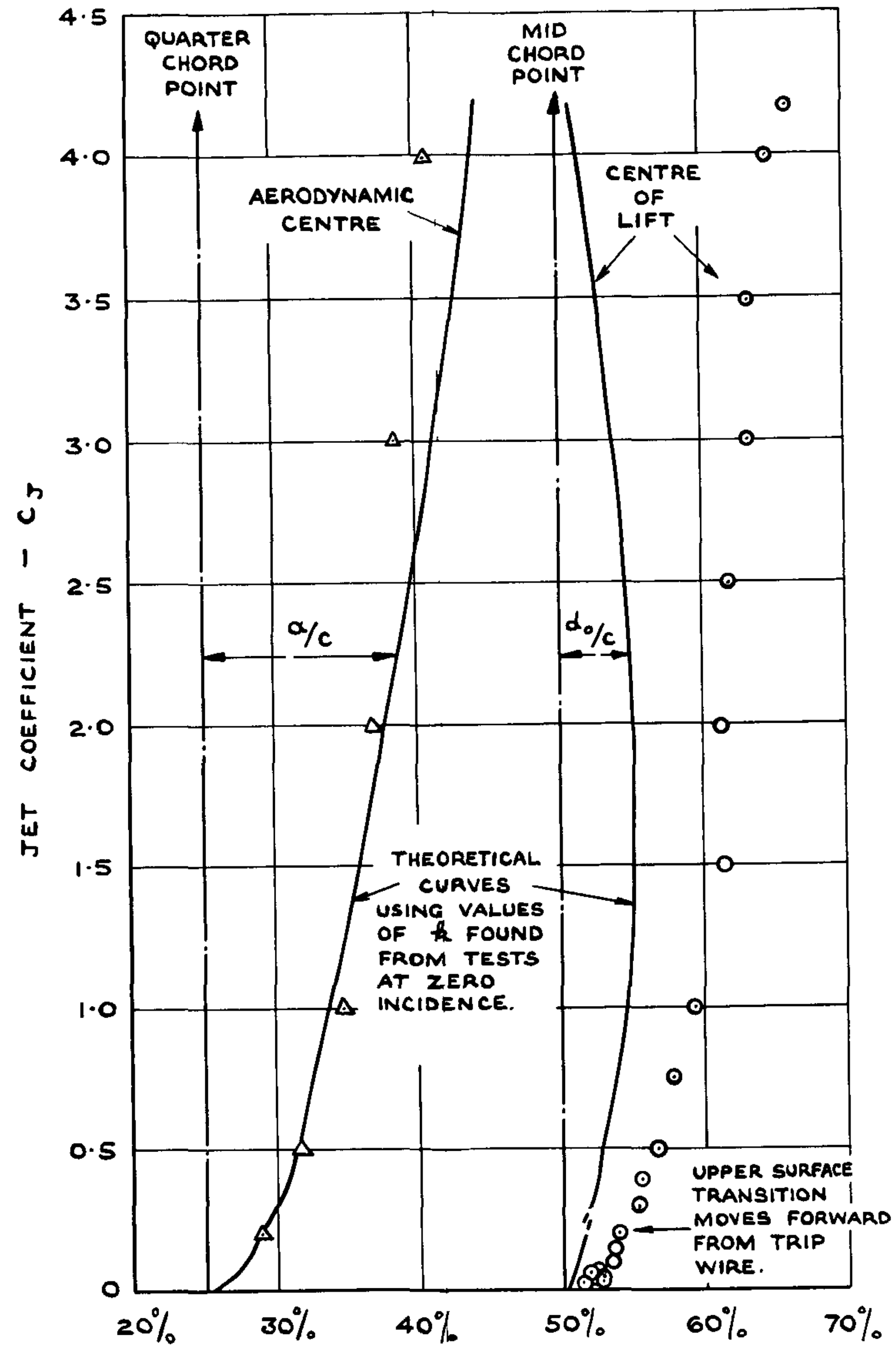

NOTE: FALSE ORIGIN

AERODYNAMIC CENTRE & CENTRE OF LIFT 30° MODEL.

FIG. 29

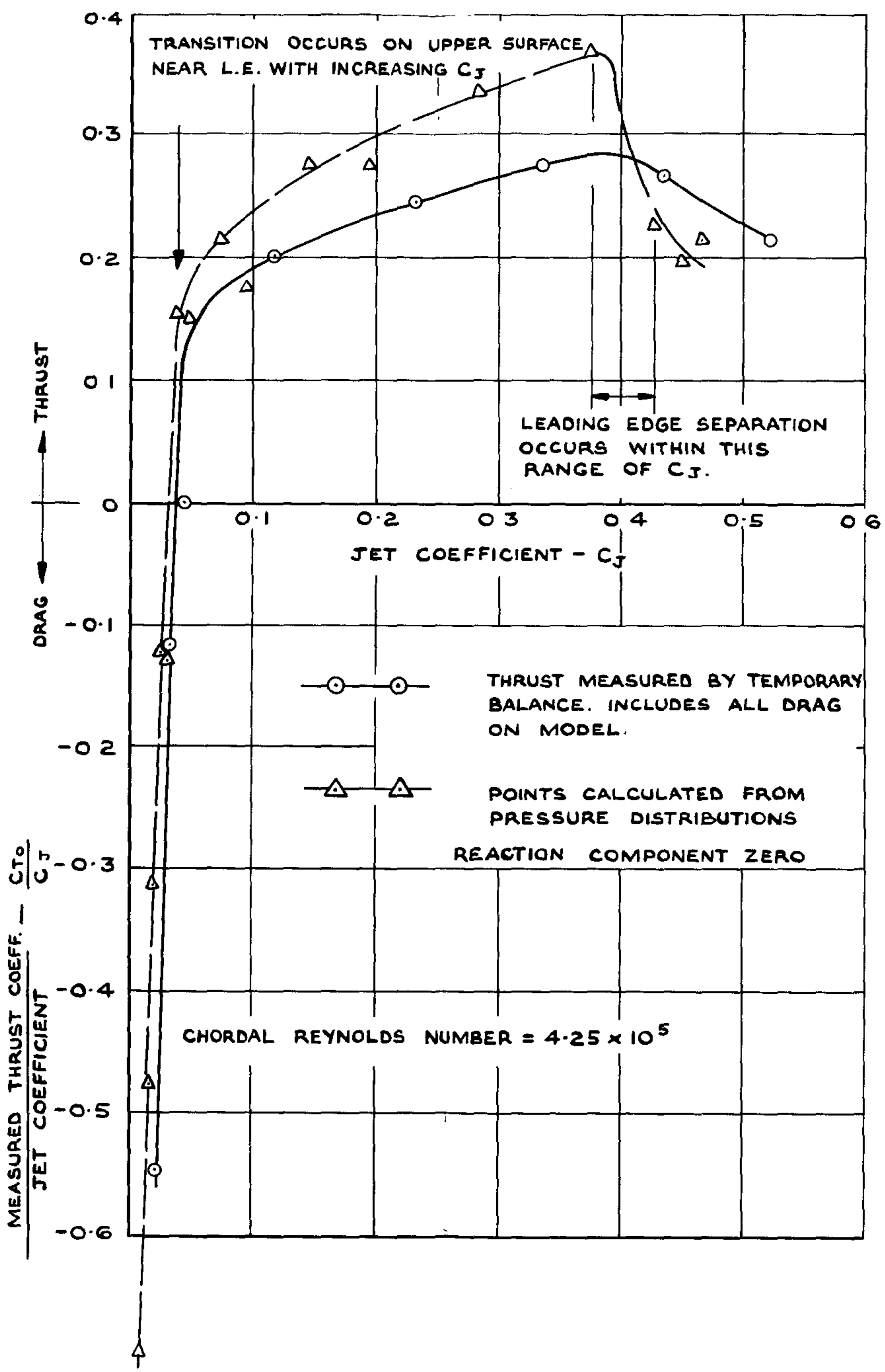

PRESSURE THRUST-90° MODEL.

FIG. 30

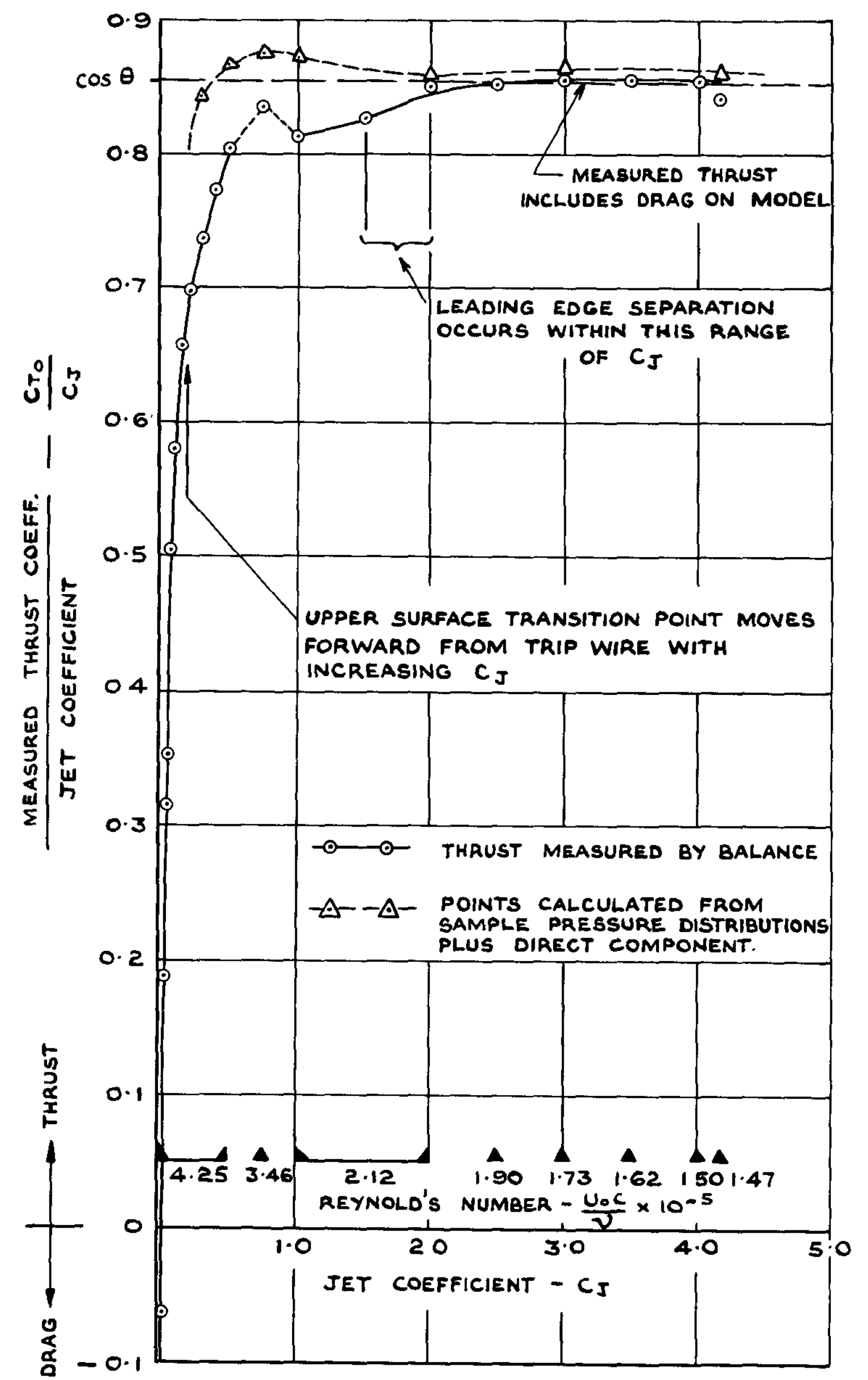

MEASURED THRUST-30° MODEL.

FIG.31

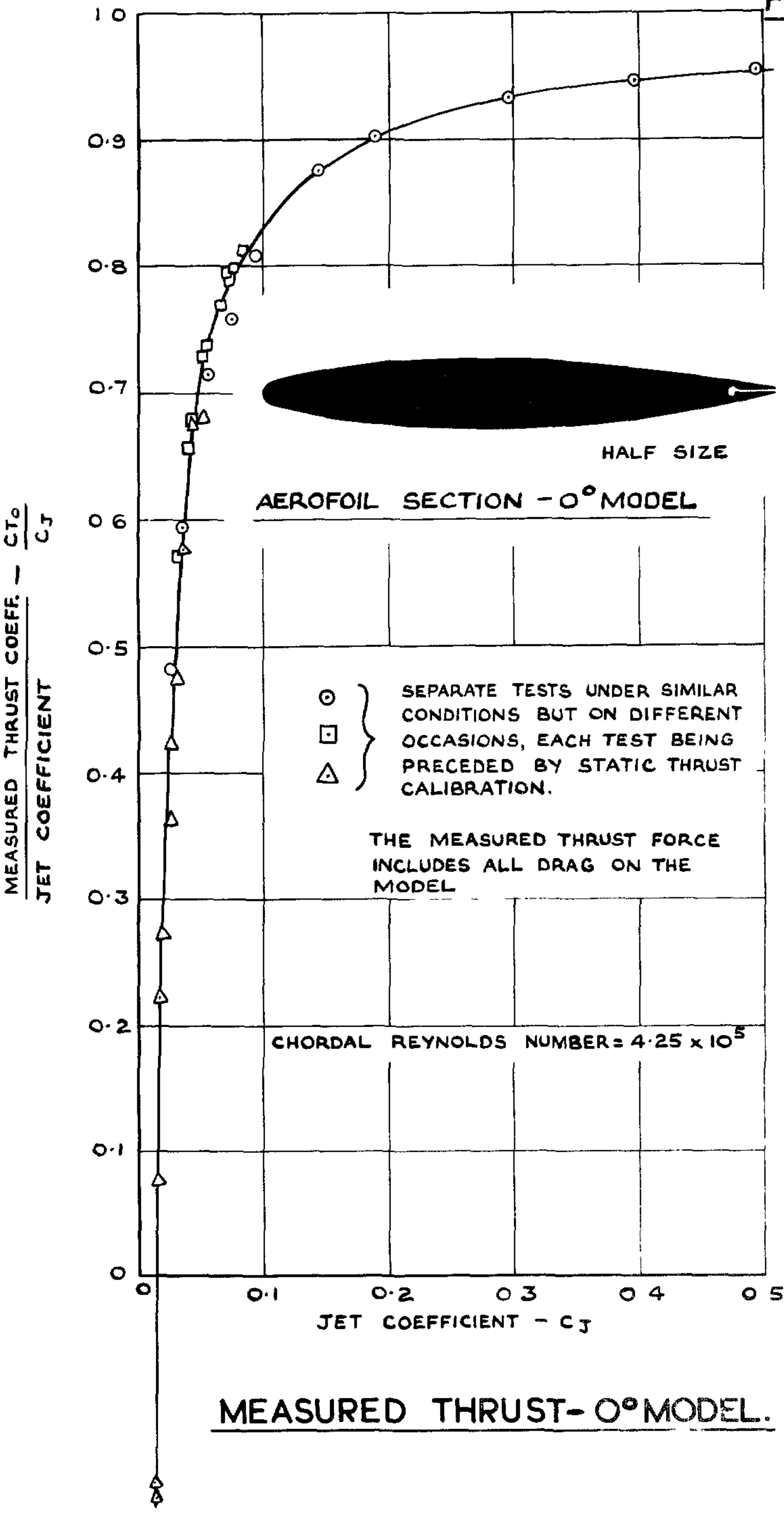

MEASURED THRUST — 0° MODEL.

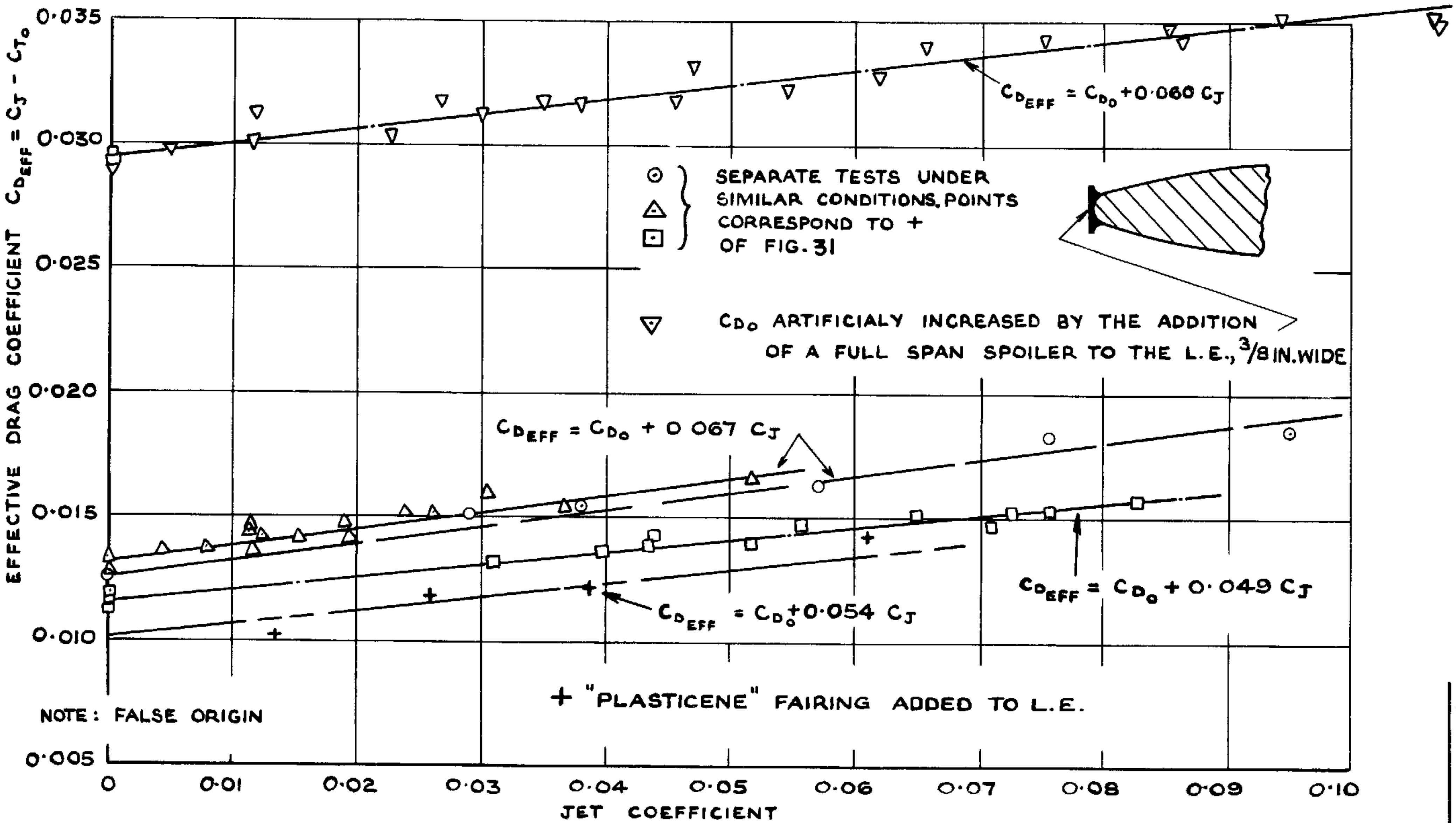

THE SINK DRAG EFFECT – 0° MODEL.

FIG. 32

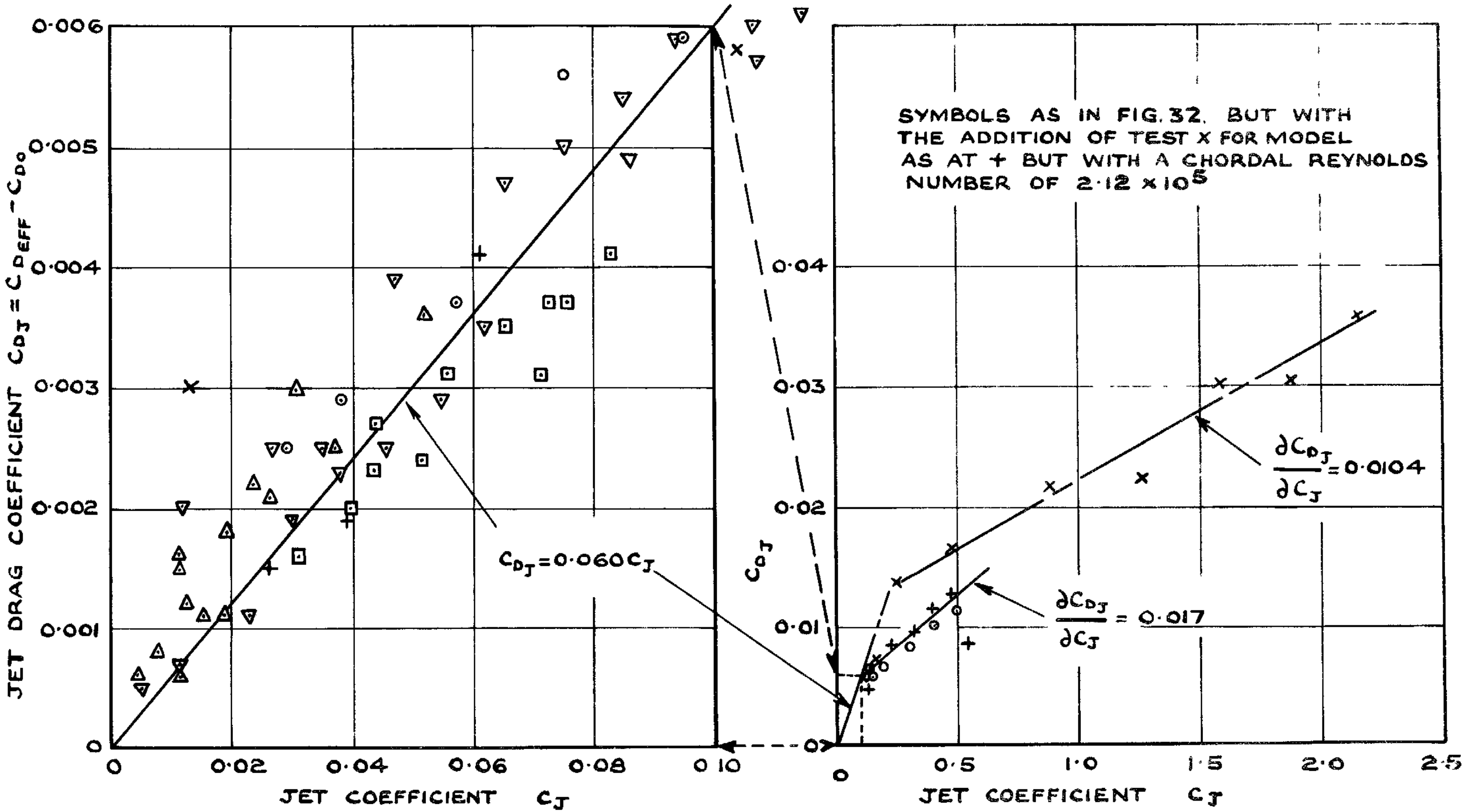

VARIATION OF C_{D_J} WITH C_J

FIG. 33.

FIG. 34

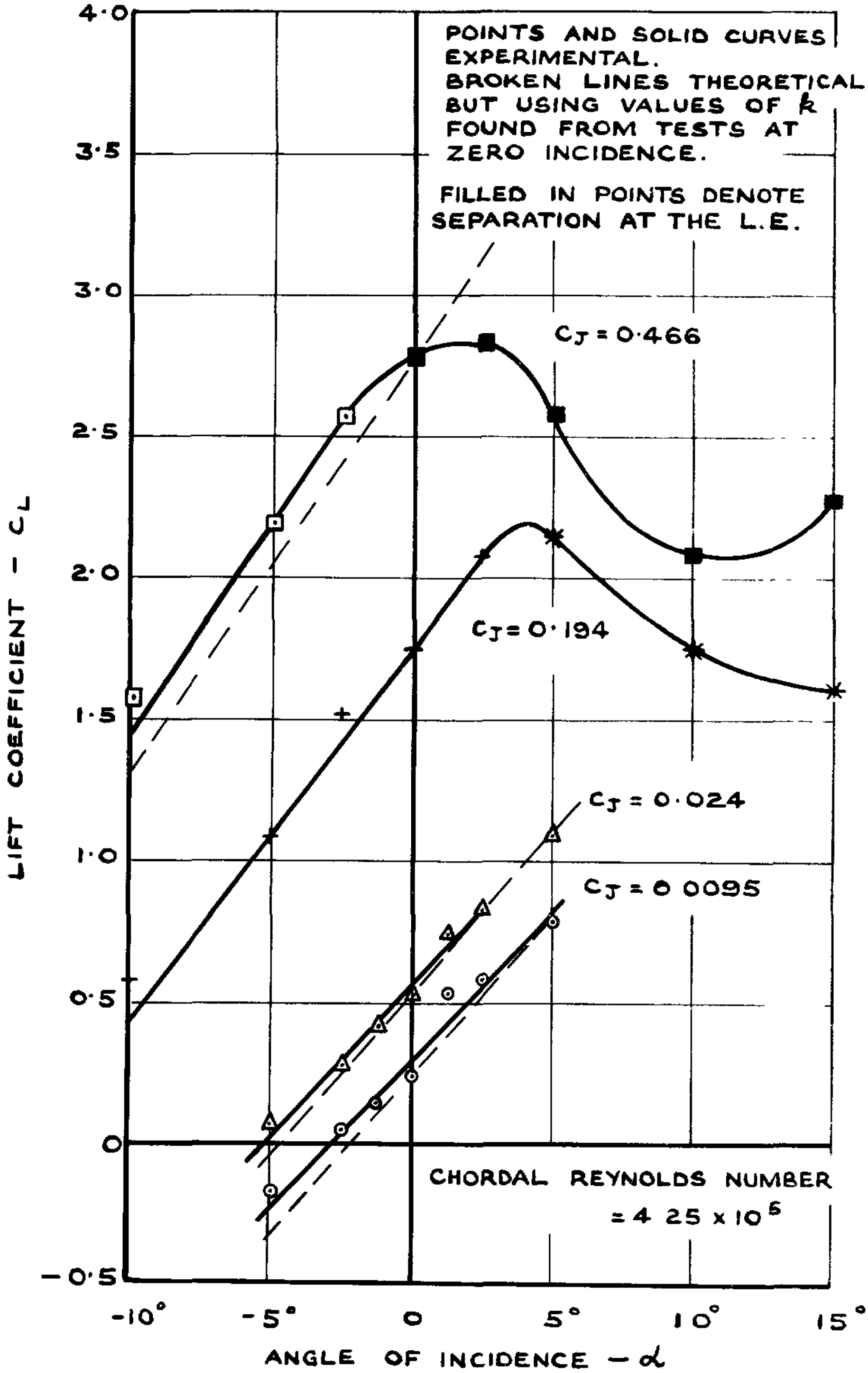

LIFT AT INCIDENCE - 90° MODEL

FIG. 35

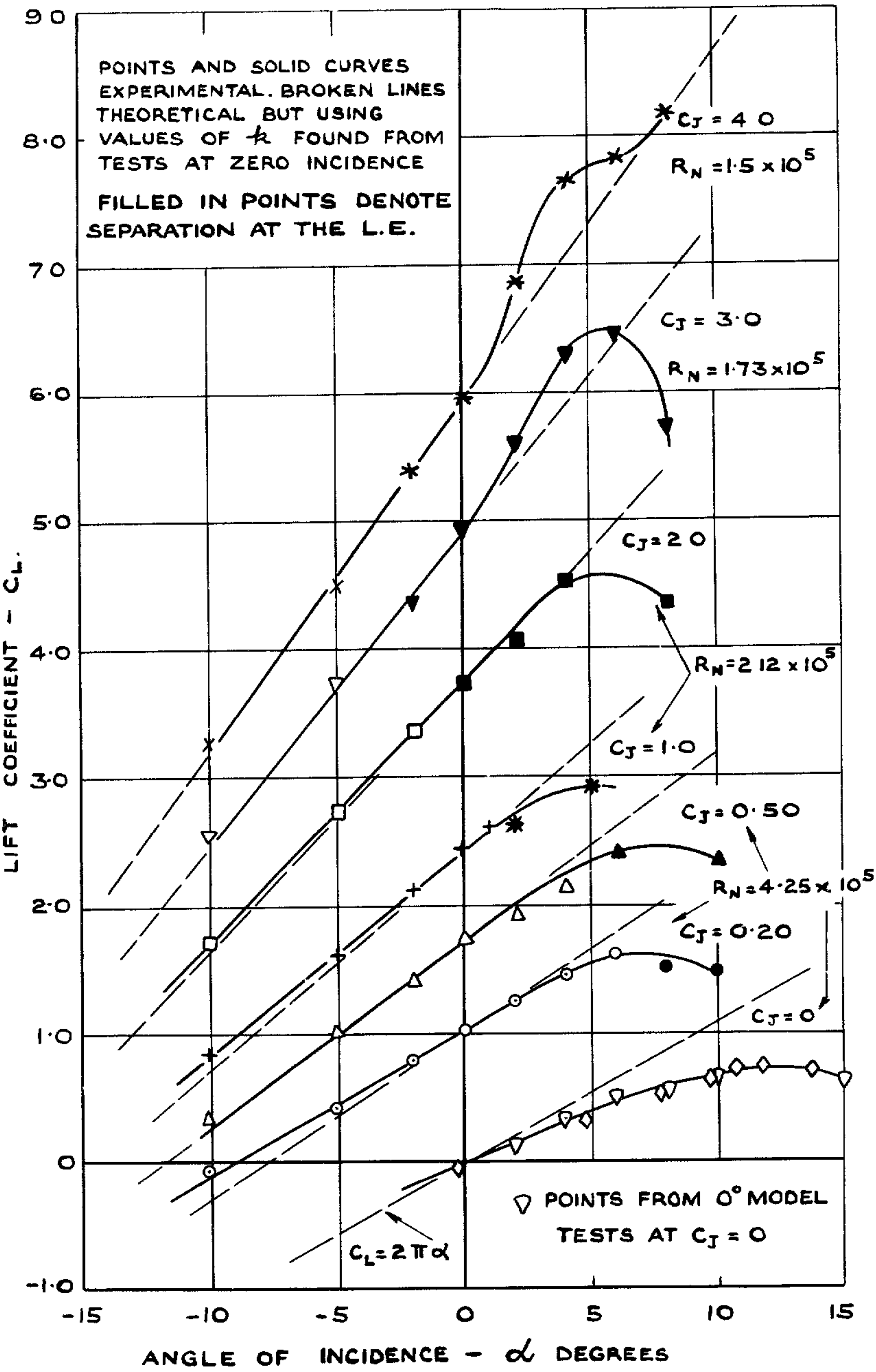

LIFT AT INCIDENCE -30° MODEL.

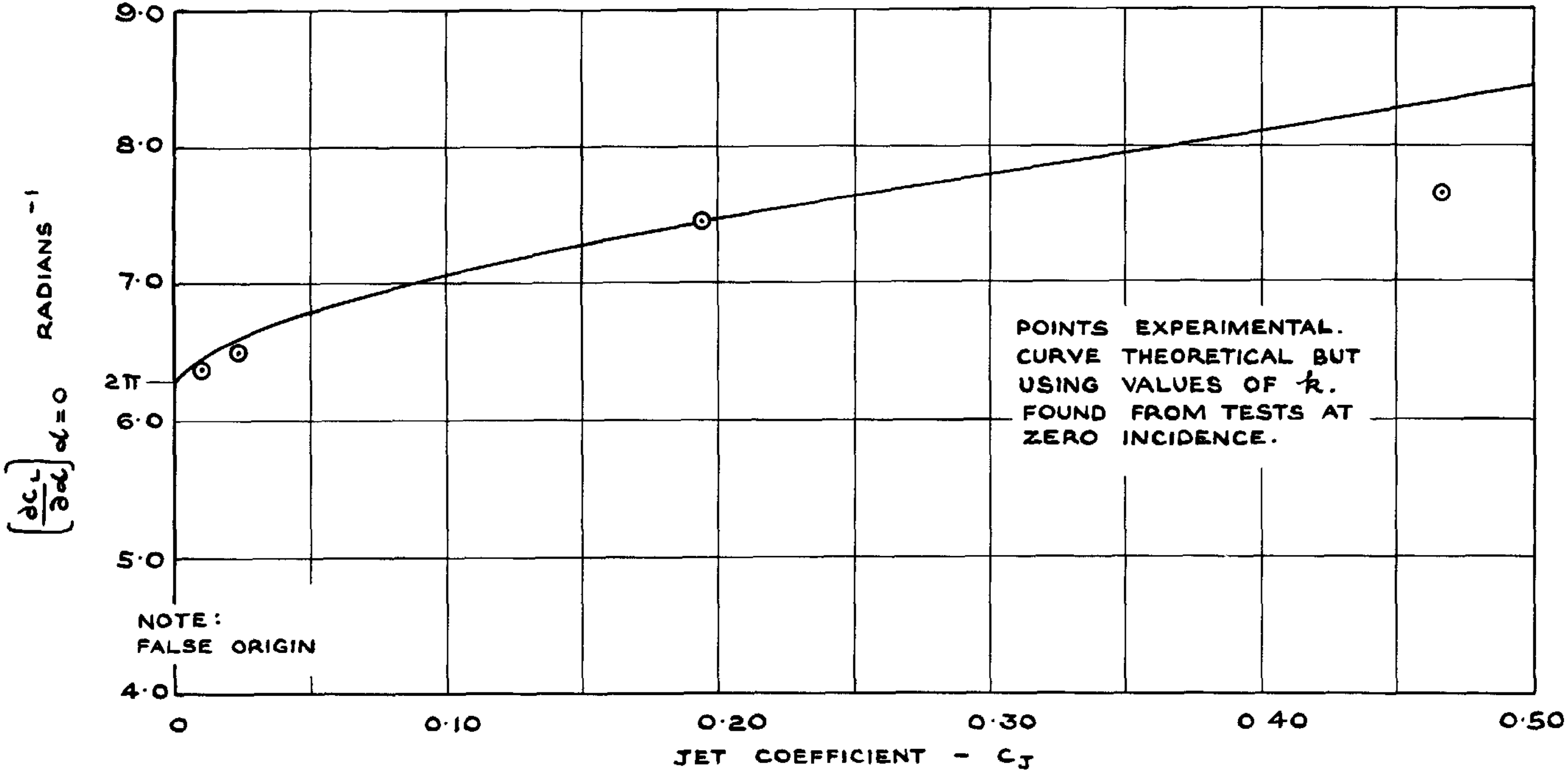

LIFT AT INCIDENCE – 90° MODEL.

VARIATION OF LIFT CURVE SLOPE WITH C_J.

FIG. 36

FIG. 37

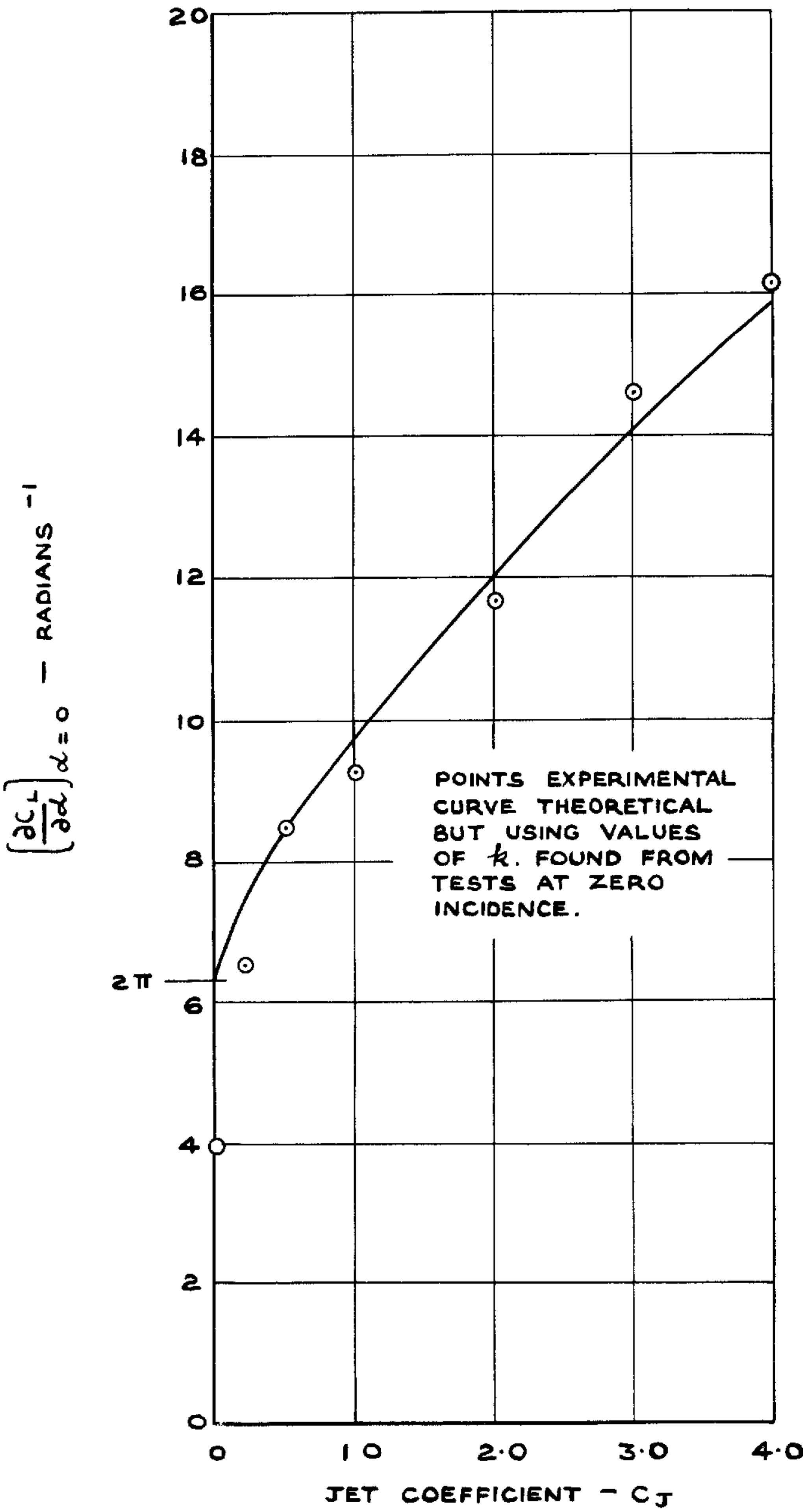

LIFT AT INCIDENCE – 30° MODEL.

VARIATION OF LIFT CURVE SLOPE WITH C_J.

FIG. 38

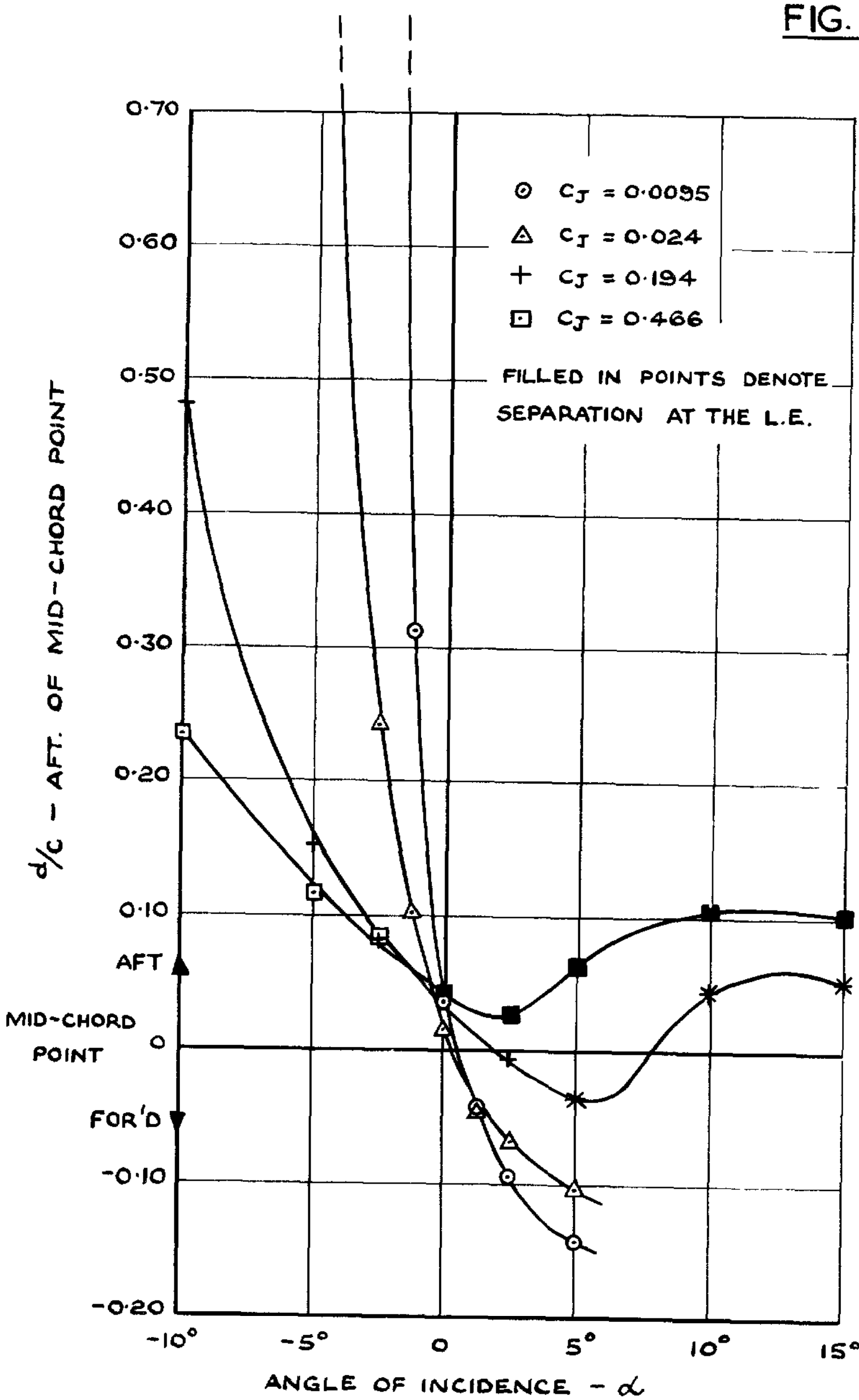

CENTRE OF LIFT — VARIATION WITH INCIDENCE
90° MODEL

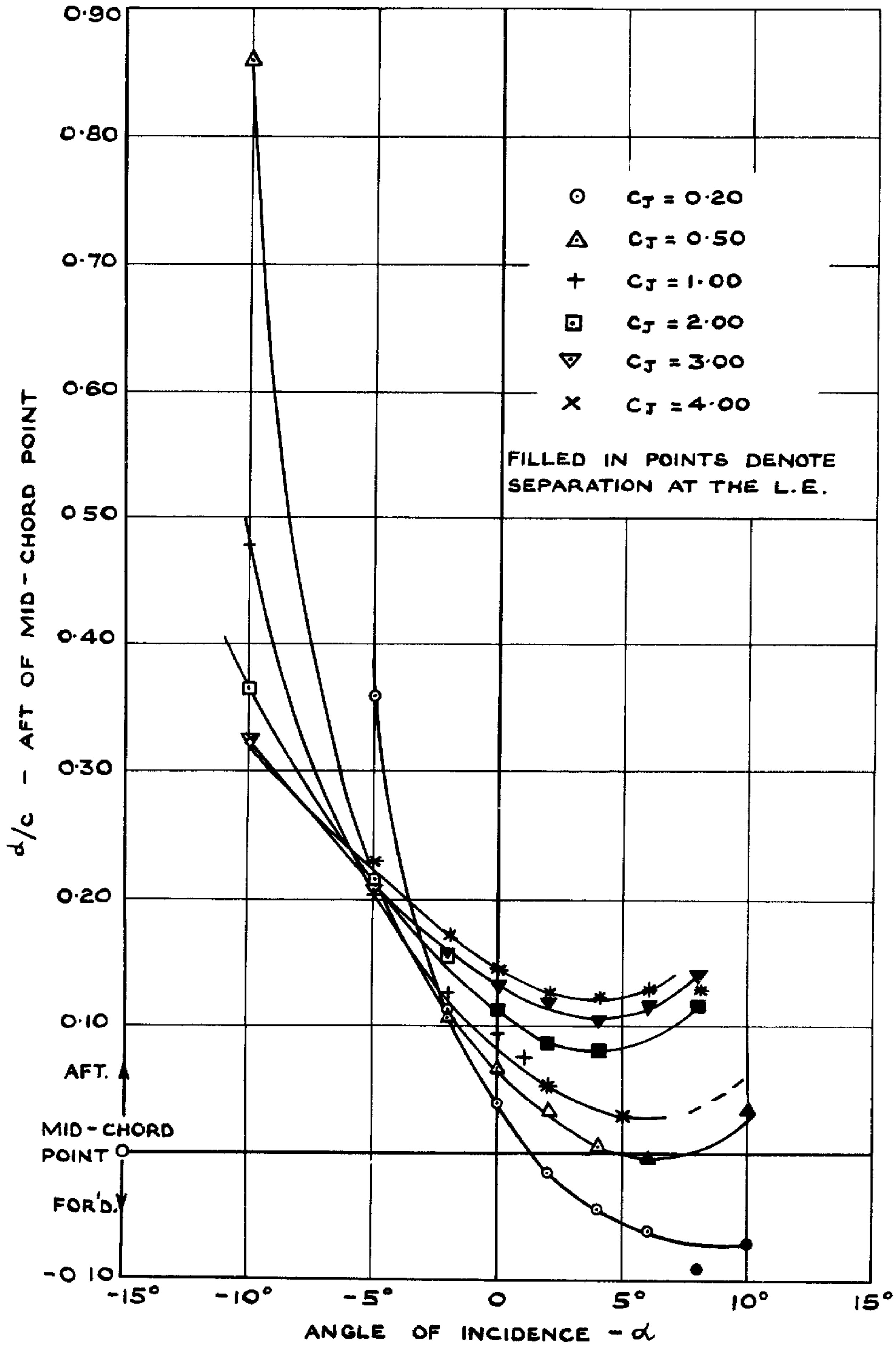

CENTRE OF LIFT – VARIATION WITH INCIDENCE.

30° MODEL.

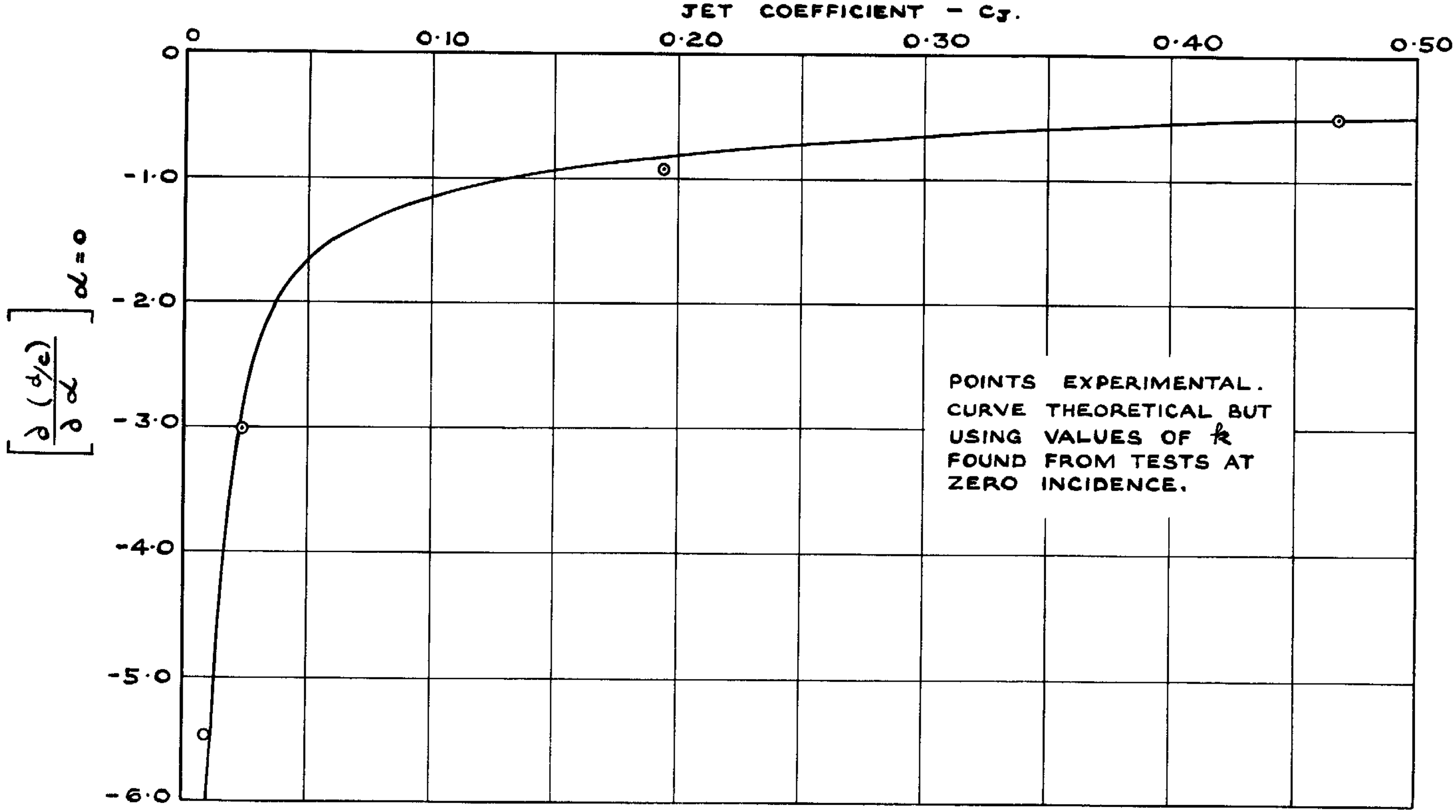

CENTRE OF LIFT MOVEMENT WITH INCIDENCE - 90° MODEL.

FIG. 40

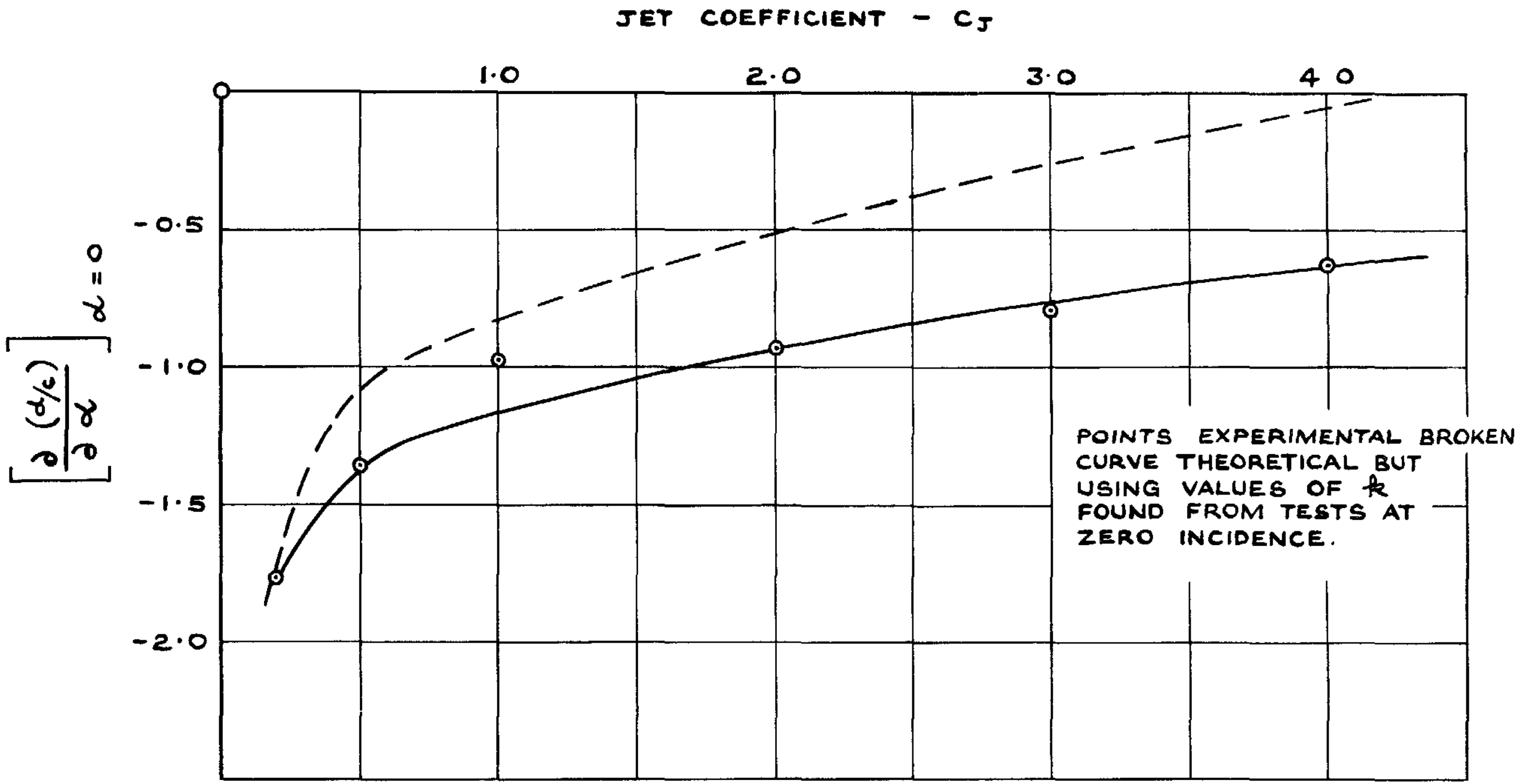

CENTRE OF LIFT MOVEMENT WITH INCIDENCE - 30° MODEL.

FIG. 41

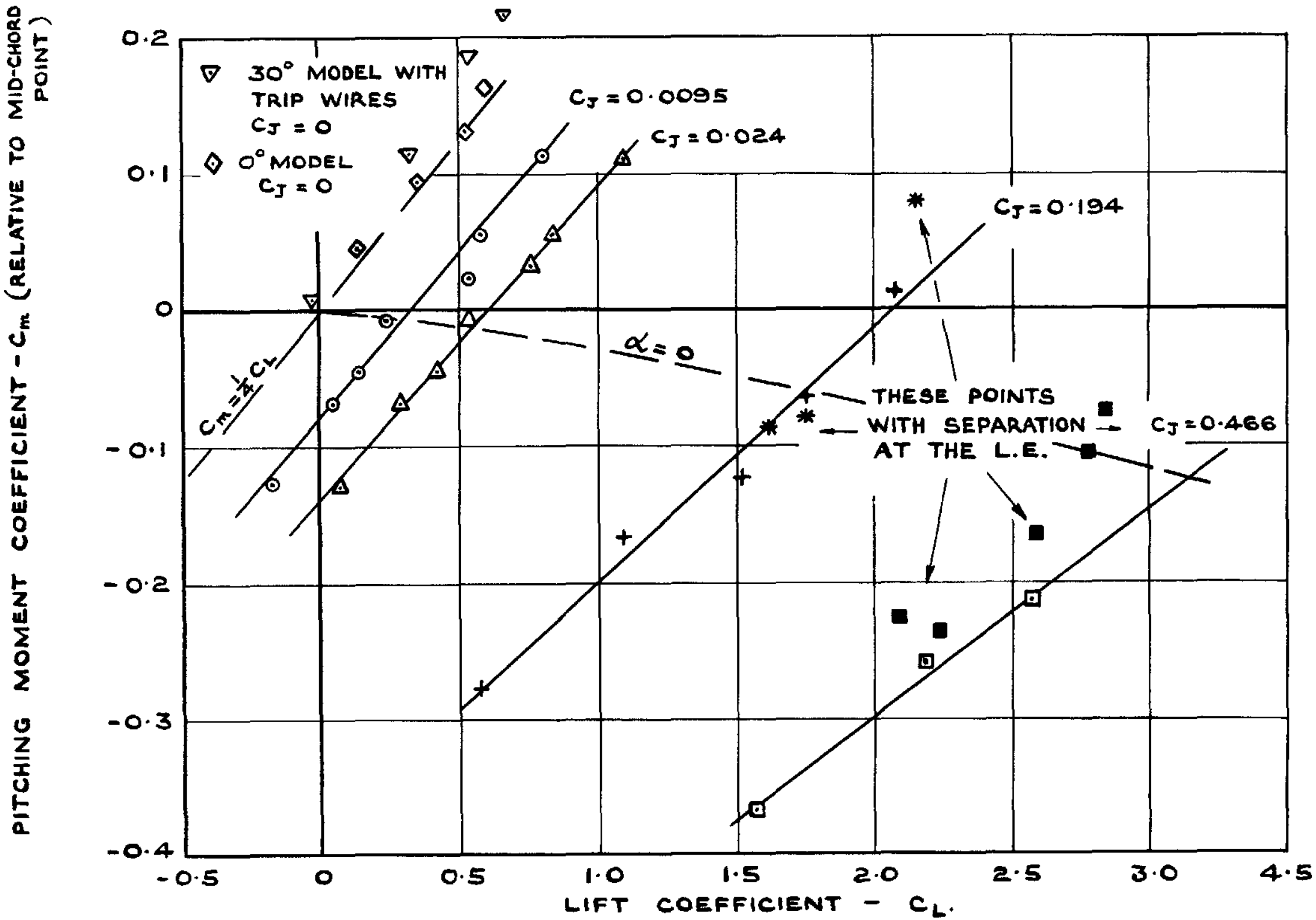

LIFT AND PITCHING MOMENT RELATIONSHIP. – 90° MODEL.

FIG. 42

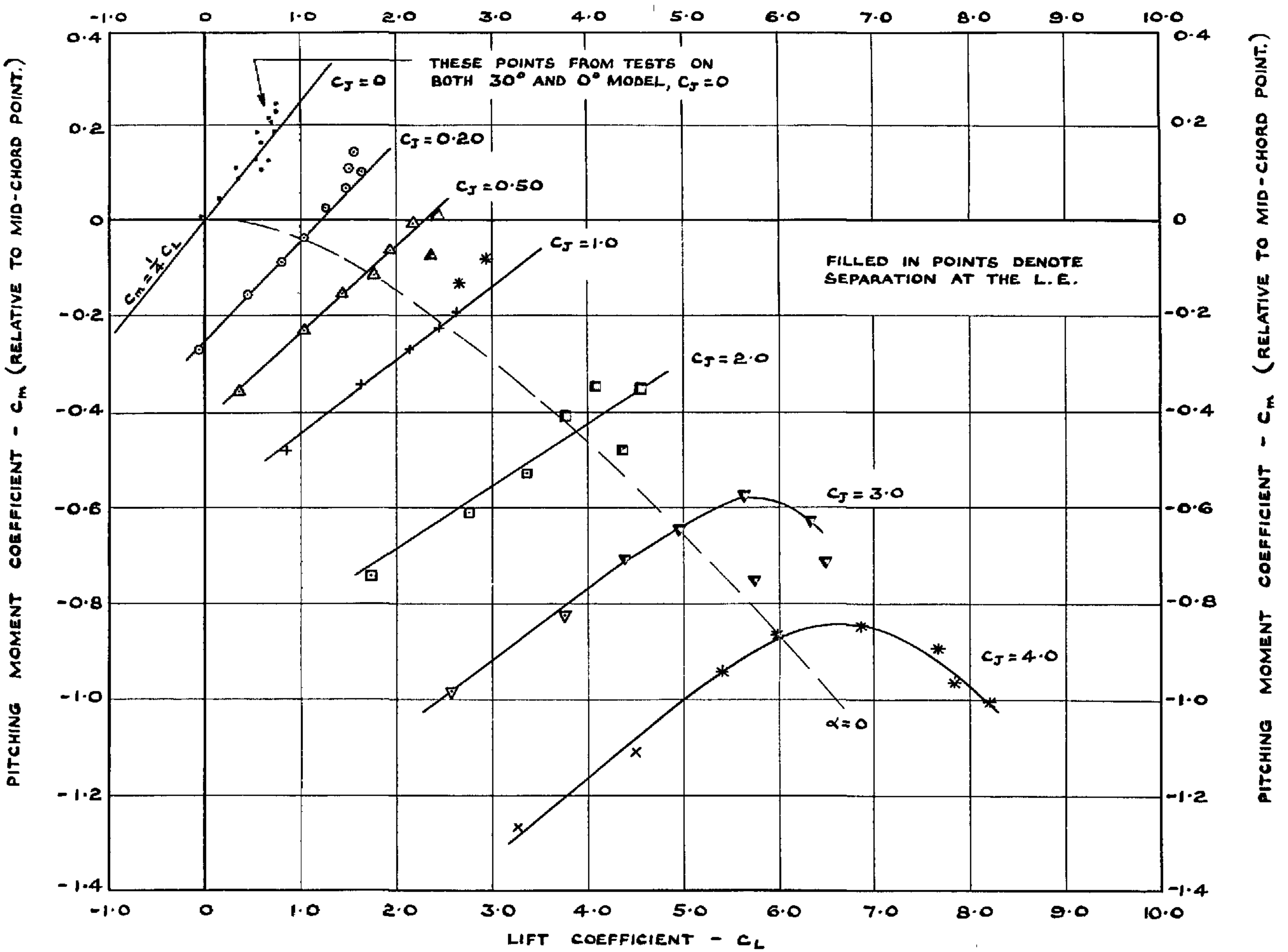

LIFT AND PITCHING MOMENT RELATIONSHIP. – 30° MODEL.

FIG. 44

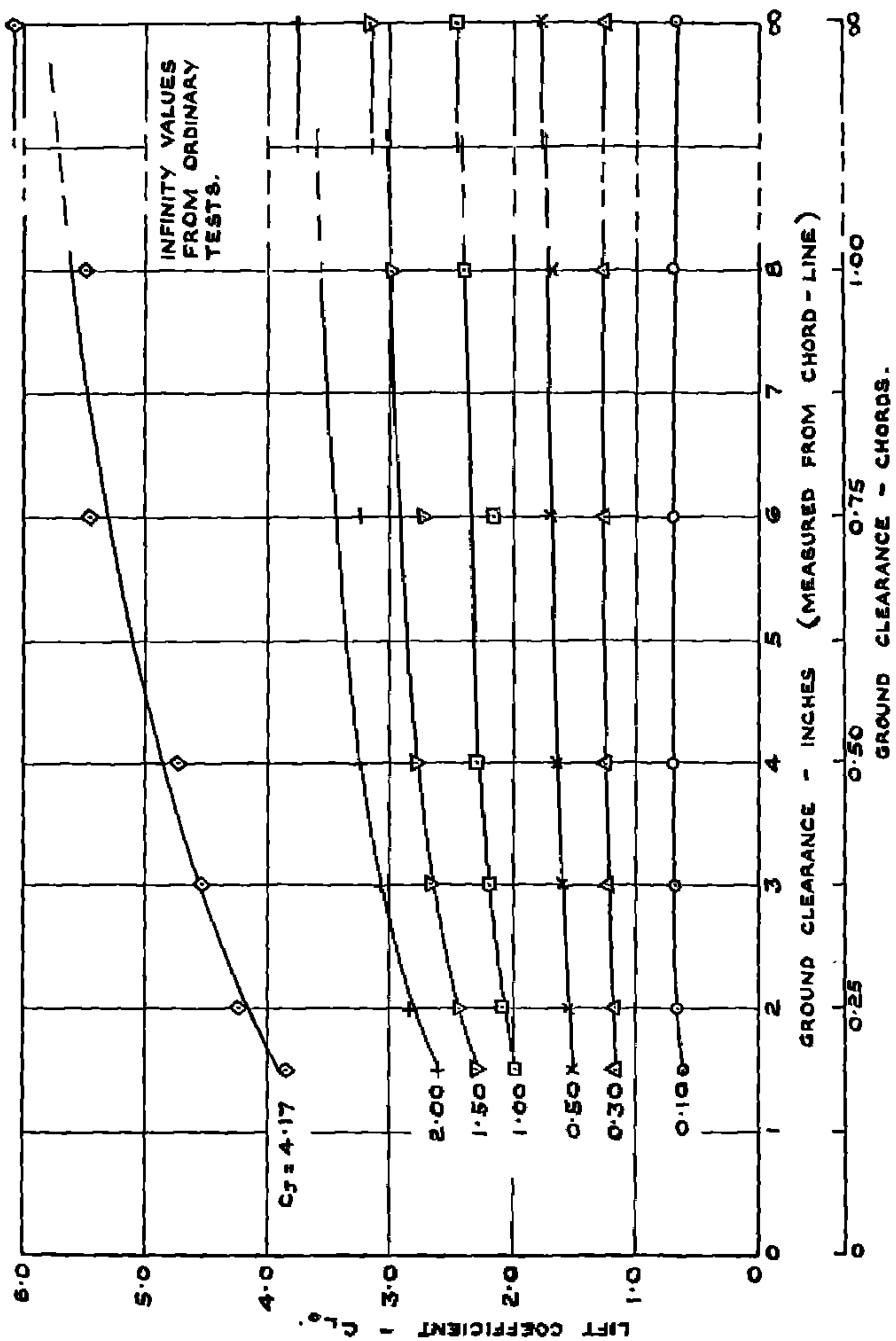

GROUND INTERFERENCE EFFECT ON LIFT COEFFICIENT AT ZERO INCIDENCE—30° MODEL.

FIG. 45

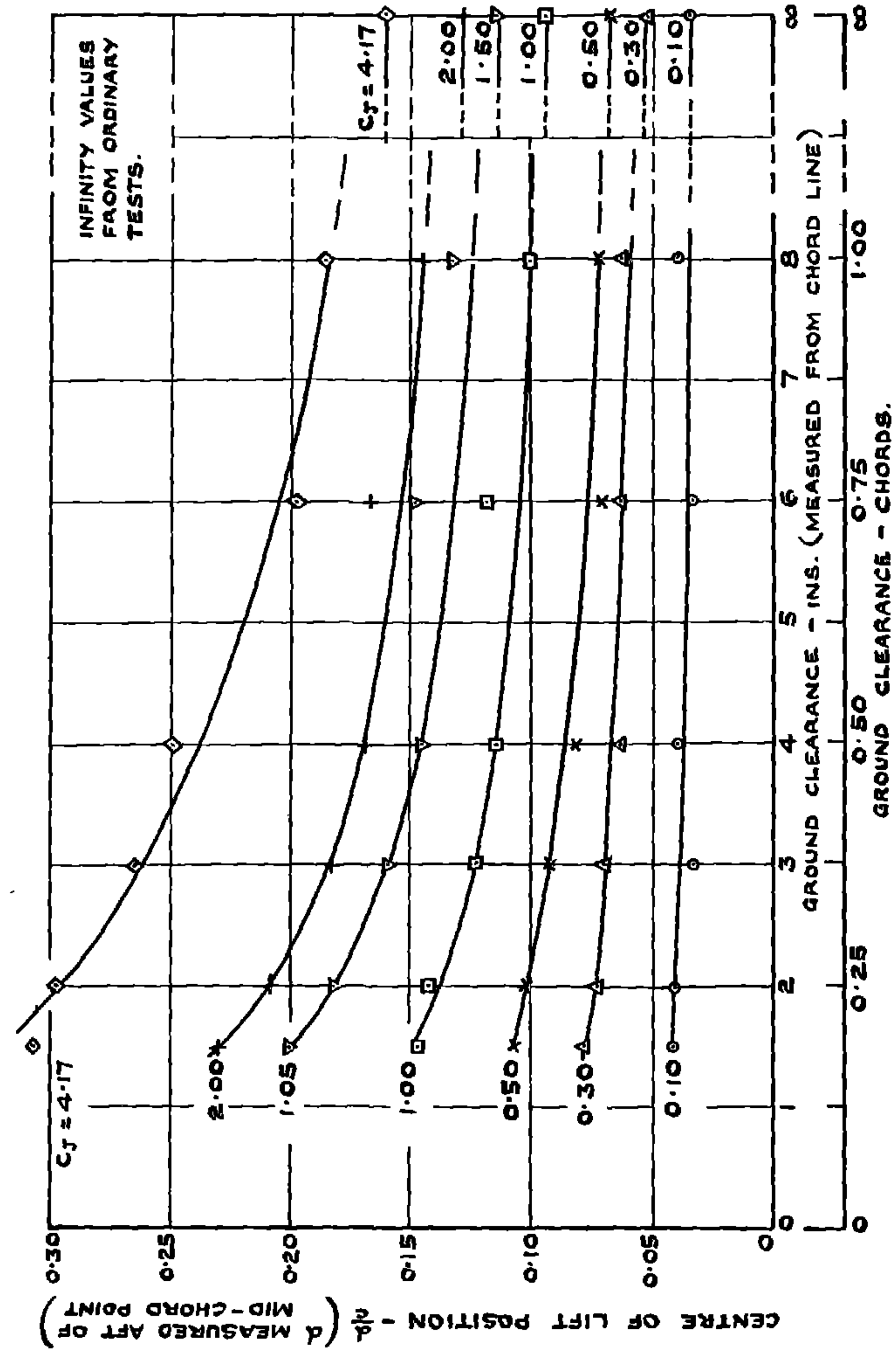

GROUND INTERFERENCE EFFECT ON CENTRE OF LIFT POSITION AT ZERO INCIDENCE—30° MODEL.

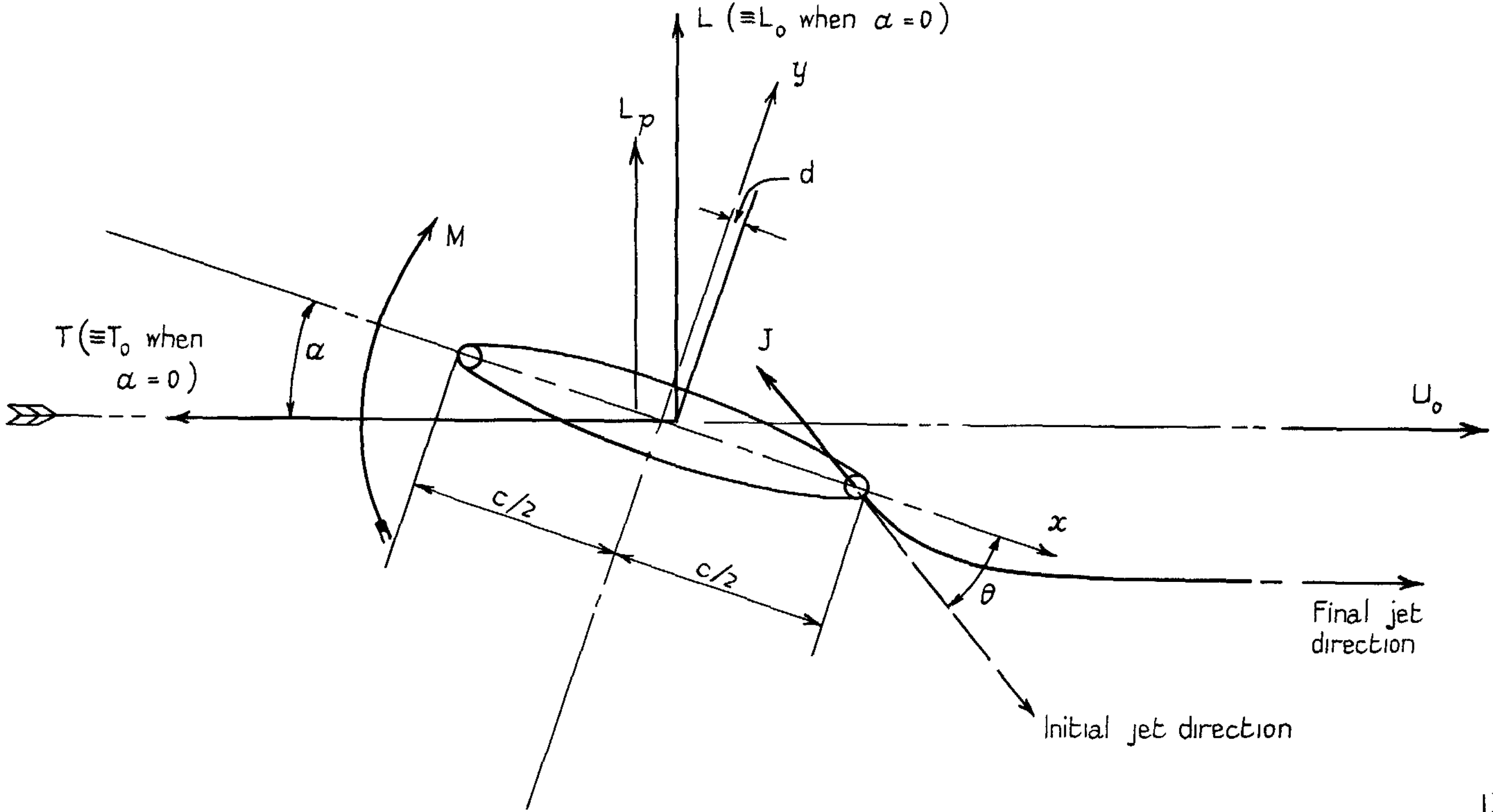

Notation — see also Appendix I

D558481/1 Wt 51 K3 7/57 CL

FIG 46.

C.P. No. 344
(18,186)
A.R.C. Technical Report

Crown copyright reserved

Printed and published by
HER MAJESTY'S STATIONERY OFFICE

To be purchased from
York House, Kingsway, London W.C.2
423 Oxford Street, London W.1
13A Castle Street, Edinburgh 2
109 St Mary Street, Cardiff
39 King Street, Manchester 2
Tower Lane, Bristol 1
2 Edmund Street, Birmingham 3
80 Chichester Street, Belfast
or through any bookseller

Printed in Great Britain

S.O. Code No. 23-9010-44

C.P. No. 344